A CORRELATION OF FRICTION FACTORS FOR PIPE FLOW OVER TWO-DIMENSIONAL, PERIODIC GEOMETRIC ROUGHNESS

A Dissertation

Presented to

the Faculty of the Department of Chemical Engineering

University of Houston

In Partial Fulfillment

of the Requirements for the Degree

Doctor of Philosophy

---

by

Emerson Clifford Gaddis, Jr.

December 1971

ACKNOWLEDGEMENTS

It is my pleasure to express my deepest thanks to the following individuals who have assisted me in the completion of this work:

the Office of Saline Water of the Department of the Interior which provided financial assistance through Grant No. 14-01-0001-1311;

the City College of the City of New York for providing financial assistance in the Boris A. Bakhmeteff Fellowship in Fluid Mechanics for the year 1969-1970;

my advisor, Dr. F. L. Worley, Jr., for his guidance and useful suggestions;

my parents, Mr. and Mrs. E. C. Gaddis, for engendering in me the perseverance and desire to accomplish, which are by far the most important prerequisites for this work;

my wife, Terry, for her assistance in typing the manuscript and especially for her willingness to have lived in the future with me for the past three years.

A CORRELATION OF FRICTION FACTORS FOR PIPE FLOW OVER TWO-DIMENSIONAL, PERIODIC GEOMETRIC ROUGHNESS

An Abstract of a Dissertation

Presented to

the Faculty of the Department of Chemical Engineering

University of Houston

In Partial Fulfillment

of the Requirements for the Degree

Doctor of Philosophy

---

by

Emerson Clifford Gaddis, Jr.

December 1971

ABSTRACT

Friction effects of two-dimensional, periodic, artificial roughness for fully roughened pipes in turbulent flow were investigated. Friction factor data over many different shapes, sizes, and spacings of roughness were compiled and examined for similarities which could be correlated. Such shapes included fins, round rods, rectangular rods, square bars, v-grooves, and sinusoids.

It was found that friction factors for two differently-shaped roughness waveforms of the same spacing, amplitude, and pipe diameter are related by the normalized crosscorrelation coefficient of their waveforms. Such roughness falls into two groups: projections, where the bulk flow interacts with the flow near the wall; and grooves, where captive vortices exist in the roughness cavities and do not interact with the bulk flow. Friction factors were related to sine waves of similar size, modified by linear combinations of roughness dimensions and plotted versus a representing parameter R, which was found to be a dimensionless group containing a measure of spacing, amplitude, and pipe diameter. Two correlation plots were developed, for projections and grooves. These show distinct regions which are shown to delineate geometries where various wall flow processes occur. Predictions can thus be made of friction factor and flow

type given only the roughness system geometry and shape.

TABLE OF CONTENTS

LIST OF FIGURES

CHAPTER I

INTRODUCTION

In pipe flows, very few surfaces approach the ideal friction characteristics as expressed by the Blasius "smooth pipe" formula:

$$f = \frac{0.3164}{N_{Re}^{.25}}$$

Consequently, much effort has been expended to gain knowledge of such flow processes for engineering design purposes. In spite of this effort, not very much is actually understood about the dynamics of flow over rough surfaces, although many empirical relations have been developed. An example is the Moody friction factor chart for randomly distributed, irregularly shaped roughness. This type is also known as sand grain roughness, as pipes roughened with sand grains have been used to approximate its effects. Sand grain roughness seems to be adequately characterized by the mean roughness height, e, usually referenced to the pipe diameter D. Friction factors can thus be estimated given the parameter e/D and the Reynolds number, $\frac{\rho D \bar{U}}{\mu}$.

Another class of roughness commonly encountered is comprised of regularly spaced geometric shapes, such as rods, bars, or sine waves. This roughness is integral with the wall in conduits for purposes of rigidity, or is placed in the conduit for augmentation of heat or mass transfer, which on the large scale is governed by the fluid transport processes.

There are numerous instances where hydraulic roughness is desirable in order to enhance turbulence for transport of mass or heat, as in nuclear reactors or water desalination plants. One might also require the optimum spacing of mine shaft timbers for ventilation and even the proper dimensions for corrugated-wall prosthetic blood vessels. In the latter case it is found that certain geometries are conducive to highly disrupted flow patterns near the walls which may result in hemolysis of red blood cells. An optimum wall configuration is thus desirable on the grounds of adequate strength and physiologically inert flow conditions.

Owing to its complexity of flow, studies of regularly spaced, geometric pipe roughness have mostly been empirical in character, following from the similarity principles of Reynolds and the universal velocity distributions of Prandtl and von Karman for smooth pipes. Clauser (8) was able to show that the velocity shift equations of Prandtl and von Karman applied to rough surface flow in the form

$$\frac{\Delta U}{U_*} = \frac{1}{k}\log \frac{yU_*}{\nu} + B$$

where B is a function of the roughness type.

Sine wave geometries are amenable to analytical approaches, as was shown by Miles (29), Benjamin (2), and Konobeev and Zhavoronkov (23), among others.

Extensions of the phenomenological theory to rough surfaces were also made by Rotta (40), and Worley (60).

In reviewing the literature on the roughness problem, it becomes apparent that there is no general way by which roughness patterns may be uniquely described, so that a correlation corresponding to the Moody friction factor charts can be made which relates friction effects, Reynolds number, and geometric parameters. Also lacking is an understanding of which geometric variables are important to the several flow processes which are known to occur over large-size pipe roughness, as reported by Morris (32), May (28), Knudsen and Katz (20) and others. Accordingly, the problem of this paper may be stated: "Can the friction factor be predicted, given only the geometry of the system and the Reynolds number?"

The roughness type considered in this work is composed of two-dimensional periodic waveforms which are tranverse to the flow direction in fully rough pipes. In analyzing or even attempting to represent such roughnesses, a basic problem lies in the number of dimensions which are required to describe them. By contrast, all microscopic or sand-grain roughnesses can be said to be similarly distributed with respect to a normal distribution of amplitudes, so that their overall dissipative processes near the wall are similarly normal and need only a mean amplitude for description. Two-dimensional periodic waveform roughnesses have additional parameters of wavelength and shape which must be considered, as well as dimensionless combinations of geometric lengths, since several combinations of shape, size and spacing may give the same overall friction effect. Any systematic method for representing this type of roughness has heretofore been lacking, so the only options left to the engineer dealing with such flows have been to use the particular sizes for which extensive friction data are available, as in the case for corrugated metal pipes (34), or to take the data himself.

This study presumes to offer a rationale by which two-dimensional periodic pipe roughness is categorized such that each roughness system consisting of a pipe diameter, amplitude, and wavelength can be assigned a solely geometric parameter which gives it a unique identity. Using this parameter as a base variable, a modified Darcy friction factor is crossplotted to give a universal correlation whereby the friction factor for virtually any shape of two-dimensional roughness can be predicted. This correlation shows how such roughness must be divided into two major groups called projections and grooves, according to the flow processes which occur near the roughness. Five distinct flow processes are shown to be outlined by the resulting correlation graphs.

CHAPTER II

REVIEW OF PREVIOUS WORK

A review of previous work is necessary for an introduction and background in flow over rough surfaces. An annotated summary and review of those works pertinent to this study will be given, with emphasis on works that have recently appeared. Previous work has progressed along lines of extensions of the similarity laws of Prandtl and von Karman, adaptations of the mixing length theories, and recently, analytical investigations which have arisen from wave theory.

Semi-empirical

Several good reviews of roughness literature and associated equations are available, such as those of Worley (60), Robertson, Burkhart, and Martin (38), Liu, Kline, and Johnson (26), and Chapters 19 and 20 of Schlicting (45).

By the 1950s, it had been well established that roughness effects were localized near the wall region, and that velocity correlations of the form

$$\frac{U}{U_*} = A + B \log \frac{yU_*}{\nu} - \frac{U_o - U}{U_*}$$

would apply, both for smooth and rough pipes, where A and B were nearly universal constants and $\frac{\Delta U - U}{U_*}$ was a function of the particular surface. The problem lay in determining this quantity for any given roughness.

Several researchers, Morris (32) for example, found that the friction factor curves could be compressed over the range of Reynolds numbers by functions of the form

$$\phi = \frac{1}{\sqrt{f}_{rough}} - \frac{1}{\sqrt{f}_{smooth}} ,$$

which, when plotted versus a "roughness" Reynolds number $\mathbb{R}$

$$\mathbb{R} = \frac{U_* \lambda}{\nu} = \frac{N_{Re} \cdot \sqrt{f}}{D/\lambda} \cdot \frac{1}{\sqrt{8}}$$

would yield graphs which showed that similarity existed among roughnesses of the same shape, as shown in Figure 1.

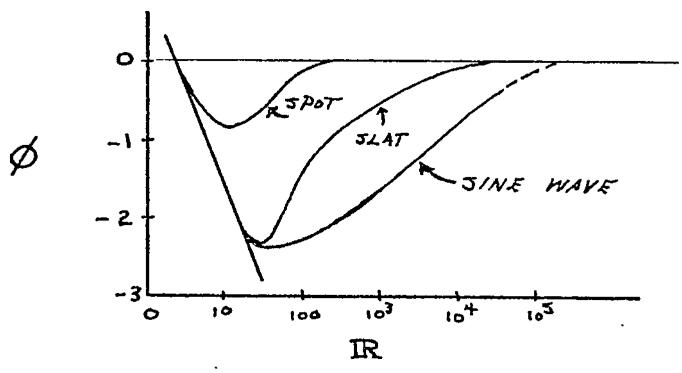

FIGURE 1

Here, the roughness spacing is the predominant length in correlation.

Velocity shift functions were also developed by Clauser (8) and Hama (15) which were universal for several roughness types, and were correlated on the basis of equivalent sand-grain height for each roughness type.

The most widely-used relation of engineering application that has been available is the friction factor chart of Moody (31) which is a summary of friction factors for all pipe flows over random roughness or sand-grain type which can be described by the single length parameter e/D.

Mechanistic

Recent works have attacked the roughness problem with a more intensive look as to the roughness mechanism.

Perry and Joubert (36) took Clauser's form of the logarithmic velocity distribution for roughness

$$\frac{U}{U_*} = \frac{1}{k} \log_e\left(\frac{yU_*}{\nu}\right) + A - \frac{\Delta U}{U_*}\left\{\frac{kU_*}{\nu}\right\},$$

and expressed it as

$$\frac{U}{U_*} = \frac{1}{k} \log_e\left(\frac{yU_*}{\nu_e}\right) + A ,$$

where

$$\frac{\nu}{\nu_e} = \exp\left(k \frac{\Delta U}{U_*}\left\{\frac{kU_*}{\nu}\right\}\right)$$

where the brackets denote a functional dependency. This amounts to shifting the smooth wall friction factor curve to the right by log ν_e/ν . If one then has friction factor data, one can read off values of $\Delta U/U_*$ for all values of Reynolds number. There are those roughness forms, however, whose friction effects (e.g., stable vortices) are independent of Reynolds number and render the above method invalid.

Perry, Schofield, and Joubert (37), recognizing that different flow regimes existed, used square bars to produce two categories of roughness, "k" type and "d" type. Flow in the "k" type consisted of vortices shedding from the cavity, and the "d" type contained captive vortices in the roughness cavities. It was found that a shift downwards, ϵ, from the roughness crest height would correlate the velocity profile data over a wavelength according to the expression

$$\frac{U}{U_*} = \frac{1}{k} \log_e \frac{\epsilon U_*}{\nu} + C$$

where for the "k" roughness, $\epsilon \propto k$, and for the "d" roughness, $\epsilon \not\propto k$. C is a constant for a given roughness shape. However, as in all such velocity shift expressions, U_* must be obtained in each case by experiment.

Betterman (3) found that the intercept C of the velocity shift function

$$\frac{\Delta U}{U_*} = A \log_{10} \frac{kU_*}{\nu} + C ,$$

where k is the sand-grain roughness height, could be correlated for boundary layer flows as summarized in the following diagram (from Dvorak (12)),

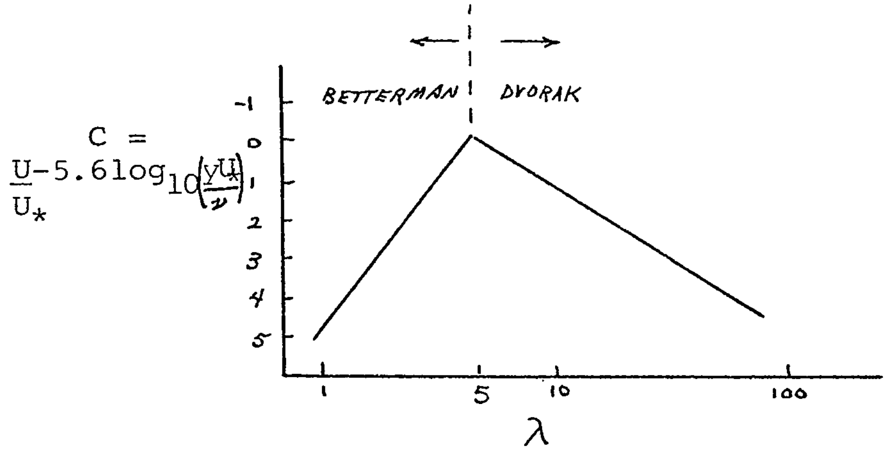

where $\lambda = \dfrac{\text{total surface area}}{\text{roughness area}}$

for the fully rough regime in zero pressure gradient. The sand-grain roughness height k must be obtained from correlations for specific roughness types.

Dvorak (12) extended Betterman's correlation to the roughness density $\lambda > 5$ and this is also shown above. Two distinct linear regions are clearly seen, and these meet in a discontinuity.

Dvorak also extended this correlation to small pressure gradients by the use of a momentum integral equation and a shape factor equation. The resulting expression seems to work well for small or zero pressure gradients.

May (28) constructed thirty-two rough pipes of different periodic rectangular roughness geometries and measured friction factors over each. Substantiating the earlier speculations of Morris (32), May concluded that five flow regimes existed near rough surfaces, which he classified as follows:

<u>Description</u>	<u>Quantifying Criteria</u>
Smooth turbulent	$1/\sqrt{f} = 2 \log_{10} N_{Re}\sqrt{f} - 0.8$ (Prandtl-von Karman)
Normal turbulent	$\frac{\Delta U}{U_*} = \frac{1}{k} \log_e (R_o/y)$
Stable vortex (Morris' "quasi-smooth")	$P/A \lesssim 1.15$
Unstable vortex	
Quasi-stable	$1.15 < P/A \lesssim 8$
Hyperturbulent	$\frac{\Delta U}{U_*} = \frac{1}{k} \log (y/\lambda) + 8.5$
Isolated roughness	$8 < P/A \lesssim 200$

The terms P and A are defined as shown below.

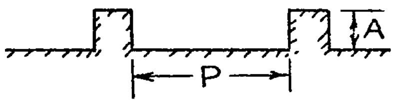

May's analytical approach is interesting in that the mechanisms of the two vortex regimes were derived based on gross assumptions of the dynamics of the vortices that exist in such flows. Also, geometric criteria are given to characterize each type of flow. The data are shown to correlate well with the semi-empirical expressions derived.

Yost (62), in a study of two-dimensional turbulent channel flow over a large-scale sawtooth roughness, measured mean velocity components very close to the roughness elements. By a momentum balance of the terms of the turbulent Navier-

Stokes equations, he showedthat the mean momentum convection terms $U_i \frac{\partial U_i}{\partial U_j}$ were of considerable importance close to the rough surface ($2y/D_o < 0.2$) and that the time-dependent terms contributed somewhat, indicating that some unsteady process takes place and that the momentum equations were balanced when averaged over a wavelength of roughness. This means that any consideration of energy effects, such as represented by the friction factor, must be wavelength-averaged.

Robertson, Burkhart, and Martin (38) showed, as Schlicting had done (44), that a maximum roughness effect occurred in the parameter k/ϵ , when plotted against a roughness density defined as

$$F = \frac{\text{(projected area of roughness on plate normal to flow)}}{\text{(unoccupied plate area)}}$$

as shown in Figure 2. Different maxima exist for rounded and slat type roughness.

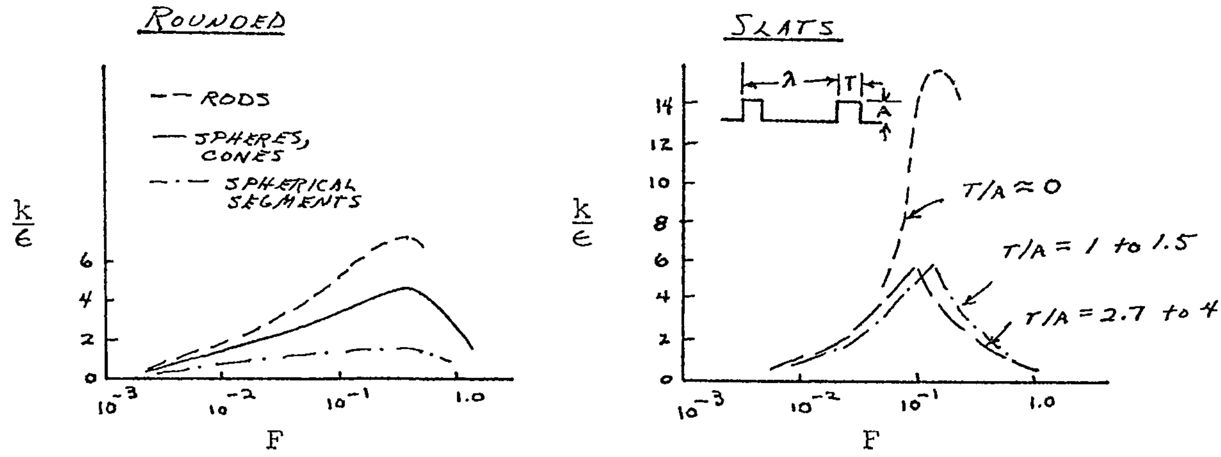

FIGURE 2

A number of investigators have used a roughness height $e^+ = \frac{e}{D} N_{Re} \sqrt{f/2}$ to correlate Stanton number data for heat transfer over rough surfaces. Among these are Dipprey and Sabersky (10), Sheriff and Gumley (46), and Sutherland (54).

Burck (4), (5) used a roughness height $e^+_{sg} = \frac{k_{sg}}{D} N_{Re} \sqrt{f/2}$ to correlate heat transfer data where k_{sg} is the equivalent sand-grain roughness height.

Webb, Eckert, and Goldstein (63) correlated friction factors for square-rib roughness by the empirical relation

$$u^+_e \left(\frac{\lambda}{e}\right)^{-.53} = \phi\ (e^+) \qquad 2.1$$

where $u^+_e = \sqrt{2/f} + 2.5 \ln\left(\frac{2e}{D}\right) + 3.75$. The function u^+_e was developed by Nikuradse (64) to correlate his sand-grain roughness data. Equation 2.1 is apparently valid only for square rods where the spacing is large compared to the amplitude. The authors argue against the feasibility of a single correlation for all roughness geometries.

It is observed that most of the friction factor correlations are based upon a measure of the roughness height, e, which conforms to the idealized sand-grain concept. The roughness height does not afford a unique representation of roughness geometry. Moreover, the roughness height is often compounded with a friction factor or wall shear velocity U_*.

Some degree of correlation is thereby assured since both abscissa and ordinate are functions of the same variables. Such correlations cannot be used for prediction purposes and serve only to correlate the data.

Phenomenological

By using an extension of Boussinesq's eddy viscosity approach to calculating total shear stress in turbulent pipe flows, Worley (60) added a roughness eddy viscosity term so that the total shear stress is

$$\tau g_c = (\eta + \varepsilon + \varepsilon') \frac{d\bar{U}}{dy} \qquad 2.2$$

The eddy viscosity was calculated from the Gill and Sher (14) equation

$$\frac{\varepsilon}{\nu} = k^2 \, y^{+2} \, (1-\exp(-\phi y^+/y^+_{max}))^2 \, \frac{dU^+}{dy^+} \qquad 2.3$$

By assuming a linear shear stress distribution and substituting equation 2.3 into 2.2, a differential equation results

$$dU^+ = \left[\frac{-(1+\varepsilon'/\nu) + \sqrt{(1+\varepsilon'/\nu)^2 + 4CD}}{2C}\right] dy^+ \qquad 2.4$$

where $C = k^2 \, y^{+2} \, (1 - \exp(-\phi y^+/y^+_{max}))^2$

$D = 1 - y^+/y^+_{max}$.

Having this expression, Worley found that there exists an ε for a velocity profile and pressure drop such that a universal correlation can be given of the form $\frac{\varepsilon'}{\nu} = A(Re)^b (f)^c$

where A,B, and C are universal constants, independent of roughness type. Unfortunately, one must have some method of predicting the pressure drop before a velocity profile can be obtained by integrating equation 2.4.

Analytical (sine wave roughness)

As a sinusoidal boundary is a nearly ideal roughness form from the point of view of ease of representation, it is not surprising that a large amount of literature is devoted to it. Also, because of its analyticity, it has lent itself to some interesting theoretical approaches. As such, it will command a section of its own in this report.

A number of investigators have measured friction factor data over sine wave roughness in pipes, including Motzfeld (33), Stanton, Marshall and Houghton (49), Gibson (13), Streeter (52), Morris and Straub (51), Webster and Metcalf (58), Chamberlain (6), and Konobeev and Zhavoronkov (23).

Morris (32) seems to have been the first of these to note the variety of flow effects which occur over sinusoidal, and indeed, all roughness forms. He recognized that all the combinations of parameters were important, such that $f=\phi(N_{Re}, A/D, \lambda/D, S/D)$. He states that the friction effect is due to viscous dissipation and form (pressure) drag which is caused by large-scale vorticity produced behind each roughness element. This vorticity interacts with the elements to the extent that three distinct flow processes exist.

1. Isolated roughness flow--the elements are spaced far enough apart so that the separated flow region reattaches before the next roughness element is encountered. The proper descriptive index is λ/A.

2. Wake interference flow--the wake is unstable and interacts with the downstream element. The proper index is D/λ .

3. Skimming flow--stable vortices exist in the cavities formed by the elements such that the mean flow is not disrupted and "skims" over the roughness. The proper index is λ/T.

Friction factor relations are derived for each type, and a correlation on the basis of a roughness Reynolds number is presented for sinusoidal roughness, which is designated as a representative geometry for wake interference flow. No criteria are given, however, to distinguish which of the three flow types will prevail for a given size and spacing.

The origin of theoretical analyses of sinusoidal waves is to be found in the works of Lamb (24), Wuest (61), and Lock (27), and formed the bases for the later work of Miles and Benjamin.

Kapitsa (18), in a pioneering work on films, analyzed the structure of moving interfacial waves by solving linearized equations of motion and continuity for a falling film to predict the velocity, wavelength, and frequency of interfacial waves.

The interest here in these and the following wave models is for the case where the boundary velocity is zero, which is equivalent to a solid, rigid roughness.

Miles (29) formulated a mechanistic model for flow over a wavy boundary, such that the boundary introduces a perturbation to the two-dimensional linearized equations of motion. Equations for the pressure and shear stress were derived and phase relations shown to exist between these stresses and the boundary profile. Such stresses out of phase with the boundary would contribute to the growth of waves at a gas-liquid interface.

Benjamin (2) expanded Miles' approach and achieved a slightly better approximation to the problem by the use of orthogonal curvilinear (sinusoidal) coordinates. Like Miles, he found certain phase relationships between the wall stresses and the boundary profile which were equivalent to effects observed in such flows, as for example, separation, where the pressure profile is out of phase with the boundary (disturbance). The Miles-Benjamin models are valid only for laminar of "quasi-laminar" flows of an inviscid fluid and for waves of small amplitude-to-wavelength ratio.

Davis (9) has extended the models of Miles and Benjamin to predict wave-induced turbulence stresses as well. Numerical solutions of the linearized turbulent Navier-Stokes equations were made with the conclusion that such models are inadequate to describe turbulent flows, since no conclusive verification of the adequacy of the Miles-Benjamin theory could be made with existing data.

Konobeev and Zhavoronkov (23) present an interesting approach to the analysis of flow over a sinusoidal boundary. They assume that the mean velocity streamlines follow the boundary (potential flow) and are exponentially damped as the distance from the wall increases. The pressure loss due to these velocity gradients is evaluated at the wall as a function of wavelength (λ) and amplitude (A). The total wall shear stress is then taken to be the sum of the smooth wall viscous dissipation and the contribution from the wall pressure profile when integrated over a wavelength, as

$$\tau_w = \tau_o + \tau = f_o\left(\frac{\rho \bar{U}^2}{8}\right) + \frac{1}{\lambda}\int_o^{\lambda} P_{y=o}\, dx$$

where τ_o = smooth wall shear stress

$P = P_o - A\,n \cdot \sin nx \cdot e^{-ny} \rho U_o^{\,2}$

U_o = centerline mean velocity.

Friction factor expressions are derived for two cases:

1. long wave roughness-- $f = 1+2.115^2\pi\beta(A/2\lambda)^2$;

2. short wave roughness--$f = 0.123/(\log^2 d/2A)$.

These expressions fit the data but contain empirical constants. The pertinent lengths are A/λ for long wave and D/A for short wave roughness, where D is the pipe diameter. No analysis is provided for roughness intermediate to these extremes, but a parameter $E = \frac{4AD}{\lambda^2}$ is proposed for this intermediate region where all three lengths are important. All the roughness sizes could be grouped by this parameter from observing the flow effects:

long wave-- $.061 < E < .32$

intermediate-- $0.35 < E < .58$

short wave-- $.61 < E < 18.4$

This grouping brings to mind the three roughness categories suggested by Morris (32).

Smith and Tait (48) used Benjamin's model to predict friction factors for seven of Konobeev's long wave geometries which were in the model's range of validity. Benjamin's equation for the viscous pressure (P_v) of a sheltered wave was used with the periodic normal stress component being assumed to lag the boundary profile by 90 degrees. The resulting wall pressure was

$$P_v = -a\, k^{13/3}\, \tau_o^{-5/3}\, \rho^{4/3}\, (U-c)^4\, \phi_1 \phi_2\, \cos(kx-\pi/2)$$

where k = wave number of boundary

U = velocity of fluid

c = velocity of wave.

The wall shear stress

$$\tau_{pv} = -a\ k\ P_v \sin\ (kx)$$

was integrated over an assumed velocity profile and wavelength-averaged to give, in friction factor form

$$\frac{\tau_v}{(U-c)^2} = \frac{1}{2}\ a^2\ k^{16/3}\ f^{-5/3}\ \rho^{-4/3}\ \mu^{4/3}\ (U-c)^{-4/3}\ \phi_1\ \phi_2$$

where ϕ_1 = Benjamin's G function

$$\phi_2 = \left[\int_0^{\infty}\left(\frac{(u-c)}{(U-c)}\right)^2 \exp\ (-k/y)\ dy\right]^2$$

f = smooth wall friction factor.

Their success (from zero to 300 per cent error) in predicting friction factors is significant, but considering the limitations of the model and the assumptions used, may be only fortuitous.

Closure

The foregoing attempts to treat the roughness problem have demonstrated the following:

1. similarity exists between bulk flows over rough and smooth surfaces, as shown by the nearly universal slope of the velocity shift equations and the friction factor correlations of Morris

2. similarity exists for energy dissipation in roughness flows as indicated by Worley's roughness eddy vis-

cosity concept and the law of the wall

3. roughness effects can be correlated by geometric parameters, the most common of which is the sand-grain roughness height.

The above declarations seem to hint at a syllogism that roughness effects could be universally related, regardless of geometric shape. Some means of proving this tantalizingly apparent similarity remains to be found. This seems to have been done only for those roughnesses of the sand-grain type, which can be directly assigned an identifying parameter, e/D.

Miles and Benjamin have shown tractable analytical approaches for sinusoidal waveforms, and the development of faster computers and algorithms using finite difference approximations, such as that by Chorin (7) may eventually provide answers.

The main problem in any case is obtaining boundary conditions, particularly the wall pressure. A correlation based purely on roughness geometry is hence needed so that the circle relating velocity profiles and pressure loss may be broken.

CHAPTER III

CORRELATION OF FRICTION EFFECTS

At the initiation of this work, it was desired to try to discover whether or not some property of pipe flow over rough surfaces could be predicted strictly on the basis of geometry. This proposition gave rise to two basic tasks:

1. finding some means of representing a roughness geometry on some general, rational basis
2. correlating some flow property after establishing this basis.

The scope of this work is limited to two-dimensional periodic roughness in fully roughened pipe flow. A fully roughened pipe is defined as a conduit having a completely rough inner periphery, with the roughness elements set transverse to the flow, as shown below:

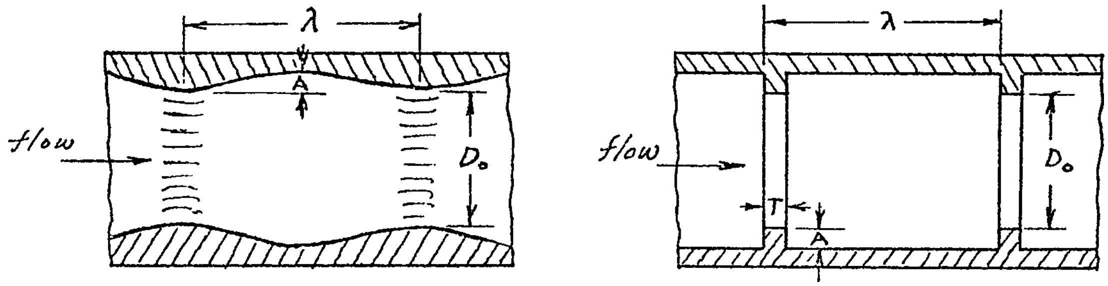

A roughness system will be defined as a conduit of hydraulic diameter D_o, having some roughness as described above of some particular shape with given amplitude A (measured peak-to-peak), and wavelength λ. The diameter is the minimum diameter of the pipe.

Sine wave roughness was considered first, on account of its analyticity, and the existence of a large amount of published friction factor data. The data of Konobeev and Zhavoronkov (23) was particularly appealing as it was measured for a wide range of amplitude, wavelength and diameter combinations, although its veracity was not yet established.

<u>Representation of a roughness system</u>

It was necessary to represent a roughness system on the basis of the minimal number of parameters needed to completely identify a sinusoidal geometry: wavelength, amplitude, and a pipe diameter. Separation of flow was thought to be a significant effect in flows over rough surfaces, so the radius of curvature R, at the roughness crest (

y(x)) was investigated. It is defined as

$$R = \left. \frac{\left[1 + \left|\frac{dy}{dx}\right|^2\right]^{3/2}}{\left|\frac{d^2y}{dx^2}\right|} \right|_{\pi/2} = C \frac{\lambda^2}{A}$$

where $y(x) = \frac{A}{2} \sin \frac{2\pi x}{\lambda}$. When made dimensionless by a characteristic flow length, which is the pipe diameter, the radius of curvature becomes $R = \frac{\lambda^2}{AD}$. Strikingly enough, this is essentially the reciprocal of the parameter $E = 4\frac{AD}{\lambda^2}$ of Konobeev, <u>et al</u>., which was shown to afford some categorization of the flow processes.* This parameter R was later modified to be more unique as $R = \frac{\lambda^2}{\sigma D}$, where σ is the root mean square (RMS) of the amplitude of the roughness waveform when averaged over a wavelength and normalized by its mean η, so that it is defined $\sigma \equiv \left[\frac{1}{\lambda}\int_0^\lambda (y(x)-\eta)^2 \, dx\right]^{\frac{1}{2}}$, where $\eta = \frac{1}{\lambda}\int_0^\lambda y(x) \, dx$. The parameter R becomes very large with increasing wavelength, for $\lambda \gg \sigma, D_o$ and $\sigma < D_o$, which approaches an effectively smooth surface. It becomes very small as $A \approx \lambda$ and $\lambda, A \ll D_o$, which also becomes effectively a smooth surface. Each sinusoidal roughness system can therefore be assigned a fairly unique numerical identity by which it can be represented graphically.

The Darcy friction factor $f = \frac{8 \tau_\omega}{\rho \bar{U}^2}$ was chosen as a flow property to be plotted against R to see if some relationship could be found. The friction factor was chosen as it contains the important properties of pipe flow for engineering purposes and is a familiar concept to all engineers.

---

*It is also noteworthy that an important result of the Miles-Benjamin theory is that the pressure supplied by the flow to the wall is proportional to the curvature of the velocity profile. The velocity is assumed to follow the boundary shape (2).

Correlation of sine wave roughness friction factors

The similarity principles set forth by Reynolds and extended by Prandtl, von Karman and many others in the analysis of fluid flows have shown that the processes may be characterized by the dimensionless physical parameters of importance to the system. The resulting expressions and criteria, such as the universal velocity distributions and dimensionless numbers, apply to any size system. Similarity analysis has thus made it unnecessary to know the exact nature of the fluid processes, but only the dimensions of importance. Were this not so, very little progress indeed would have been made in this field, owing to the complexity of the processes.

For the case of two-dimensional, periodic pipe roughness, two dimensionless quantities, f and R, had been selected to represent, respectively, the flow process and the system geometry. The friction factors were chosen at a Reynolds number of 10^5 so that any Reynolds number effect would be absent for initial considerations. The friction factors for each of Konobeev's roughness systems were then simply plotted against R, resulting in Figure 3a. After much appraisal, certain regularities could be seen, so the friction factors were then succesively modified by various dimensionless conbinations of system dimensions, such as A/λ, A/D_o, λ/D_o, etc., and these

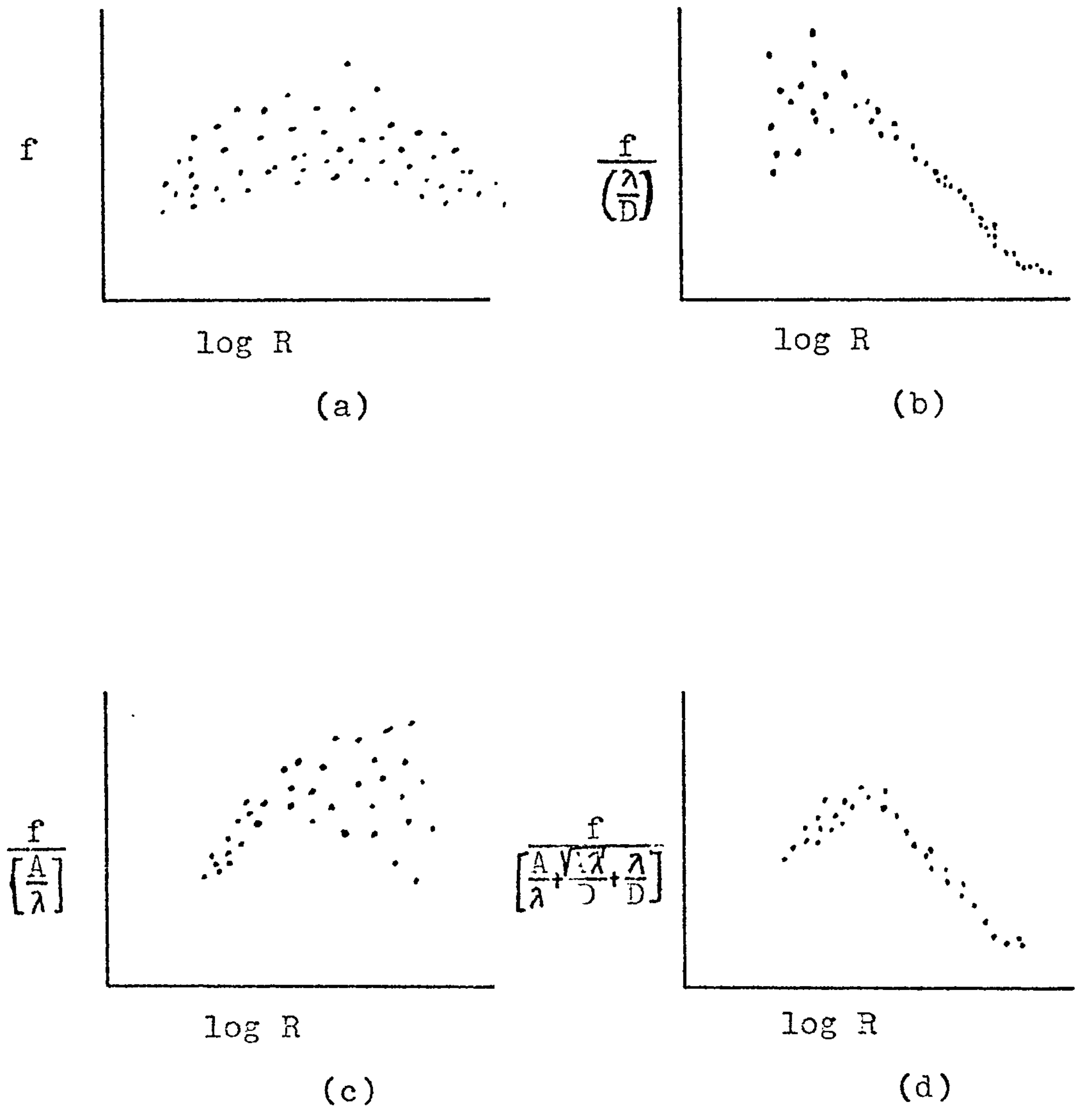

FIGURE 3. METHOD OF CORRELATING FRICTION FACTORS OF SINE WAVE ROUGHNESS

modifications likewise plotted against R. The use of a digital computer and plotting subroutine greatly accelerated the process of testing these combinations. It was observed that the modified friction factors clustered together over certain portions of the R-space as shown in Figure 3b, 3c, and 3d. This was encouraging as it meant that a correlation could be accomplished strictly on the basis of geometry and that f was a viable representation of the friction effect. It was subsequently established that a linear combination of modifying parameters was necessary for correlation to account for the overlap of portions of R-space where the parameters were individually dominant. The combination which produced the best statistical fit for all the data was $\dfrac{f}{[A/\lambda + \sqrt{A\lambda}/D_o + \lambda/D_o]}$. The parameters A/λ and λ/D_o are dominant for small and large values of R, respectively. The combination $\sqrt{\lambda A}/D_o$ was added for the intermediate values of R, where evidently all three dimensions are important.

The resulting correlation for sine wave roughness is presented in Figure 4. The traces of three regions can be discerned and are labeled 1, 2, and 3. These regions will become more distinct as the correlation is extended to all roughness waveforms in the subsequent section. The parameter E of Konobeev is seen to compare approximately to the regions shown in

Figure 4. The obvious conclusion is that friction factor data can be correlated by means of dimensionless combinations of geometrical system parameters.

The correlation procedure also involved a great deal of trial and error. For example, it was not known at the outset which of the dimensions that could properly be called a diameter was the correct one to use. This and other fine adjustments had to come after the correlation had been extended to other waveform shapes. It was found that D_o, the minimum flow diameter, and σ, instead of A, worked best. This was determined by varying one parameter at a time and performing the correlation calculations.

Parametric limits in the correlation

Over the range of the variable R, it is observed that as R becomes small, the amplitude of the roughness is approximately the order of magnitude of the wavelength and each is much smaller than the diameter. The effective roughness approaches a smooth surface and the modifying parameter becomes

$$\lim_{\substack{A \Rightarrow \lambda \\ A,\lambda \ll D_o}} \left[\frac{A}{\lambda} + \frac{\sqrt{\lambda A}}{D_o} + \frac{\lambda}{D_o} \right] \Rightarrow \frac{A}{\lambda} \Rightarrow 1$$

so that the modified friction factor approaches that for a smooth pipe. For large values of R, the wavelength becomes

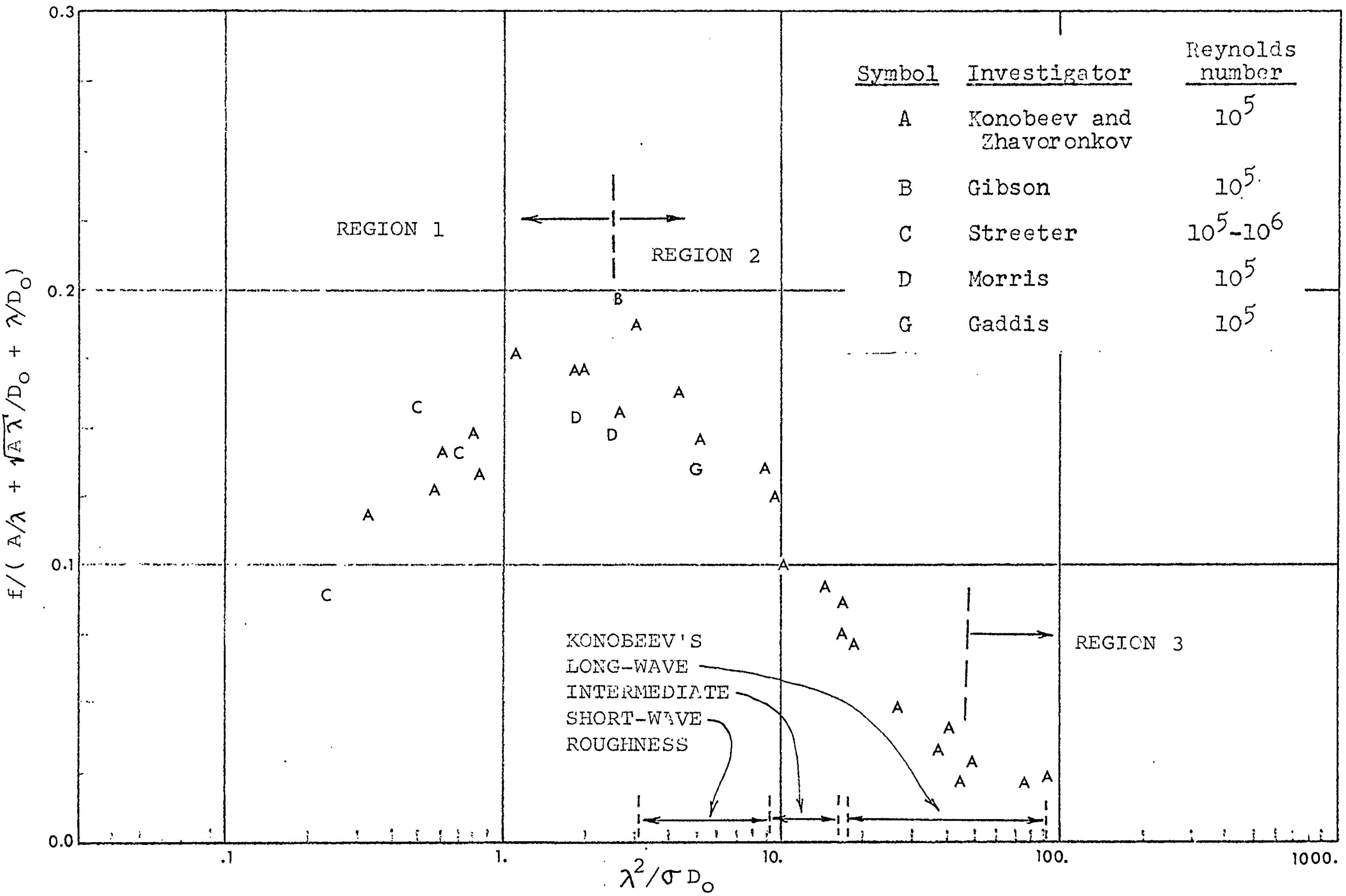

FIGURE 4. FRICTION FACTOR CORRELATION FOR SINE WAVE ROUGHNESS

larger than the diameter and much larger than the amplitude so that no corresponding smooth pipe limit exists for the modified friction factor. It becomes vanishingly small, instead. Although not esthetically pleasing, this is apparently a consequence of using λ/D_o as a modifier, as λ may increase without bound in relation to the diameter. There appear to be no other options, however, as the correlation in this range of R requires λ/D_o as a modifier. Although sine wave data are lacking throughout this range, the validity of the correlation will be strengthened later. The intermediate range of R-space evidently requires the inclusion of the term $\sqrt{\lambda A}/D_o$, implying the dominance of a process characterized by all three length scales. This ratio can also be written as $(\lambda/D_o)/\sqrt{A/D_o}$, which is a combination of the two independent parameters, A/D_o and λ/D_o.

<u>Reynolds number effect</u>

A definite Reynolds number effect on the friction factor was noted for several of the sine wave roughness systems. Data points as $N_{Re} = 10^4$ are shown in Figure 5. Previous points from Figure 4 at $N_{Re} = 10^5$ are shown as boxes.

There is a different Reynolds number effect in very large pipes ($D_o > 10$ inches), in that a maximum friction effect is attained at N_{Re} of 10^6 and higher. Also, the Reynolds number corresponding to this maximum increases as the pipe diameter increases. In smaller pipes, the friction factor either decreases or remains constant as N_{Re} increases. Most data for these large pipes were taken at high Reynolds numbers, mainly because of the difficulty of having the pipe flow full at lower Reynolds numbers. A direct comparison with the small-pipe data thus is not possible except where extrapolations can be made. The extrapolated data of Morris and Straub (51) at $N_{Re} = 10^5$ fit the small pipe correlation.

Also shown in Figure 5 are data taken from a design manual for corrugated pipes prepared by Norman and Bossy (34), which presents data for five different standardized sine wave sizes at a variety of diameters. These are summarized in the following table:

Amplitude	Wavelength	
½"	2 2/3"	
1"	6"	all for
2"	6"	
1"	3"	$1' \leq D_o \leq 20'$
2½"	9"	

The Darcy friction factor had been correlated for a given sine wave size along lines of constant $Q/D^{2.5}$, which is a common design parameter for hydraulic engineers. These data are presented in Figure 5 (Y's and Z's) for two common values of

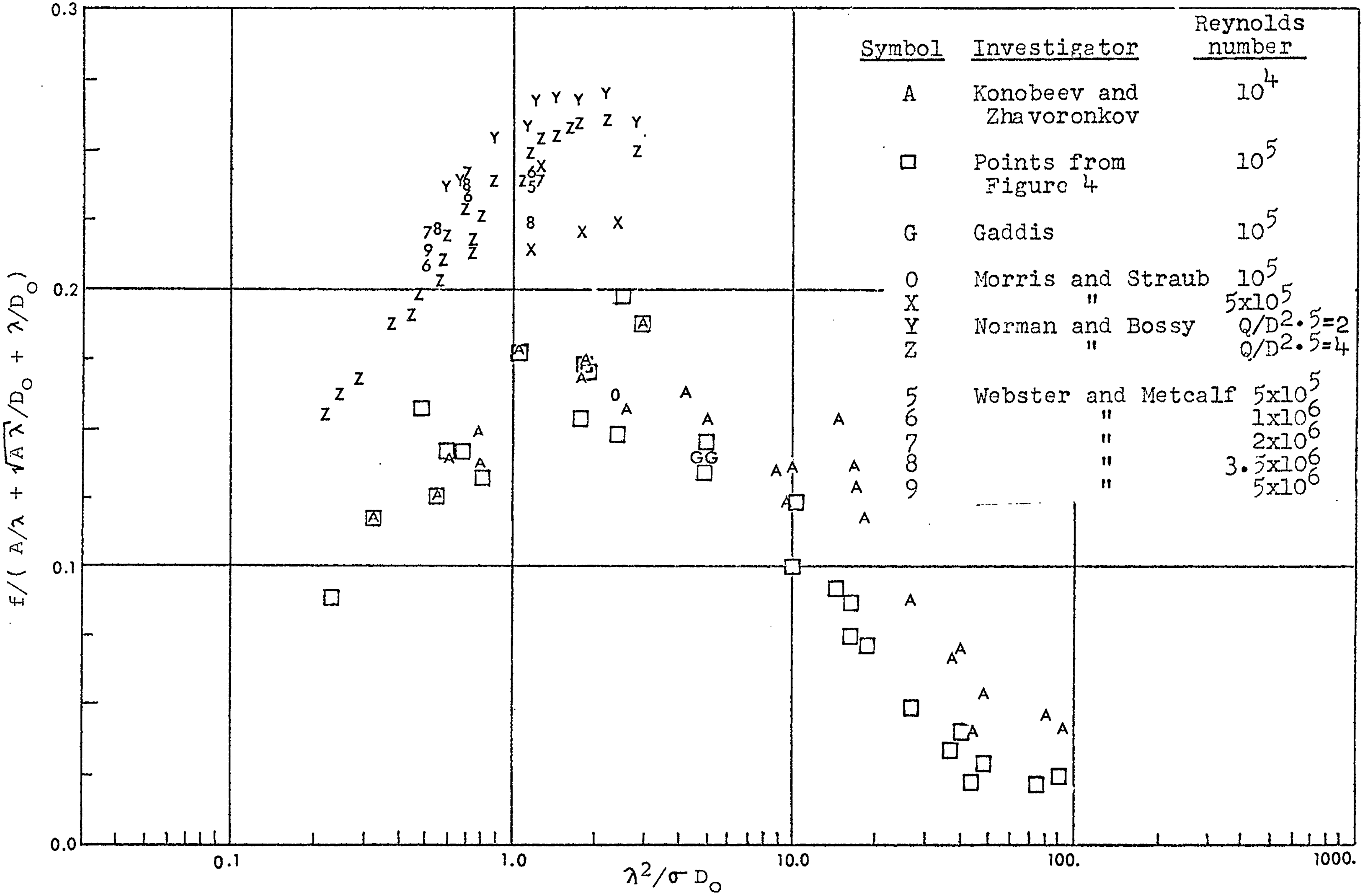

FIGURE 5. FRICTION FACTOR CORRELATION FOR SINE WAVE ROUGHNESS WITH EFFECT OF REYNOLDS NUMBER

$Q/D^{2.5}$, which correspond to the range $5x10^5 < N_{Re} < 5x10^6$.

It is interesting to note that the trend of the curve for smaller diameter pipes is followed, but the large-pipe curve is displaced upwards by an almost constant amount. The friction factor is therefore not general enough to account for such Reynolds number effects in this correlation. There seems also to be a lack of similarity between large and small diameter pipes. Kellerhals (19) compared friction factor data from a 60" diameter, ½" x 2 2/3" size sine wave corrugated pipe to that of a 1/16.6 scale model (D=3.6"). It was found that the friction factor of the scale model reached a lower maximum value at a lower Reynolds number than that of the large pipe. This suggests that dynamic and geometric similarity do not exist between pipes of small and very large diameter. The critical diameter seems to be from 10 to 18 inches, on the basis of the data which have been presented.

Some typical Reynolds number effects on friction factor are shown in Figure 6.

If the discrepancy between flow dynamics of large and small diameter conduits is momentarily ignored, the correlation of Figure 5 can be used with good accuracy to predict friction factors for a very wide range of sine-wave-roughened pipe sizes and a wide range of Reynolds numbers. The error for

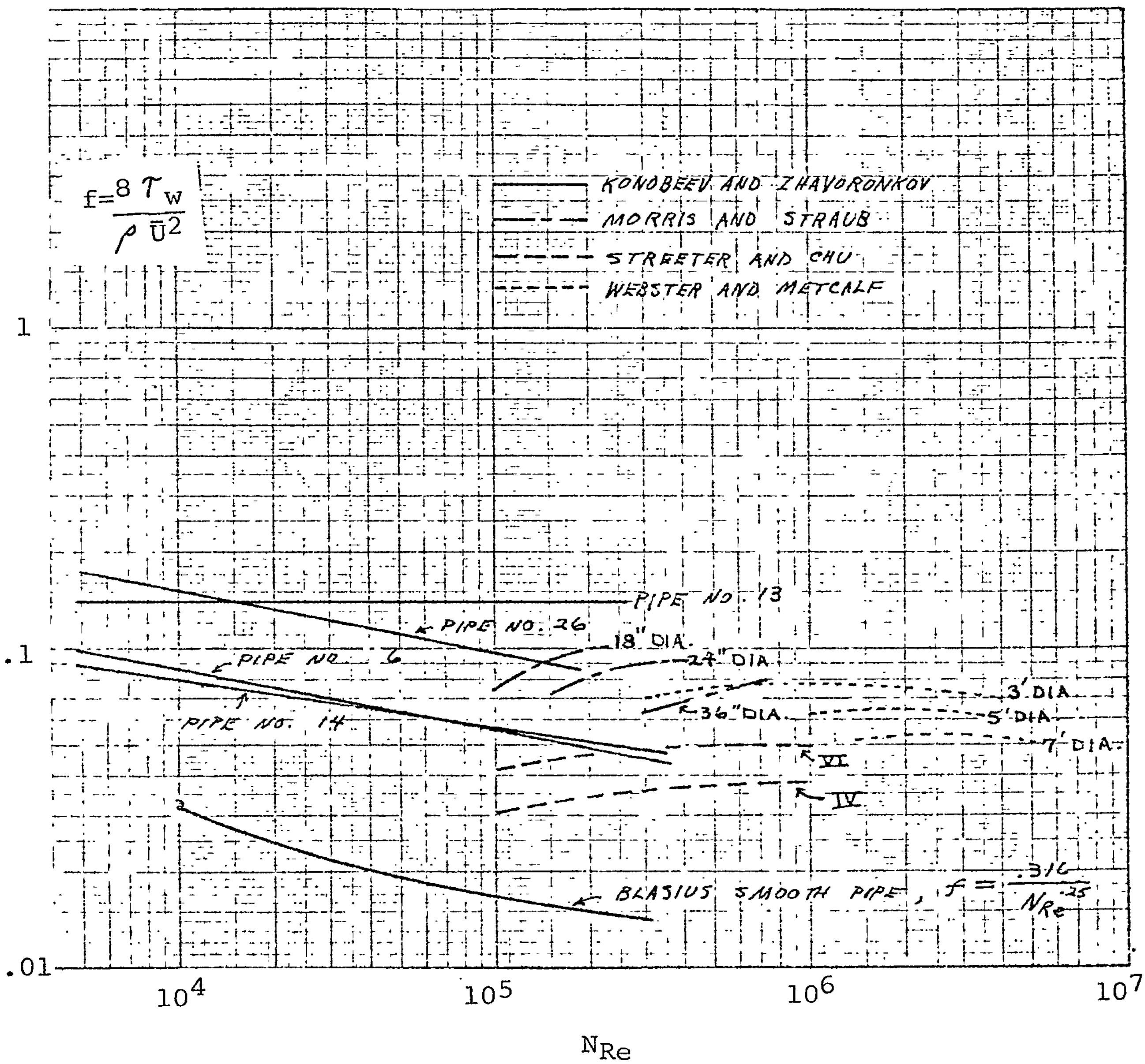

FIGURE 6. FRICTION FACTOR DATA FOR TYPICAL SINE WAVE ROUGHNESS

small pipes is a maximum of ± 25% from the mean, and for large pipes is at most ± 5%. The implication of the regions of the correlation plot will be discussed in Chapter 4.

Extension to other roughness waveforms

A fair degree of success has been obtained in correlating sine wave roughness on the basis of geometry, notwithstanding the high-Reynolds-number effect in large pipes. It was logical to desire to extend this correlation to roughness waveforms of other shapes, for which a plenitude of data were available. Such an extension would not only strengthen the correlation, but serve to prove the existence of similarity of friction effects for roughness of different shapes.

The method of attack was to use the sine wave as a reference waveform, and relate friction factor data for other waveforms to it. It was necessary as a consequence to find some flow property which could be directly related to the waveform of the boundary. This referencing approach requires that the modifying parameters A/λ, $\sqrt{A\lambda}/D_o$, and λ/D_o be universally valid.

The crosscorrelation coefficient

In communications theory, it is often necessary to compare one waveform with another for purposes of assessing its information content. This may involve extracting a signal from noise or comparing the power of one signal with another. This is done by an averaging procedure called correlation. A cross-correlation coefficient $R_{12}(L)$ may be defined for two waveforms $F_1(x)$ and $F_2(x)$, here taken to be periodic with phase difference L, as follows (25):

$$R_{12}(L) = \frac{\langle (F_1(x+L)-\eta_1)(F_2(x)-\eta_2)\rangle}{\sqrt{\langle (F_1(x+L)-\eta_1)^2\rangle \langle (F_2(x)-\eta_2)^2\rangle}} \qquad 3.1$$

The mean η_i is the average of $F_i(x)$ over a wavelength λ. The variance $\sigma_i = \langle (F_i(x)-\eta_i)^2 \rangle^{\frac{1}{2}}$ is the root mean square average of $F_i(x)$ about its mean. The brackets $\langle\rangle$ denote averaging over a statistically significant interval, which here is a wavelength. The average is defined as

$$\langle g(x)\rangle \equiv \frac{1}{\lambda}\int_0^{\lambda} g(x)\ dx.$$

The crosscorrelation coefficient $R_{12}(L)$ in equation 3.1 is normalized with respect to the mean and variance of its component functions, which centers each waveform about its mean and makes $R_{12}(L)$ independent of wave amplitude. Normalization sets the bounds for $R_{12}(L)$ so that

$$-1.0 \leq R_{12}(L) \leq 1.0 \ .$$

The autocorrelation coefficient (for $F_1(x) = F_2(x)$) is

$$R_{11}(0) = 1.0 \ .$$

The crosscorrelation coefficient is thus potentially useful as a modifying factor to relate two quantities which are thought to be linked by their shapes. As a multiplier, it should necessarily always be positive to give a meaningful, non-zero product when compounded with positive physical quantities.

It is found that the friction factors for pipe flow over two different wall waveforms can be related by the crosscorrelation coefficient of the wall waveforms, as

$$\frac{\langle f_1 \rangle}{\langle f_2 \rangle} = R_{12}(L) . \qquad 3.2$$

Hence, if $\langle f_1 \rangle$ corresponds to the wavelength-averaged friction factor for flow over a sine wave wall roughness $F_1(x)$, one need only multiply the friction factor $\langle f_2 \rangle$ of an arbitrary roughness waveform $F_2(x)$ by their crosscorrelation coefficient and the friction factors are universally related. This means that, with regard to the correlation presented previously for sine wave roughness, if the friction factor $\langle f_2 \rangle$ is modified as $\dfrac{\langle f_2 \rangle \cdot R_{12}(L)}{[A/\lambda + \sqrt{A\lambda}/D_o + \lambda/D_o]}$ and plotted versus $\dfrac{\lambda^2}{\sigma D_o}$, it will coincide with the cluster of points delineated by the sine wave correlation of Figure 4. The factor $R_{12}(L)$ then relates the two friction factors according to their shape. The modifying factor $(A/\lambda + \sqrt{A\lambda}/D_o + \gamma/D_o)$ adjusts the friction factors for the system size, and the parameter $R = \frac{\lambda^2}{\sigma D_o}$ identifies the roughness system. This correlation is given in Figures 10 and 11 and will be discussed in detail in Chapter 4. Equation 3.2 will be derived heuristically in the next section on the basis of some simplistic assumptions about the nature of flow over rough surfaces.

It became evident that this approach was not adequate to correlate friction factors for all the systems considered as the factor $R_{12}(L)$ became negative for some waveforms. These waveforms were closely spaced and had generally lower friction factors than those which would correlate with sine wave roughness according to equation 3.2. Another approach was necessary to account for these waveforms and was developed from the realization that a different flow process was involved which might require different parameters for representation. Morris (32), May (28) and others had shown that several flow processes exist near the wall for different rough surfaces.

It was found that the class of roughness examined in this work was separable into two groups:

1. projection type, which is characterized by a strong interaction between the bulk flow and flow near the boundary

2. groove type, which is characterized by a weak interaction between bulk flow and flow near the boundary.

These definitions will be refined as the development proceeds.

An assessment was made of the flow processes which could occur over the two roughness types. It had to be that some dynamical property of the flow in common with sine wave roughness occurred over projections which in turn could be directly related to the wall shape so that the heuristic equation 3.2 would result. A program of experimentation using a 9" diameter corrugated metal pipe was instituted to explore flow effects near the wall. The results are given in the next section as a basis for the analysis of projection type roughness.

Experimental work

The friction factor embodies only the pressure drop and the velocity as entities which would potentially deviate most from the effect of large-size wall roughness. These quantities were examined in the wall pressure distribution and the velocity behavior near the wall.

Wall pressure profiles had been previously measured for air flow over fixed sine wave boundaries by Motzfeld (33), and Stanton, Marshall, and Houghton (49). Stanton, *et al.* found that the wall pressure distribution was not harmonic with the boundary, but contained substantial second and third harmonics of the wall wave number. Motzfeld's distribution was somewhat similar, but he used only three wavelengths as a test section. It was thought that the flow pattern was therefore not fully developed.

Measurements of wall pressure distributions and flow visualization studies were carried out on a 9" nominal diameter commercial corrugated steel pipe. This equipment is located in the Fluid Mechanics Laboratory of the Chemical Engineering Department of the University of Houston. The observation and measuring section was located 32 diameters from the inlet to ensure fully developed turbulent flow.

The air mover was a Buffalo Forge size 30 MW centrifugal fan which could produce Reynolds numbers from 60,000 to 270,000. Pressure drop data were measured by taking centerline dynamic pressure differences of two Pitot tubes set apart in the pipe so that the tips were positioned over the roughness crests. This method was found to be far less sensitive to longitudinal positioning than measuring static pressure differences from wall taps.

The friction factor was found to be independent of Reynolds number in the range $60,000 < N_{Re} < 270,000$. The longitudinal wall static pressure distributions were measured from 18 static pressure taps set perpendicularly to the wall and uniformly spaced over 1½ wavelengths. The wall pressure distribution was not harmonic with the wall wave, and resembled the distributions of Motzfeld. A comparison of wall pressure distributions is shown in Figure 7.

For flow visualization, a suspension of carbon black in kerosene was painted on an area inside the pipe near the outlet and allowed to be dried by the airstream. The resulting streak pattern left by the carbon black traces is shown in Figure 8 and in Appendix A. An irregular pattern in a space bounded by lines of accumulated carbon black indicates the existence of a separated region, which begins slightly downstream of the roughness crest and reattaches at the trough. No evidence of vortex shedding could be detected, as the carbon black pattern was steady, so it is interpreted that a sheltered unsymmetrical vortex is a characteristic of flow near the boundary for this geometry, and the axial velocity streamlines follow approximately the roughness waveform over most of the wavelength. The results of the above investigations are included in Appendix A.

As a result of these experiments, the quantity which could be related most directly to the wall waveform was found

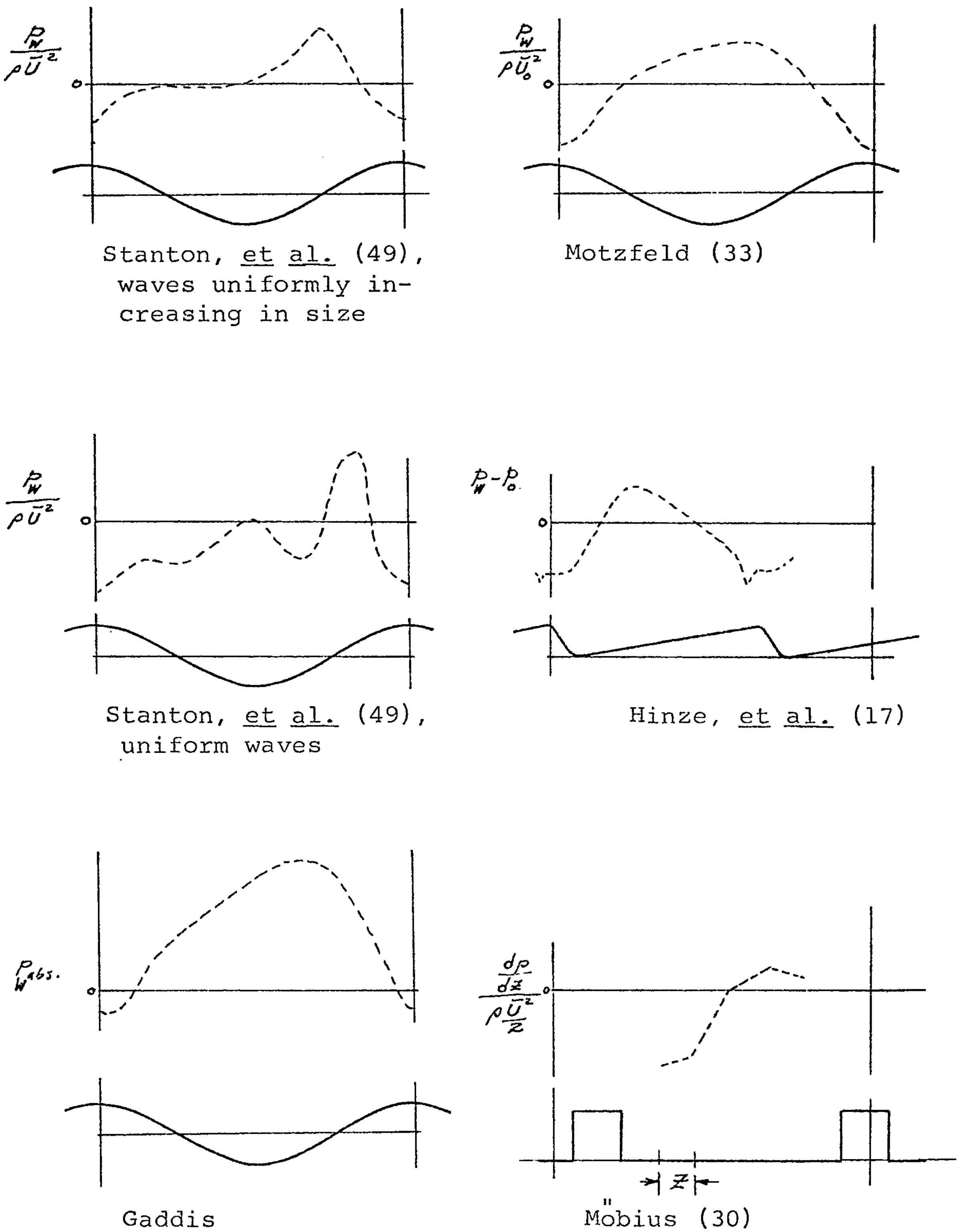

FIGURE 7. WALL PRESSURE DISTRIBUTIONS OVER VARIOUS ROUGHNESS WAVEFORMS

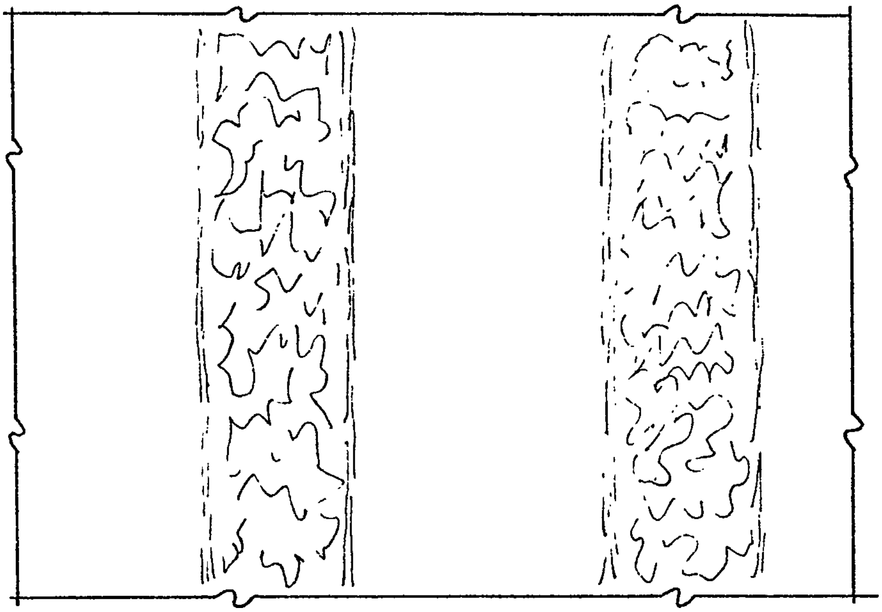

A. TOP VIEW OF VISUALIZATION SECTION

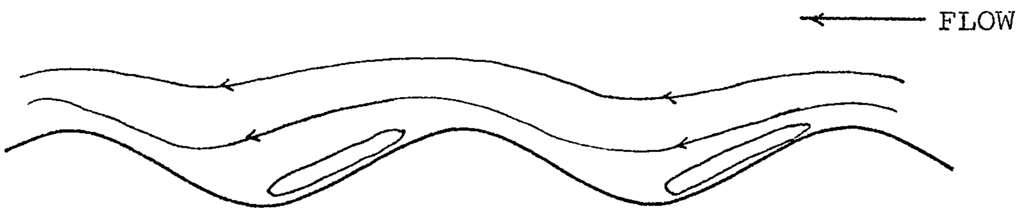

B. IMPLICATION OF VISUALIZATION SHOWN ABOVE

FIGURE 8. FLOW VISUALIZATION AT WALL OF 9" DIAMETER, ½"x2.67" WAVE CORRUGATED PIPE

to be the time-averaged velocity near the wall.* The longitudinal wall pressure distributions presented in Figure 7 have a similarity in that the lowest values occur near the roughness crest and reach a maximum about halfway between the crests. These two observations will be applied in the following analysis of projection roughness.

Analysis of projection type roughness

The friction factor for an arbitrary two-dimensional periodic pipe roughness will be related to that for a sine wave roughness of similar size and hydraulic diameter. The friction factors will be written as a ratio, and the observations made earlier about the wall pressure distributions and velocities will be applied. All other unknown quantities will divide out or become unity in the ratio. The resulting expression will be integrated over a wavelength.

The friction factor was originally defined to be a measure of energy loss due to fluid friction over a length of smooth-walled conduit. When applied to large-size periodic pipe roughness, it is calculated as an average over a discrete number of roughness wavelengths. The friction factor may be

---

*The steady-state velocity at a point in which turbulence fluctuations are averaged out is termed "time-averaged" and is distinct from the time-averaged velocity averaged over a length, which is termed the "average" velocity.

expressed as a local function of the longitudinal direction x, as follows:

$$f(x) = \frac{8 \quad \tau_w(x)}{\rho \; U^2(x,y)} \qquad 3.3$$

where f(x) is the Darcy friction factor,

$\tau_w(x)$ is the local wall shear stress,

U(x,y) is the local time-averaged mean velocity.

The friction factor $f_1(x)$ for roughness waveform $F_1(x)$ will be related to the friction factor $f_2(x)$ for roughness waveform $F_2(x)$ as follows:

$$\frac{f_1(x+L)}{f_2(x)} = \frac{8 \; \tau_{w1}(x+L)}{\rho \; U_1{}^2(x+L,y)} \; \frac{\rho \; U_2^2(x,y)}{8 \tau_{w2}(x)} \qquad 3.4$$

The length L has been included for complete generality to allow for a phase difference in comparing the waveform-related quantities. The individual quantities will now be evaluated and substituted into equation 3.4.

According to Konobeev and Zhavoronkov (23) the normal (y) velocity component U_y may be assumed to follow the boundary and be damped exponentially with the distance from the wall. For a sinusoidal boundary the normal velocity will be

$$U_y = A \sin nx \; e^{-ny} \qquad 3.5$$

From the two-dimensional equation of continuity for the time-averaged mean velocity

$$\frac{\partial U_x}{\partial x} + \frac{\partial U_y}{\partial y} = 0 \qquad 3.6$$

the longitudinal velocity, U_x, is

$$U_x = U_o \left(1 - \Delta n \sin(nx)\; e^{-ny} \right) \qquad 3.7$$

where n is the wave number,

U_o is the centerline velocity,

Δ is the amplitude of the boundary.

It will be assumed that for a generalized function F(x) which has continuous derivatives the velocity is

$$U_x = U_o \left(1 - \quad F(x)\; e^{-ny} \right). \qquad 3.8$$

For some of the roughness shapes in question, Konobeev's method is not strictly true, since the derivatives of F(x) may not yield convergent derivatives for discontinuous waveforms (e.g. orifice type). Nevertheless, it is assumed that the fluid streamlines "smooth out" any discontinuities of the roughness waveform and hence the velocity function near the wall can be written as F(x) in equation 3.8.

Substituting U(x,y) from equation 3.8 into equation 3.4 gives

$$\frac{f_1(x+L)}{f_2(x)} = \frac{\tau_{w1}(x+L)\; U_{o2}^2 (1- \quad F_2(x)\; e^{-ny})^2}{\tau_{w\;2}(x)\; U_{o1}^2 (1- \quad F_1(x+L)\; e^{-ny})^2} \qquad 3.9$$

The fluctuating part $F_i(x)$ of the velocity must be normalized with respect to its mean η_i and variance σ_i. The term $\eta_i U_{oi} \cdot e^{-ny}$ is added and subtracted in equation 3.8 to give

$$U_i(x,y) = U_o(1-\eta_i \cdot e^{-ny} - (F_i(x)-\eta_i)e^{-ny}). \tag{3.11}$$

The velocity can be made dimensionless by dividing the fluctuating term by the variance of F(x) while dividing the unity term by a quantity nearly equal to σ_i, say σ_u, which effectively preserves the order-of-magnitude relationship between the velocity in bulk flow and the velocity near the wall. Also, σ_u must be a universal constant to preserve the relative values of a ratio of velocities, as written in equation 3.9. The resulting dimensionless velocity U_i' is

$$U_i'(x,y) = U_o\left(\frac{1}{\sigma_u} - \frac{\eta_i \cdot e^{-ny}}{\sigma_i} - \frac{(F_i(x)-\eta_i)e^{-ny})}{\sigma_i}\right. . \tag{3.12}$$

The shear stress for circular pipes is

$$\tau_w(x) = \frac{dP}{dx}\,\frac{D_i(x)}{4} \tag{3.13}$$

where $D_i(x)$ is the local diameter of the pipe. The diameter is written

$$D_i(x) = D_o + \underbrace{2F(x)}_{\text{neglect}} \tag{3.14}$$

where the fluctuating part is neglected. D_i is therefore a constant, equal to the minimum diameter across the pipe from roughness crest to roughness crest.

The pressure at the wall can be written as the sum of a term linear in x which is the dissipation from the microscopic wall roughness, and a non-linear term arising from the separation of flow and other friction effects. The functional form of the non-linear term cannot be predicted so it will be assumed to have a similar shape for all roughness types. The pressure profile is then

$$P(x) = px + P_o\, g(x)\, e^{-ky} \tag{3.15}$$

where p is the microscopic ("smooth wall") dissipation,

$g(x)$ is the generalized pressure distribution,

P_o is the pressure amplitude.

Taking the differential of equation 3.15 gives

$$\frac{dP}{dx} = p + P_o\, g'(x)\, e^{-ky}. \tag{3.16}$$

Since, for most of the surface textures encountered, the constant "smooth wall" dissipation is about an order of magnitude smaller than the other term, it will be neglected. Equation 3.16 is

$$\frac{dP}{dx} = P_o\, g'(x)\, e^{-ky}. \tag{3.17}$$

Substituting equation 3.17 into the friction factor ratio equation 3.9 gives

$$\frac{f_1(x+L)}{f_2(x)} = \underbrace{\frac{P_{o1} g'(x) e^{-ky}\, U_{o2}^2}{P_{o2} g'(x) e^{-ky}\, U_{o1}^2}}_{I} \frac{D_1 \left[\frac{1}{\sigma_\upsilon} - \frac{\eta_2 \cdot e^{-ny}}{\sigma_2} - \frac{(F_2(x) - \eta_2) e^{-ny}}{\sigma_2}\right]^2}{D_2 \left[\frac{1}{\sigma_\upsilon} - \frac{\eta_1 \cdot e^{-ny}}{\sigma_1} - \frac{(F_1(x+L) - \eta_1) e^{-ny}}{\sigma_1}\right]^2}. \tag{3.18}$$

Consider the term I in equation 3.18:

$$I = \frac{P_{o1}\ g'(x)\ e^{-ky}\ U_{o2}^2}{P_{o2}\ g'(x)\ e^{-ky}\ U_{o1}^2}. \qquad 3.19$$

It is further assumed that the pressure amplitude P_o is related to the square of the velocity maximum U_o^2 by a universal constant so that

$$\frac{P_{o1}\quad U_{o2}^2\ e^{-ky}}{U_{o1}^2\quad P_{o2}\ e^{-ky}} = 1\ . \qquad 3.20$$

Also, the damping coefficients are assumed to be equal. The friction factor ratio now becomes

$$\frac{f_1(x+L)}{f_2(x)} = \frac{\left[A_2 - \left(\frac{F_2(x)-\eta_2}{\sigma_2}\right)e^{-ny}\right]^2}{\left[A_1 - \left(\frac{F_1(x+L)-\eta_1}{\sigma_1}\right)e^{-ny}\right]^2}. \qquad 3.21$$

where $A_1 = \frac{1}{\sigma_\upsilon} \frac{-\eta_1 \quad e^{-ny}}{\sigma_1}$,

$A_2 = \frac{1}{\sigma_\upsilon} \frac{-\eta_2 \quad e^{-ny}}{\sigma_2}$.

Expanding the square terms in equation 3.21 and multiplying by unity with the factor $\frac{(F_1(x+L)-\eta_1)\sigma_1}{(F_1(x+L)-\eta_1)\sigma_1}$ results in

$$\frac{f_1(x+L)}{f_2(x)} = \frac{\left[A_2^2\left(\frac{F_1(x+L)-\eta_1}{\sigma_1}\right) - A_2\left(\frac{F_2(x)-\eta_2}{\sigma_2}\right)\left(\frac{F_1(x+L)-\eta_1}{\sigma_1}\right)e^{-ny} + \left(\frac{F_2(x)-\eta_2}{\sigma_2}\right)^2\left(\frac{F_1(x+L)-\eta_1}{\sigma_1}\right)e^{-2ny}\right]}{\left[A_1^2\left(\frac{F_1(x+L)-\eta_1}{\sigma_1}\right) - A_1\left(\frac{F_1(x+L)-\eta_1}{\sigma_1}\right)^2 e^{-ny} + \left(\frac{F_1(x+L)-\eta_1}{\sigma_1}\right)^3 e^{-2ny}\right]} \qquad 3.22$$

The third order terms are neglected because the factors $(F_i(x)-\eta_i)/\sigma_i$ are less than one; also there are squared negative exponential terms. Equation 3.22 is cleared of fractions preparatory to being integrated over a wavelength:

$$\frac{1}{\lambda}\int_0^{\lambda} f_1(x+L)\left[A_1^2\left(\frac{F_1(x+L)-\eta_1}{\sigma_1}\right)-A_1\left(\frac{F_1(x+L)-\eta_1}{\sigma_1}\right)^2 e^{-ny}\right]dx \tag{3.23}$$

$$=\frac{1}{\lambda}\int_0^{\lambda} f_2(x)\left[A_2^2\left(\frac{F_1(x+L)-\eta_1}{\sigma_1}\right)-A_2\left(\frac{F_2(x)-\eta_2}{\sigma_2}\right)\left(\frac{F_1(x+L)-\eta_1}{\sigma_1}\right)e^{-ny}\right]dx.$$

The friction factors are now taken as an average over a wavelength and removed from inside the integral. The integration is performed, to yield

$$\langle f_1\rangle\left[A_1^2\overset{\nearrow 0}{\left\langle\frac{F_1(x+L)-\eta_1}{\sigma_1}\right\rangle}-A_1\left\langle\left(\frac{F_1(x+L)-\eta_1}{\sigma_1}\right)^2 e^{-ny}\right\rangle\right]$$

$$=\langle f_2\rangle\left[A_2^2\overset{\nearrow 0}{\left\langle\frac{F_1(x+L)-\eta_1}{\sigma_1}\right\rangle}-A_2\left\langle\left(\frac{F_2(x)-\eta_2}{\sigma_2}\right)\left(\frac{F_1(x+L)-\eta_1}{\sigma_1}\right)e^{-ny}\right\rangle\right], \tag{3.24}$$

where the brackets denote wavelength-integration. It is observed that the first order terms in $F_i(x)$ are zero, and only the second order terms are significant. The factors A_1 and A_2 are nearly equal and can be divided out, as can the exponential terms, to yield

$$\langle f_1\rangle R_{11}(0)=\langle f_2\rangle R_{12}(L) \; . \tag{3.25}$$

This is rewritten as

$$\frac{\langle f_1 \rangle}{\langle f_2 \rangle} = R_{12}(L) \qquad 3.26$$

since by definition, $R_{11}(0) = 1.0$ with the result that $R_{12}(L)$ is the normalized crosscorrelation coefficient between the two waveforms. This is the heuristic equation 3.2. The phase difference L is a consequence of the correlating scheme and must by determined by trial and error in correlating the data. Physically, this means that there is an equivalent effect in the reference (sine wave) pipe and the test pipe if the friction effects are evaluated with respect to a common longitudinal datum as shown in Figure 9. Thus the correlation is made by referencing the friction factor for pipe flow over an arbitrary waveform to that for a sine wave of similar dimensions in the same pipe diameter, D_o.

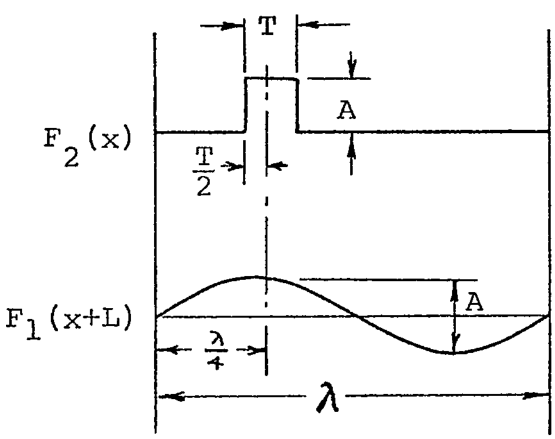

Figure 9

Equation 3.26 actually says that two friction factors are so related regardless of their respective amplitudes. This is a consequence of the definition of the dimensionless velocities made so that a normalized correlation coefficient could be obtained. These were very strong conditions and have removed the dependence on amplitude. Hence, it must be additionally specified that equation 3.26 is true only for friction factors for waveforms of the same amplitude.

The resulting correlation for projection type roughness is shown in Figures 10 and 11. A list of the roughness shapes correlated is given in Table 1. It is noted that the data points of the many investigators represented coincide with the sine wave correlation plots of Figure 5. The data for the large diameter pipes are not represented here. It is emphasized that each point on the graphs represents a roughness flow system of a shape, size, and pipe diameter. The Reynolds number ranges in the legend are those over which the friction factor value is nearly constant.

The validity of the correlation is shown from the diversity of roughness types correlated and the fact that the deviations from the means of the plots appear to be random. A complete listing of the data used and pertinent calculated quantities is given in Appendix B.

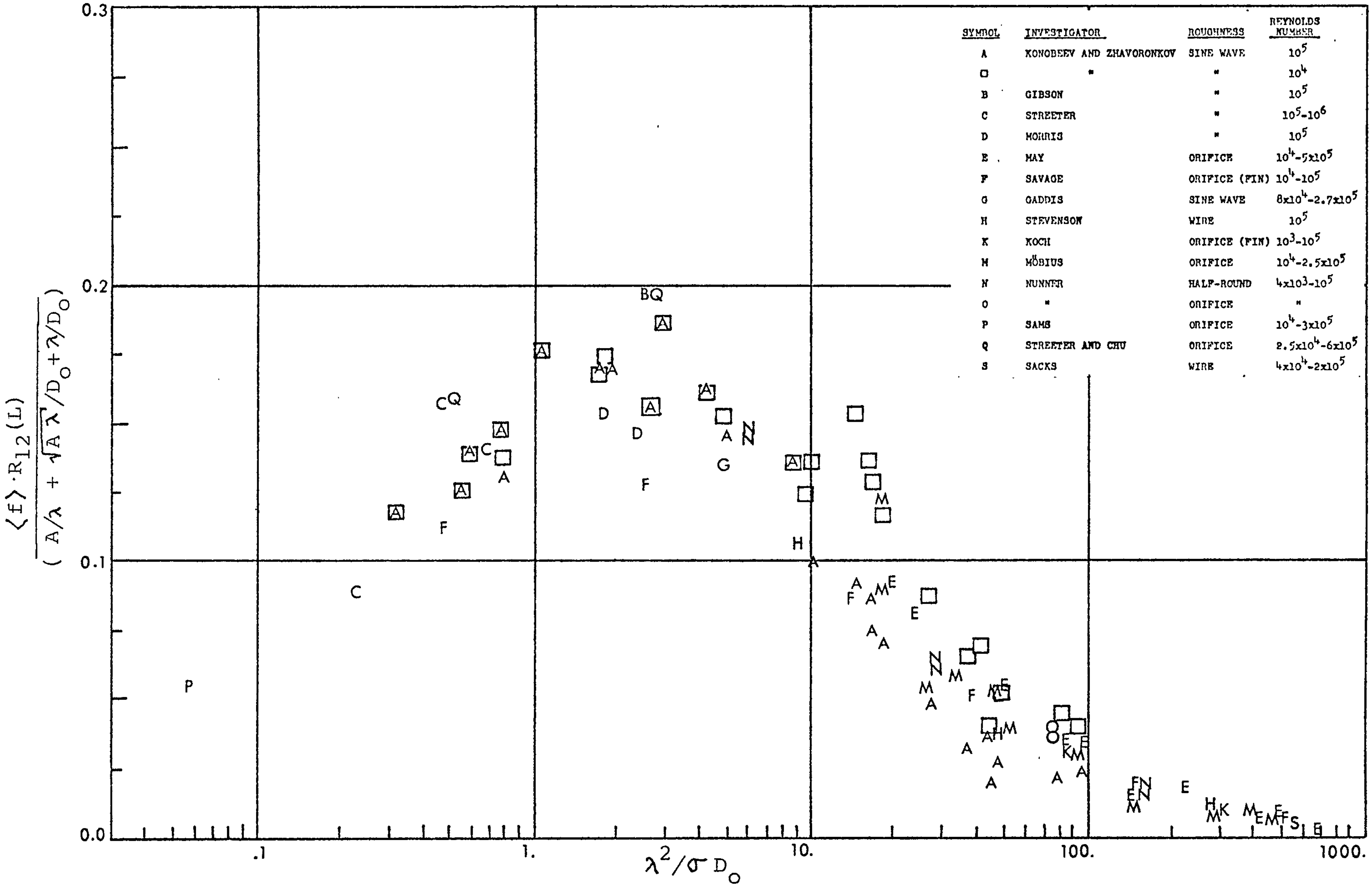

FIGURE 10. FRICTION FACTOR CORRELATION FOR PROJECTION ROUGHNESS ON SEMILOG COORDINATES

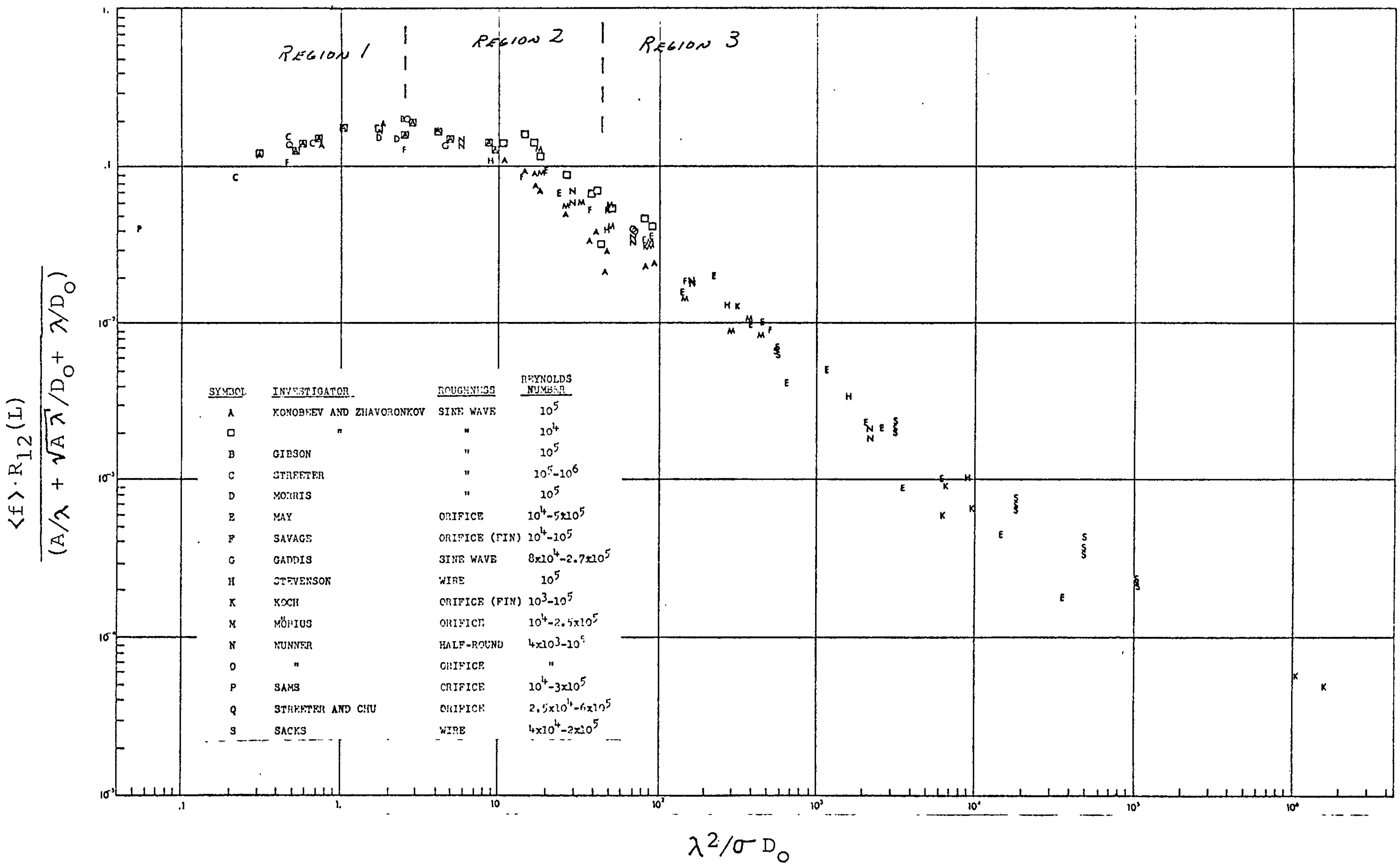

FIGURE 11. FRICTION FACTOR CORRELATION FOR PROJECTION ROUGHNESS ON LOG-LOG COORDINATES

TABLE I

SUMMARY OF ROUGHNESS GEOMETRIES CORRELATED

Investigator and reference	Typical roughness pattern	Pipe cross section	How ΔP was measured
Konobeev and Zhavoronkov (23)		round	not given
Gaddis		round	Δ(dynamic P) at centerline
Streeter (52)	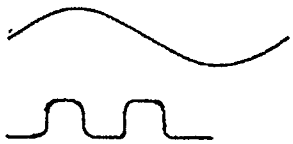	round	static pressure tubes set halfway to centerline
Morris (32)		round	not given
Webster and Metcalf (58)		round	ΔP from static tubes set 6" into pipe
Gibson (13)		round	ΔP from static wall taps at crests and troughs
Norman and Bossy (34)		round	-------
Stevenson (50)		54"x4" rectang. channel	static wall taps
Sacks (41)		round	static wall taps
Nunner (35)	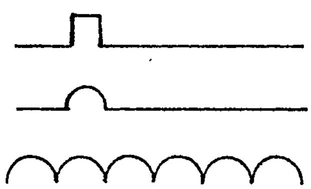	round	static wall ΔP over entire rough section; smooth entrance section

TABLE I (continued)

Investigator and reference	Typical roughness pattern	Pipe cross section	How ΔP was measured
Streeter and Chu (53)		round	static pressure tubes set halfway to centerline
Sams (42)		round	static wall ΔP over entire rough section; no smooth entrance
Koch (21)		round	same as Nunner but isothermal
Möbius (30)		round	wall taps in troughs
May (28)		round	wall taps at crests
Savage (43)		round	static ΔP at centerline
Tripp (56)	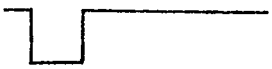	rectang.	not given
Kolar (22)	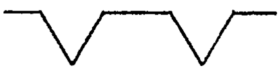	round	wall ΔP over entire rough section; smooth entrance section
Skoglund (47)	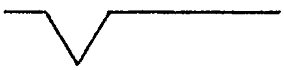	rectang.	wall taps on crests

Reynolds number effects

As a generalization, it can be stated that the friction factor-Reynolds number curves are fairly horizontal for roughness waveforms with discontinuities, i.e. sharp edges as in the orifice type. Those friction factor curves for rounded roughnesses are in general influenced by the Reynolds number, as shown in Figure 12.

Since flow separation is involved, the point of separation is evidently dependent primarily on velocity for rounded waveforms, but is well-defined by the edges of orifice-type roughness.

Groove type roughness

The existence of stable vortices within cavities produced by certain waveforms is well documented by May (28), Knudsen and Katz (20), Perry, et al.(37), Liu, et al. (26), and Morris (32). These processes are very different from those common to projection type roughnesses and require a different analysis for correlation.

This type of roughness has characteristically lower friction factors than the projection type having similar dimensions and was apparently denoted by Morris as producing "skimming flow." Since the roughness elements do not provide

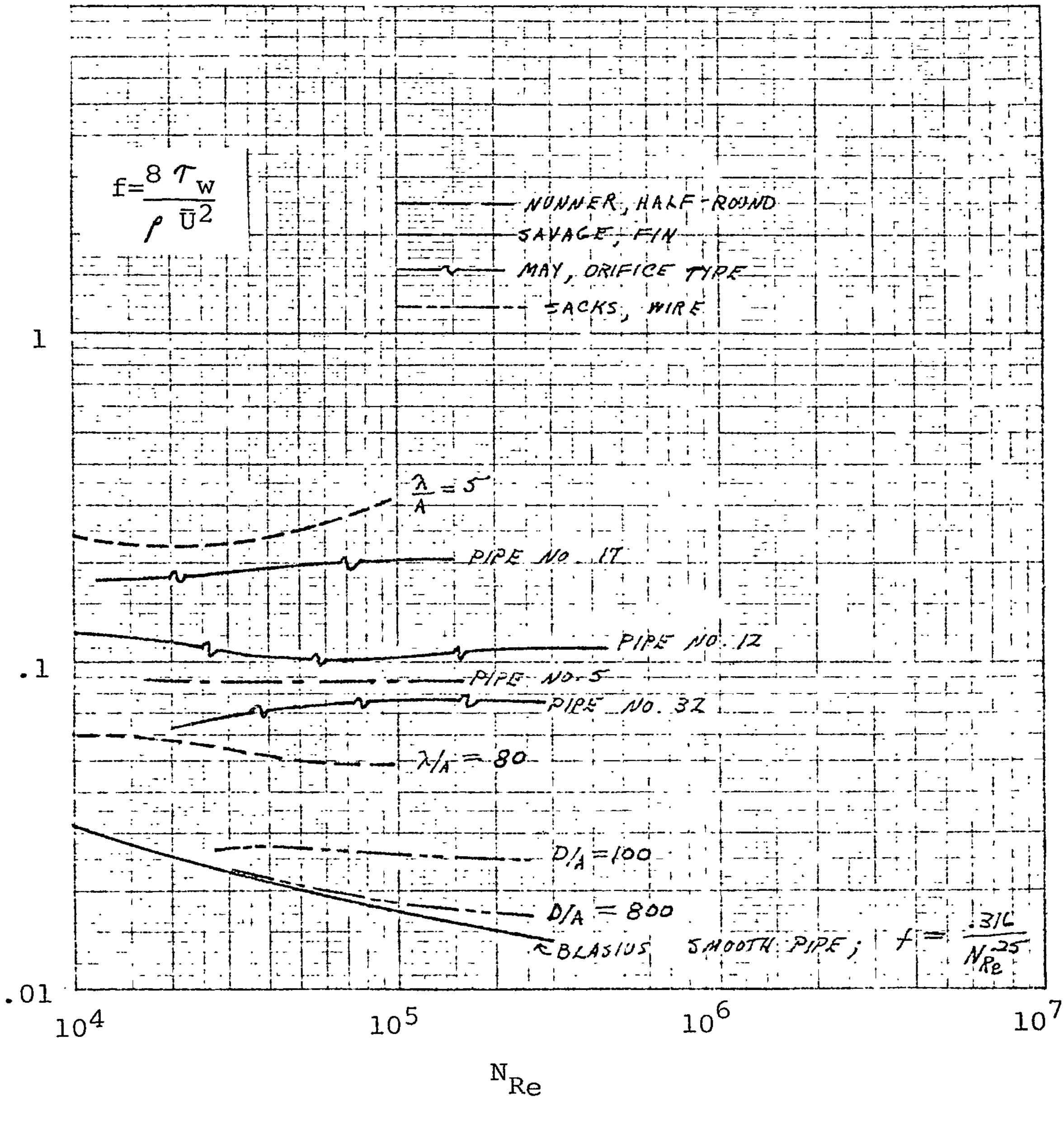

FIGURE 12. FRICTION FACTOR DATA FOR TYPICAL PROJECTION ROUGHNESS

obstacles to the mean velocity streamlines, the only energy loss results from maintaining the vorticity plus the usual viscous dissipation at the wall.

A new problem also arises because the representation parameter $\frac{\lambda^2}{\sigma D_o}$ is not sufficient to characterize this roughness type. The wavelength is no longer a useful parameter, since different friction effects may be produced by waveforms having the same wavelength, as shown below:

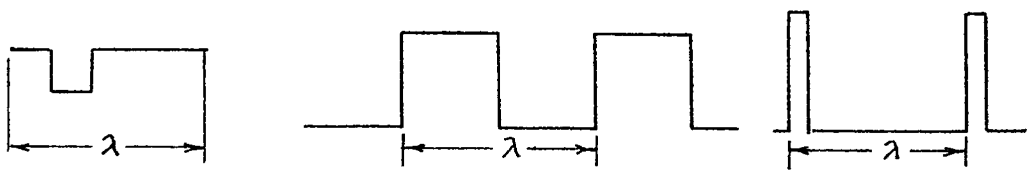

Criteria also had to be developed to distinguish geometries amenable to stable vortex formation from those which have characteristics of projection roughness.

When do projections become grooves?

By examining several waveforms for this type roughness, it is noted that the cavity length P and crest length T are the significant dimensions rather than the wavelength and amplitude. A new classifying parameter $\frac{P^2}{TD_o}$ is created, similar in form to that necessary for projections, except that an amplitude is not included. The dimensions P and T combine to approach smooth surfaces as shown below, where on the one hand P becomes very small in relation to T (widely spaced cavities), and on the other hand P becomes larger than T (widely spaced projections):

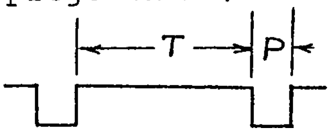

$T > P$ and $P \ll D$

$\frac{P^2}{TD_o} \Rightarrow$ small

approaches smooth surface

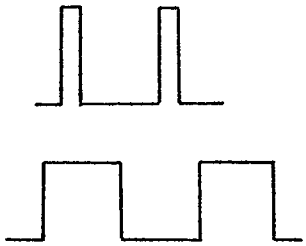

$T, P < D$

$\frac{P^2}{TD_o} \Rightarrow$ intermediate

$T \approx P$ or $\frac{A}{P} \approx 1$

$P \gg T, D_o$

$\frac{P^2}{TD_o} \Rightarrow$ large,

approaches projection roughness

This combination of parameters seemed to afford a fairly unique identity for the waveform types considered, and approached projection roughness as P increased. The limits where the amplitude becomes large (deep grooves) were not considered, as the parameter A seemed not to be important. Such deep grooves have been studied by Atherton and Thring (55) and Knudsen and Katz (20). The effect of amplitude in such cases is to afford containment for several superimposed vortices within the cavity.

Analysis of groove type roughness

The following analysis was conceived from the heuristic analysis for projections, and was used as a basis to correlate friction factor data over groove roughness of different shapes and sizes.

The friction factors for roughness waveforms $F_1(x)$ and $F_2(x)$ are written as a ratio

$$\frac{f_1(x)}{f_2(x)} = \frac{8\,\tau_{w1}(x) \quad \rho U_2^2(y)}{\rho\, U_1^2(y) \quad 8\,\tau_{w2}(x)} \tag{3.27}$$

where $f_1(x)$ is the local friction factor over the reference waveform $F_1(x)$ and $f_2(x)$ is the local friction factor over the arbitrary roughness waveform $F_2(x)$. Now, a new reference waveform is defined as a groove with a sinusoidal half-wave for a cavity as shown below:

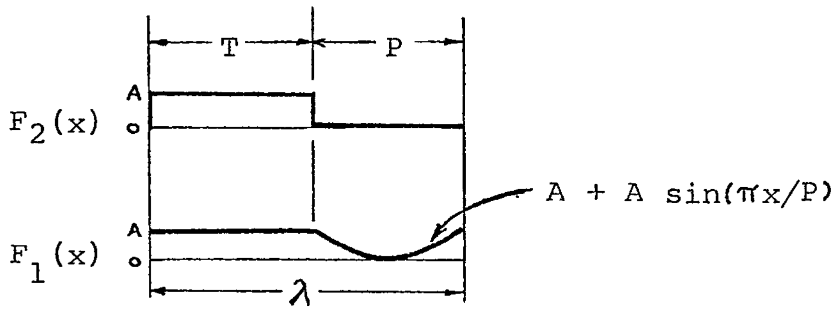

Here the phase difference L is zero on account of a common longitudinal datum.

There are no friction factor data extant for such a reference waveform, but this is inconsequential, since if a correlation is achieved for the variety of waveforms for which data exist, it will be for the reference waveform in the identity limit that $R_{12}(0) = 1$.

It is now assumed that the waveform of the roughness does not disturb the mean velocity streamlines near the waveform, so that the time-averaged local velocity U_x can be written in a power-law form:

$$U(y) = U_o\left(\frac{y}{R_o}\right)^m \tag{3.28}$$

where U_o is the centerline velocity,

m is a universal constant,

R_o is the radius of the pipe.

The shear stress at the wall, τ_ω, is

$$\tau_\omega(x) = \frac{dP}{dx}\frac{D(x)}{4} . \qquad 3.29$$

For this case, the local diameter is

$$D_i(x) = D_o + 2\,F_i(x).$$

The fluctuating part must be normalized by its mean and variance. Adding and subtracting the waveform mean η_i gives

$$D_i(x) = D_o + 2\eta_i + 2\,(F_i(x) - \eta_i).$$

A dimensionless diameter D_i' can be defined where the wall term $F_i(x)$ is divided by its variance σ_i and the bulk flow term D_o is divided by a constant, say σ_D, to give

$$D_i' \cong \frac{D_o}{\sigma_D} + \frac{2\eta_i}{\sigma_i} + 2\,\frac{(F_i(x) - \eta_i)}{\sigma_i} \qquad 3.30$$

The variance and σ_D are of the same order of magnitude, but not necessarily equal, to preserve the order-of-magnitude relationship between the wall term and the bulk flow term. However, σ_D must be unique for a given D_o, so that in the ratio, $\frac{D_i'}{D_j'} = 1$ for $D_{o_i} = D_{o_j}$.

The wall pressure profile is assumed to be composed of a term linear in x for the viscous dissipation, and a generalized function h(x) which is assumed to be universal for any groove type roughness. The pressure distribution decays exponentially away from the wall so that it is written

$$P_i(x) = px + P_{oi}\ h(x)\ e^{-ky}. \qquad 3.31$$

The differential is

$$\frac{dP}{dx} = p + P_{oi}\ h'(x)\ e^{-ky}. \qquad 3.32$$

Substituting equations 3.28, 3.29, 3.30, and 3.32 into equation 3.27 gives

$$\frac{f_1(x)}{f_2(x)} = \frac{p+P_{o1}\ h'(x)\ e^{-ky}\left[\frac{D_o}{\sigma_D} + \frac{2\eta_1}{\sigma_1} + \frac{2(F_1(x)-\eta_1)}{\sigma_1}\right] U_{o2}^2\left(\frac{y}{R_o}\right)^{2m}}{p+P_{o2}\ h'(x)\ e^{-ky}\left[\frac{D_o}{\sigma_D} + \frac{2\eta_2}{\sigma_2} + \frac{2(F_2(x)-\eta_2)}{\sigma_2}\right] U_{o1}^2\left(\frac{y}{R_o}\right)^{2m}} \qquad 3.33$$

It is now assumed in equation 3.33 that $p \ll P_{oi}\ h'(x)\ e^{-ky}$. It is further assumed that the pressure amplitude and square of the maximum velocity are related by a universal constant, so that

$$\frac{P_{o1}\ U_{o2}^2}{U_{o1}^2\ P_{o2}} = 1.$$

Equation 3.33 becomes

$$\frac{f_1(x)}{f_2(x)} = \frac{\left[\frac{D_o}{\sigma_D} + \frac{2\eta_1}{\sigma_1} + 2\ \frac{(F_1(x)-\eta_1)}{\sigma_1}\right]}{\left[\frac{D_o}{\sigma_D} + \frac{2\eta_2}{\sigma_2} + 2\ \frac{(F_2(x)-\eta_2)}{\sigma_2}\right]}. \qquad 3.34$$

In order to avoid the result $\langle f_1\rangle = \langle f_2\rangle$ upon wavelength averaging, equation 3.34 is multiplied by unity in the factor $\frac{(F_1(x)-\eta_1)\sigma_1}{(F_1(x)-\eta_1)\sigma_1} = 1$.

Equation 3.34 is expanded and cleared of fractions preparatory to integration:

$$\frac{1}{\lambda}\int_0^{\lambda} f_1(x)\left[\left(\frac{D_o}{\sigma_D}+\frac{2\eta_2}{\sigma_2}\right)\left(\frac{F_1(x)-\eta_1}{\sigma_1}\right)+2\left(\frac{F_1(x)-\eta_1}{\sigma_1}\right)\left(\frac{F_2(x)-\eta_2}{\sigma_2}\right)\right]dx$$

$$=\frac{1}{\lambda}\int_0^{\lambda} f_2(x)\left[\left(\frac{D_o}{\sigma_D}+\frac{2\eta_1}{\sigma_1}\right)\left(\frac{F_1(x)-\eta_1}{\sigma_1}\right)+2\left(\frac{F_1(x)-\eta_1}{\sigma_1}\right)^2\right]dx. \qquad 3.35$$

Now, it is assumed that the friction factors are defined as averages over a wavelength and brought outside the integral sign. Equation 3.35 is integrated to yield:

$$\langle f_1\rangle\left[\left(\frac{D_o}{\sigma_D}+\frac{2\eta_2}{\sigma_2}\right)\cancelto{0}{\left\langle\frac{F_1(x)-\eta_1}{\sigma_1}\right\rangle}+2\left\langle\left(\frac{F_1(x)-\eta_1}{\sigma_1}\right)\left(\frac{F_2(x)-\eta_2}{\sigma_2}\right)\right\rangle\right]$$

$$=\langle f_2\rangle\left[\left(\frac{D_o}{\sigma_D}+\frac{2\eta_1}{\sigma_1}\right)\cancelto{0}{\left\langle\frac{F_1(x)-\eta_1}{\sigma_1}\right\rangle}+2\left\langle\left(\frac{F_1(x)-\eta_1}{\sigma_1}\right)^2\right\rangle\right]. \qquad 3.36$$

It is observed that the first order terms are zero, and the second order terms are correlation coefficients. Equation 3.36 is rewritten as

$$\langle f_1\rangle\, R_{12}(0) = \langle f_2\rangle\, R_{11}(0). \qquad 3.37$$

By definition, $R_{11}(0) = 1.$, so equation 3.37 is

$$\langle f_1\rangle = \frac{\langle f_2\rangle}{R_{12}(0)}\,. \qquad 3.38$$

The derivation was similar to that for projection roughness but here the crosscorrelation coefficient is in the denominator.

Equation 3.38 shows that friction factors for flow over groove type roughness can be related in shape by the reciprocal of the crosscorrelation coefficient of the roughness waveforms. As before, the normalization has removed any specification of the waveform amplitudes so that equation 3.38 is valid for friction factors over waveforms of the same amplitude.

The friction factors so modified for groove roughness were correlated by further modification with dimensionless combinations of length parameters. This correlation was done by trial and error.

Although several combinations of parameters appeared to cause the friction factor data to cluster after some fashion, the best from a least squares basis was the combination

$$\left[\frac{P}{S} + \frac{\sqrt{AP}}{D_o} + \sqrt{\frac{P}{D_o}}\right]$$

where S is the perimeter of the waveform along a wavelength and P, A, and D_o are defined as for projections. The physical implication of S is that the wall dissipation is prevalent in the space where P^2/TD_o becomes small and a smooth surface is approached. The modifiers were established for large and small values of the base variable P^2/TD_o and are mutually negligible in the other's domain. The modifier $\sqrt{AP}/D_o$ was added to better the correlation in the intermediate region of P^2/TD_o.

The resulting correlation for groove type roughness is presented in Figure 13. Each point represents the friction factor of a roughness system of a different shape, size and pipe diameter. The friction factor is nearly constant over the Reynolds number range given in the legend.

A trend is observed which forms two regions that can be fit with straight lines. These regions are labeled 4 and 5. At $P^2/TD_o = 70$, the data no longer are correlated as the geometries approach the long-wave projection type roughness, which correlates with sine wave roughness. The data of May and Savage which fit the projection correlation were plotted to show this divergence as the cavity length P becomes very large in relation to T. The correlation is judged to be valid since the data group about the means such that any deviations appear to be random. The data cover the extreme types of groove roughness as shown below:

 Skoglund

 Nunner

 Kolar

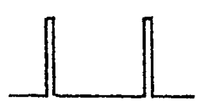 Savage, Koch

 Tripp

 May

A listing of the data and calculated quantities for the groove roughness is given in Appendix C.

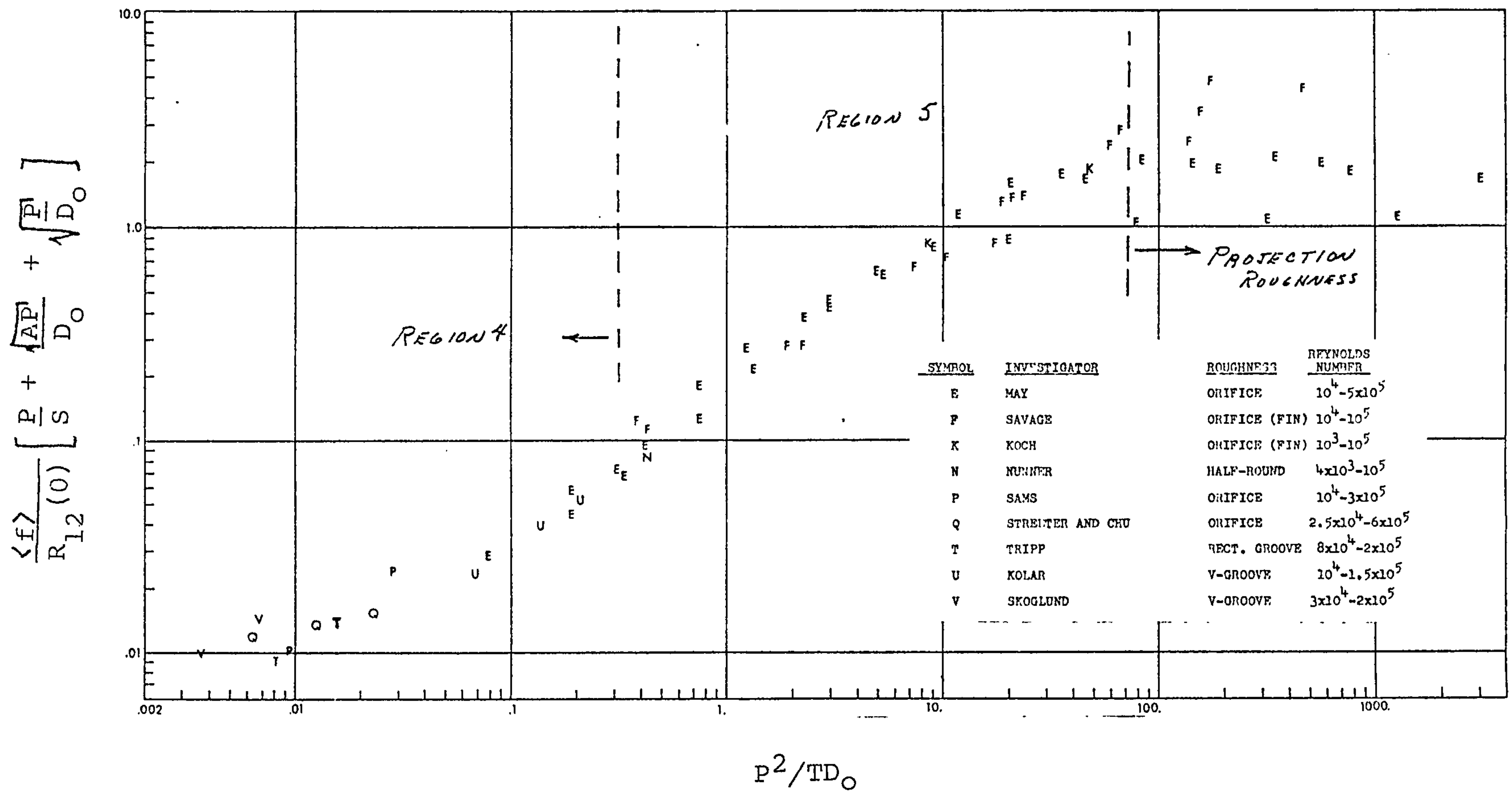

FIGURE 13. FRICTION FACTOR CORRELATION FOR GROOVE ROUGHNESS

Reynolds number effects

The graph of friction factors for some of the various groove geometries given in Figure 14 shows slight dependence on the Reynolds number. The correlation graph can be used with little error for a wide range of Reynolds numbers.

Closure

The essence of the analytical correlating scheme has been to reference all arbitrary roughness geometries to a single reference shape of similar dimensions. The unknown quantities and y-direction dependence were eliminated by division, and the resulting expression integrated over a wavelength. The result is that the friction factors are related by the cross-correlation coefficients of their waveforms. This procedure has necessitated the division of roughness into two major groups, which will be shown to have distinct flow processes occurring within the roughness cavities.

All the available data on two-dimensional periodic pipe roughness fit either of the two correlation graphs according to the generalized precepts for representing such geometries. The graphs are valid in the Reynolds number range of $5X10^3 \leq N_{Re} \leq 5X10^5$ The waveforms represented have friction factors from 0.01 to 1.0 on a smooth-pipe basis, and have λ/D_o ratios from 0.006 to 24. Interpretations of the correlation graphs will be given in

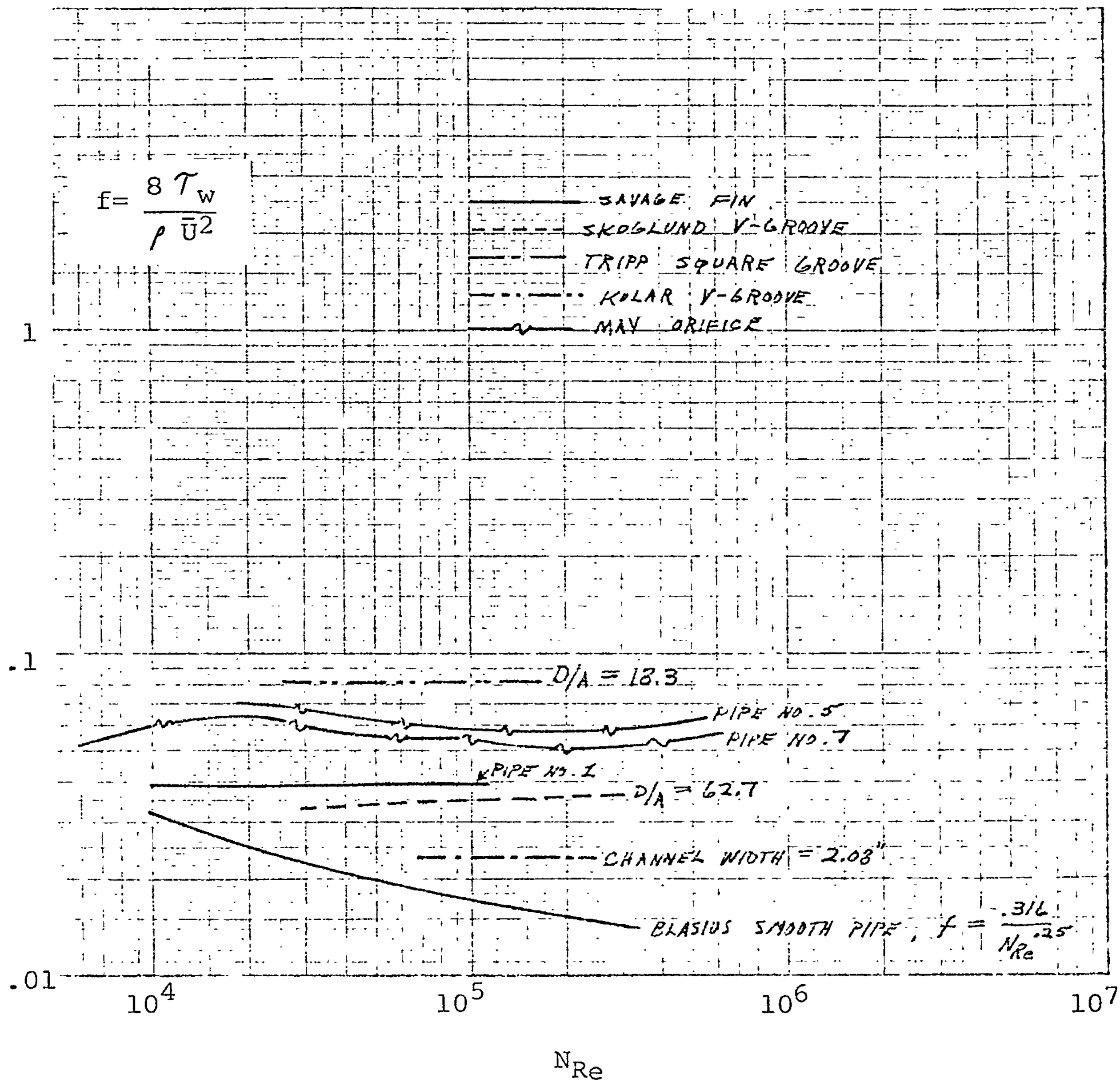

FIGURE 14. FRICTION FACTOR DATA FOR TYPICAL GROOVE ROUGHNESS

Chapter 4 as well as numerical criteria for predicting which of the two predominant flow classifications will be produced by a given geometry.

CHAPTER IV

DISCUSSION OF RESULTS

The two correlation graphs are presented in usable form in Figures 15 and 16, which are the least squares lines of fit of the data points of Figures 11 and 13. The regions were all fit by straight line equations in the appropriate semilog or log-log form according to standard least squares procedures (11).

The accuracy that may be expected from using the least-square equations for prediction of friction factors is given in Table 2 as the average deviation from the mean based on the total number of data points used in each region. It is also shown that σ is a better correlating variable than A in $\lambda^2/\sigma D_o$ on a sum-of-squares basis.

It is seen from Figures 11 and 13 that the points of intersection are least well fit by the regression lines. It is thought that these intersections represent an unsteady process of flow, hence are not accounted for in the analyses given in Chapter 3. Another region, 3a, seems to begin in Figure 11 for $\lambda^2/\sigma D_o > 3x10^4$. This region represents geometries where $A \ll \lambda$ and $\lambda > D_o$ so that another effect, that which is largely smooth wall dissipation, may start to predominate here and not be represented by the correlation. At the other approach to a

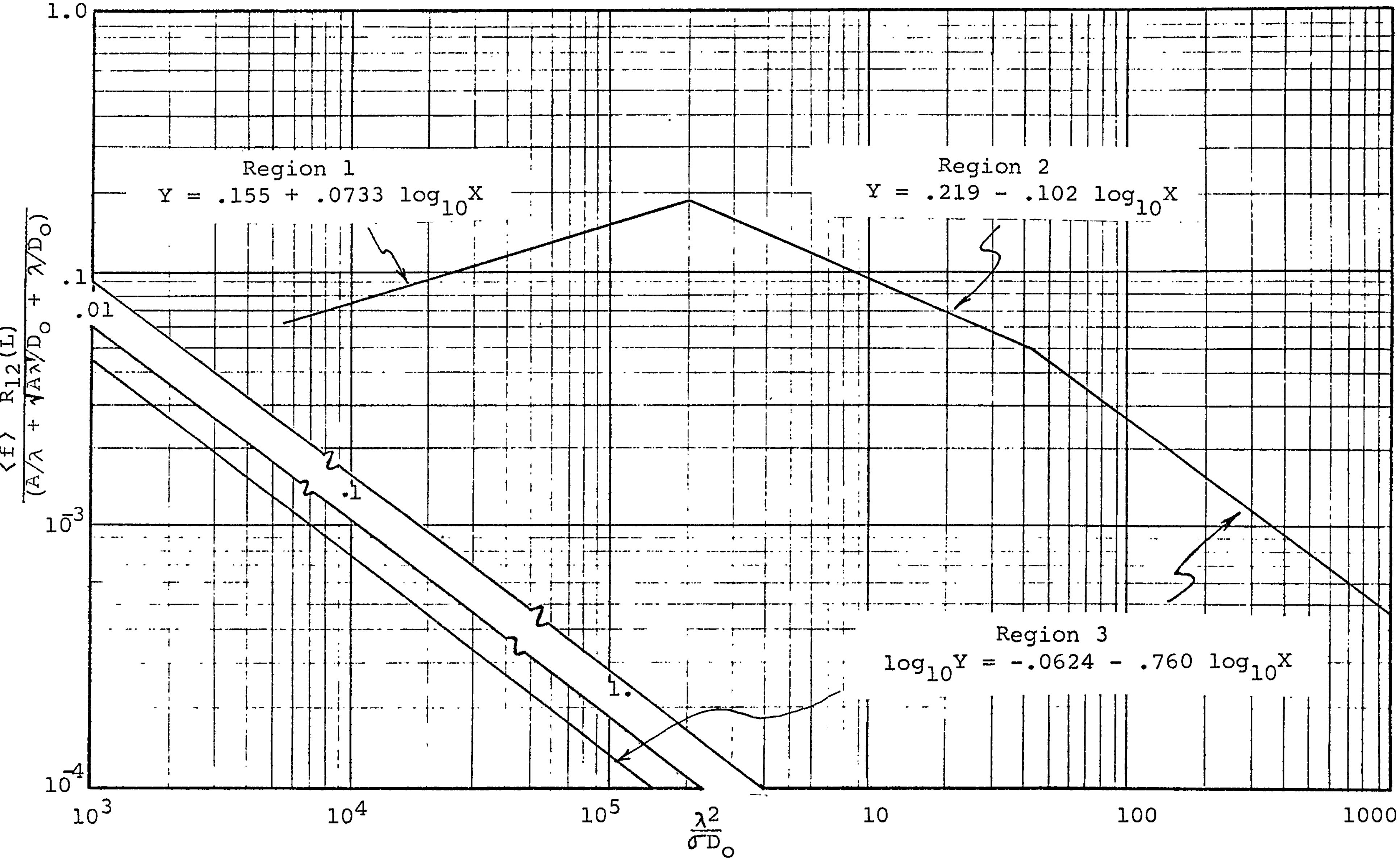

FIGURE 15. LEAST SQUARES FIT OF CORRELATION FOR PROJECTION ROUGHNESS

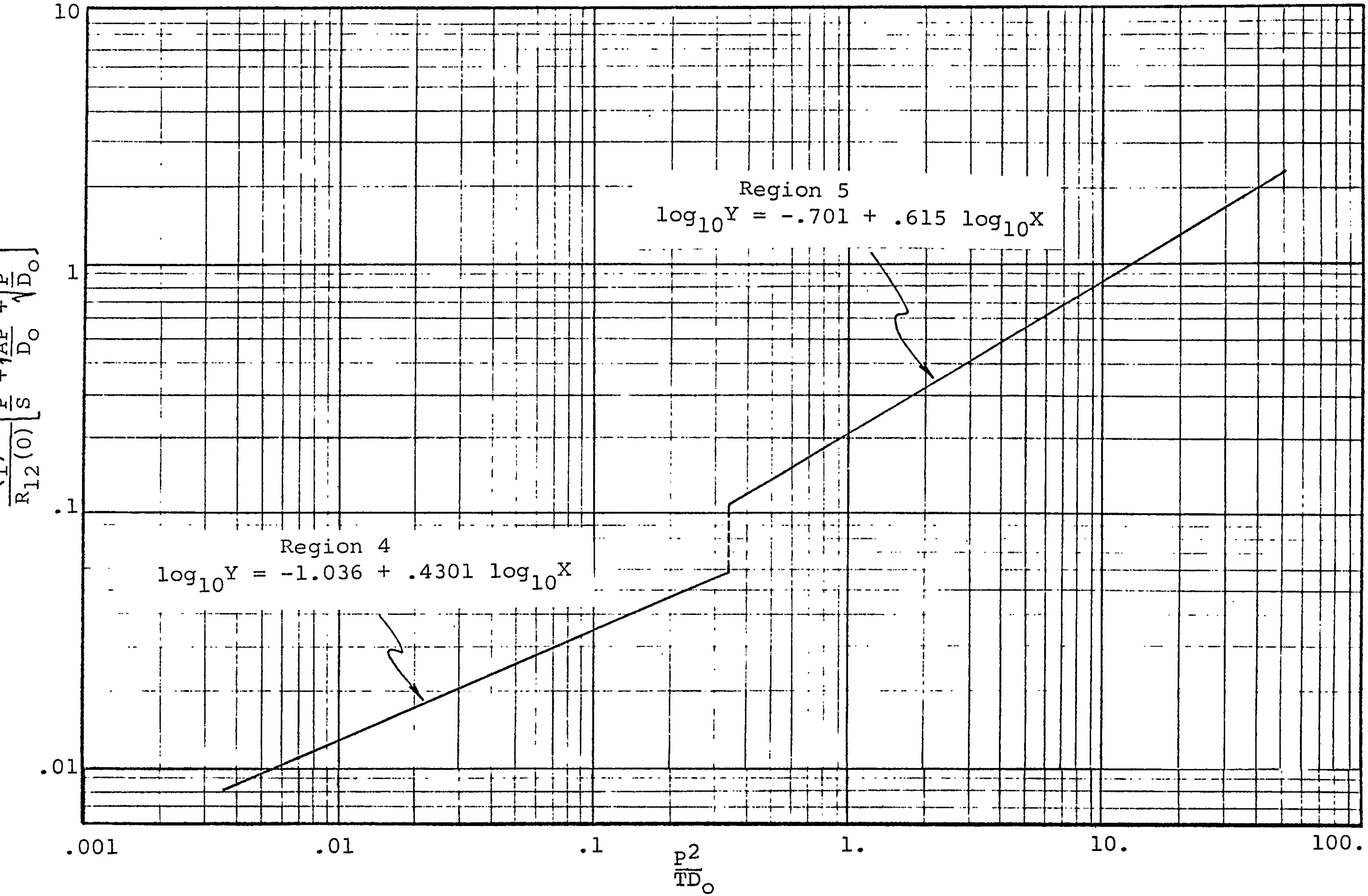

FIGURE 16. LEAST SQUARES FIT OF CORRELATION FOR GROOVE ROUGHNESS

TABLE II

SUMMARY OF STATISTICS
OF CURVE FIT EQUATIONS

REGION	EQUATION	SUM OF SQUARES	NO. OF DATA POINTS	% AVG. ERROR
Projections, $X = \lambda^2/\sigma D_o$				
1	$Y = .1556 + .0733 \log_{10} X$	.0087	23	10.4
2	$Y = .2188 - .102 \log_{10} X$	.2095	52	16.7
3	$\log_{10} Y = -.0624 - .760 \log_{10} X$	.0491	61	22.4
Projections, $X = \lambda^2/AD_o$				
1	$Y = .1825 + .0766 \log_{10} X$	.0106	23	12.5
2	$Y = .1709 - .1183 \log_{10} X$	.4042	52	18.3
3	$\log_{10} Y = -.1577 - 1.0539 \log_{10} X$	.1723	61	36.3
Grooves				
4	$\log_{10} Y = -1.036 + .4301 \log_{10} X$	.0008	17	17.9
5	$\log_{10} Y = -0.701 + .615 \log_{10} X$	.0077	29	14.2

For projections, $$Y = \frac{\langle f \rangle R_{12}(L)}{\left[\frac{A}{\lambda} + \frac{\sqrt{A\lambda}}{D_o} + \frac{\lambda}{D_o}\right]} .$$

For grooves, $Y = \dfrac{\langle f \rangle}{R_{12}(0)} \left[\dfrac{P}{S} + \dfrac{\sqrt{AP}}{D_o} + \sqrt{\dfrac{P}{D_o}}\right]$ and $X = P^2/TD_o$.

smooth surface ($\lambda^2/\sigma D_o < .01$) no data exist, but it is thought that another region will occur here, where again viscous effects should be predominant as $\lambda \approx A$ and $\lambda, A \ll D_o$.

Interpretation of the correlation graphs

The salient features of each correlation graph of Figures 15 and 16 are the linear regions and apparent discontinuities at their junctures. It will be shown that these regions represent the parametric space of $\lambda^2/\sigma D_o$ and P^2/TD_o where different flow processes occur near the rough surface. This will be assessed on the basis of available flow visualization studies. These flow effects can be quantified parametrically so that they may be predicted for a given geometry of roughness.

It is observed that the data points in Figures 11 and 13 delineate distinct regions, and these have been given straight line fits in Figures 15 and 16. These regions have been labeled 1, 2, and 3 for projections and 4 and 5 for grooves. The regions can be quantified in terms of the base variables, but a further quantification is necessary in order to distinguish projections from grooves. This was done by comparing flow visualization observations for certain roughnesses and observing where these corresponded, parametrically, on the correlation graphs. The general nature of the wall flow processes was then inferred to occur over a particular region. Geometric criteria were then established for each region.

Projections

Region 1 is characterized by wavelengths and amplitudes which are very small in relation to the diameter. Recent visualization studies by Verma and Cermak (57) for flow over sine waves in a 6'x6' cross section wind tunnel indicate a flow pattern as shown below, which is a shedding vortex located centrally in the roughness trough. The wavelength and ampli-

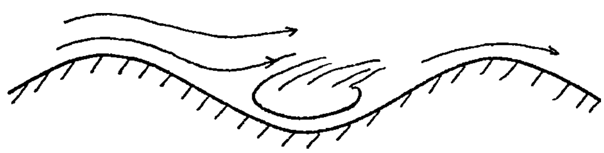

tude range studied was λ=4.2", with A=1.7", 1.0", and 0.5" so that $0.4 < \lambda^2/\sigma D_o < 1.37$, which places the roughnesses in region 1.

In a recent paper by Williams and Watts (59), studying rib roughness configurations for augmenting heat transfer, extensive flow visualization studies were made on square, chamfered, and sawtooth ribs of different spacings and amplitudes. These shapes were used to roughen one sidewall of a rectangular 46 cm. by 62 cm. duct. The dimensions were such that all geometries illustrated were in region 1. The friction data could not be compared directly because only one wall was roughened. The visualization diagrams are presented in Figure 17

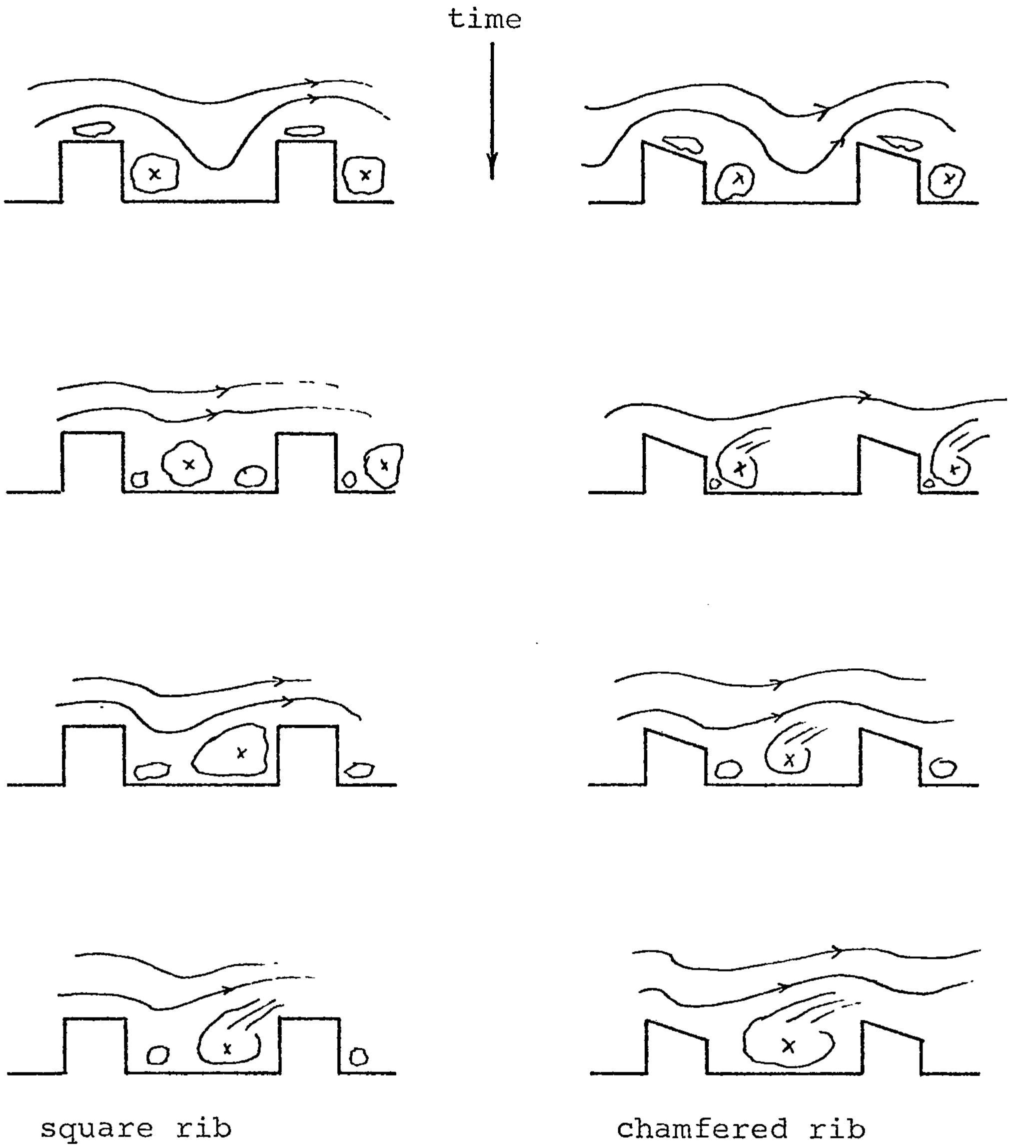

FIGURE 17. FLOW PATTERNS FOR ROUGHNESS IN REGION 1 (FROM WILLIAMS AND WATTS (59))

and show that vortices are produced in fairly regular growth sequences and are ultimately shed into the bulk flow. The manner of growth varies with the waveform shape, however. Heat transfer data presented indicate that the closely spaced (λ/A=3) chanfered rib produces the best performance for improved heat transfer, where the performance was measured by the ratio of the Stanton number to friction factor. It is concluded that geometries in this parametric region produce vortices which are shed into the bulk flow.

Region 2 represents waveforms where $A \approx \lambda$, but neither is very small in relation to D_O. Studies by the author on a 9" diameter corrugated pipe show that an unsymmetrical vortex exists as shown below which occupies less of the cavity than those for region 1. This region seems to compare with Morris'

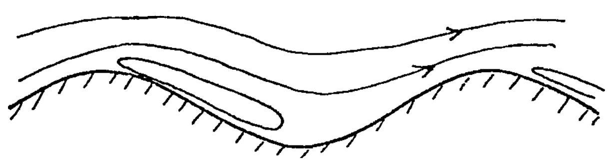

"wake interference flow."

Region 3 apparently represents Morris' "isolated roughness flow," in that the roughness elements are far apart, and the wavelength is on the order of the diameter, or greater. It is also possible to suggest a flow regime on the basis of studies by Liu, <u>et al.</u> (26). Their studies were done in an open channel in zero pressure gradient and no equivalent diameter can be deduced from their data. However, from the work of May, $8 < P/A \leqslant 200$ is a criterion for this parametric region. A flow pattern is presented by Liu, et al. for $P/A > 8$ which is shown below. It is seen that small vortices exist near the

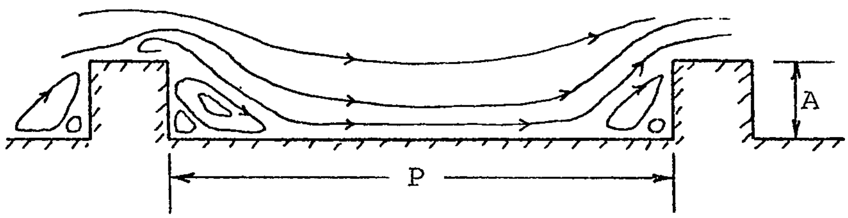

roughness elements and the flow streamlines follow the roughness contours. It is expected that the presence of a pressure gradient would not alter the separation structure except perhaps to shift the points of attachment somewhat.

It is seen for projection roughness, in general, that the bulk flow interacts to a great extent with the roughness cavities. At present, it is not possible to predict the precise flow pattern which will occur over a given roughness shape. It is possible to generalize about the flow patterns which correspond to the regions on the correlation graphs.

Grooves

Region 4 consists of geometries which produce low friction factors (2--10 times smooth pipe values), and whose cavity lengths are the measures of spacing. Also, it is also observed that $P/A \leqslant 1$. Flow patterns for the four data points of May in this region show that stable, circular vortices having constant rotational speed exist in the cavities as shown below. Likewise, work by Knudsen and Katz (20) and

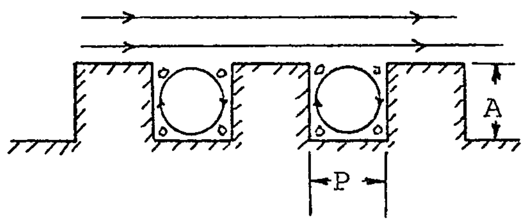

Roshko (39) shows that cavities for which $P/A \lessgtr 1.15$ are conducive to this type of flow pattern. From observing the correlation of Figures 13 and 16 it is seen that Savage's roughness pattern #1 has P/A=1 but lies in region 5. The parameter P/A is not sufficient to predict when this type of flow will prevail, so it must be specified that $P/A \leq 1$ and $P^2/TD_o < 0.32$ for this stable vortex pattern to occur.

Region 5 has geometries where, nominally, $1 < P/A < 10$. This is also the approximate point where such geometries fit the projection curve well. Liu, _et al._, show that a large, unsteady captive vortex exists which tends to fill the space of the cavity as shown below, for $1. < P/A < 8$. It is concluded

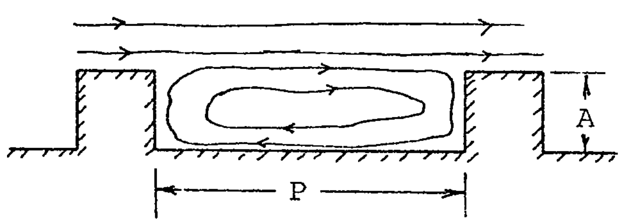

that such a vortex system exists in pipe flow for $1. < P/A < 10$ and $0.32 < P^2/TD_o < 70$. May's work and the values of P/A for the data which lie in region 5 support this conclusion.

Note that Nunner's pattern of adjacent half-round rings also fits in region 5. This roughness pattern () did not correlate with projection roughness, nor did it fit the groove correlation scheme as no dimension "T" exists for it. T was arbitrarily chosen as T=A/4 and correlation done on that basis. T was varied by ± 20 % and still fit the groove correlation in region 5, which indicates that a captive vortex occurs in this roughness type which conforms to the cavity shape. From this example, it is seen that the parameters are somewhat compensatory if some dimensions must be chosen arbitrarily for waveforms otherwise difficult to represent.

The arguments given above afford numerical criteria for predicting which flow patterns at the wall will occur for a given roughness geometry in pipe flow. These criteria are summarized in Table 3.

Statistical assessment of the correlations

All the regions of the correlations were fit by standard least squares techniques to linear models of the form

$$\hat{Y} = \beta_o + \beta_1 \log_{10} X$$

or

$$\log_{10}\hat{Y} = \beta_o + \beta_1 \log_{10} X$$

where $\hat{Y}$ is the ordinate and X is the abscissa. These regres-

TABLE III

SUMMARY OF CRITERIA FOR DEFINING REGIONS OF THE ROUGHNESS CORRELATIONS

Region	Parametric criteria	Basis for evaluation
1	$P/A > 1$ and $\lambda^2/\sigma D_o \leq 2.5$	Verma and Cermak (57), Williams and Watts (59)
2	$1 < P/A < 10$ and $2.5 < \lambda^2/\sigma D_o \leq 45$	this work, May (28)
3	$P/A > 10$ and $45 < \lambda^2/\sigma D_o$	Liu, *et al.* (26), May (28)
4	$P/A \leq 1$ and $P^2/TD_o \leq .32$	Liu, *et al.* (26), May (28)
5	$1 < P/A \leq 10$ and $1 < P^2/TD_o \leq 70$	Liu, *et al.* (26), May (28)

sions are given in Figures 15 and 16.

To assess the validity of such models, consideration must be given the number of data points used, mean square errors (F-test) and an examination of the residuals (Y(actual) -Y(estimated)).

The significance of each data point in this work is that it represents the friction factor of a roughness flow system at a particular Reynolds number. Multiple points for those systems which were Reynolds-number-dependent account for most of the variance shown in Figures 10, 11, and 13. For those systems which exhibit no great Reynolds number dependency, the scatter to be observed results only from the inadequacy of the models and variation between results of different investigators. It is fairly certain that the data used are in themselves precise, so any variation about the means will be random and the data points will be distributed randomly about the regression lines. Hence, although an infinite number of such points could have been chosen, the correlations would not have any greater statistical significance.

Significance of the regression can be judged by an F-test which compares the mean square due to regression $(\Sigma(\hat{Y}_i-\bar{Y})^2)$ with the estimated variance ($s^2 = \frac{\Sigma(Y_i-\hat{Y})^2}{n_p-2}$) to form the statistic $F = \Sigma(\hat{Y}_i-\bar{Y})^2/s^2$. For significance of regression, i.e., that the postulated model adequately describes the cluster of data, then $F_{calculated} > F_{distribution}$. This was found to be true for all correlation regions.

Finally, an examinations of the residuals was done to see if the models were adequate over the range of the X-variable. The residual plots of $Y-\hat{Y}$ versus $\log_{10}X$ were distributed in a uniform band about $Y-\hat{Y}=0$, indicating that the models were adequate over the X-variable range. Tabulations of the statistical tests done are given in Appendix D for all 5 regions. It is concluded that the straight line models are adequate and that regression is significant for pipes of $D_o < 18''$. The data for very large pipes were not considered further because of limited roughness shapes, although those represented in Figure 5 are closely grouped by the correlation for a wide range of sizes and Reynolds numbers.

Analysis of variance

The lack of fit observed on the correlation graphs may be attributed to several factors.

1. Imperfect assumptions in the analyses--This is judged to be the greatest effect, as available visualization data show that the assumptions of velocity following the wall waveform is not very realistic, except in the case of wake interference flow (region 3) where, indeed, the fit is least good. The assumption of pressure profile similarity is of uncertain validity since few data exist for evaluation.

2. Choice of dimensions used to represent roughness and modify the friction factor--The method of analysis is one of comparing one process to another as a ratio, averaging, and then evaluating the moments which are said to describe these processes. Therefore, the thesis of this paper is refuted, since one cannot hope to find all the geometric moments, much less represent then on a two-dimensional graph. Considering the success of the attempt, it must be that moments of higher order than two can be neglected. This also explains why σ causes a better fit of the data than A in the base parameter $\lambda^2/\sigma D_o$, as it is a second-order moment.

3. Variation between individual experimental studies--One can expect an experimental error of several per cent in collecting friction factor data. This error could be greater, perhaps to 5 or 10 percent when comparing the diversity of techniques and equipment as represented in this work. Heretofore, there has been no such general basis for comparing friction factor data for geometric roughness, so the correlation may be more accurate than it appears from the data fit.

A study was made to determine the effect on the correlation of a 1% deviation of the dimensions used in the function

$$Y = \frac{\langle f \rangle R_{12}(L)}{\left[\frac{A}{\lambda} + \frac{\sqrt{A\lambda}}{D_o} + \frac{\lambda}{D_o}\right]} = \frac{2\,\Delta P\, D_o^5\, R_{12}(L)}{\rho\, l\, Q^2 \left[\frac{A}{\lambda} + \frac{\sqrt{A\lambda}}{D_o} + \frac{\lambda}{D_o}\right]}$$

and

$$Y = \frac{2\,\Delta P\, D_o^5 \left[\frac{P}{S} + \frac{\sqrt{AP}}{D_o} + \sqrt{\frac{P}{D_o}}\right]}{\rho\, l\, Q^2 \quad R_{12}(0)} \,.$$

A total derivative of Y was taken as a function of those parameters considered most important as a source of scatter due to lack of precision in the original measurements:

$$dY = \frac{\partial Y}{\partial A}dA + \frac{\partial Y}{\partial D_o}dD_o + \frac{\partial Y}{\partial \lambda}d\lambda + \cdots$$

The results are presented in Table 4. The total deviation is the sum across the rows. The deviation in Y was expressed as a fraction of Y evaluated for each geometry and presented as an average over the parametric region, as the function is sensitive to different dimensions in different regions of the correlations. The analytical expression for Y has been derived for the case of the orifice type roughness. It is expected that the sensitivities given are typical, as the analytical procedure becomes very difficult for all other shapes. The results for A and D_o are valid for all shapes, however. It will be noted that the most important single parameter is the diameter D_o, as it appears to the fifth power in Y. Also, the fin thickness T is important for widely spaced fins. Errors in pressure drop cause 1:1 errors in Y.

TABLE IV

SENSITIVITY ANALYSIS OF ROUGHNESS CORRELATION

SHAPE	% DEVIATION IN Y FOR 1% DEVIATION IN			
Projections	A	D_o	λ	T
sine wave	.08--.7	5.2--6.0	.03--.45	----
orifice	.05--.2	5.9	.40--.50	.10--18.0
Groove				
all	.02--.2	4.5--4.9	----	----

Use of the correlations

The following procedure is given as a guide in using the correlations to predict friction factors in pipe flow for any arbitrary roughness waveform, provided that it is two-dimensional, piecewise, periodic and otherwise conforms to the Dirichlet conditions. Some typical examples of waveforms which conform to the conditions set forth above are shown below:

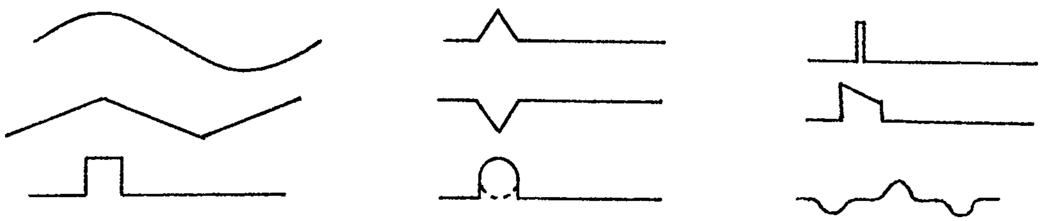

The calculation procedure is as follows:

1. specify the shape and size of roughness and the diameter of pipe
2. determine whether it is a projection or groove according to the criteria of Table 3
3. calculate the value of the abscissa of Figure 15 or 16
4. locate value of ordinate, calculate the modifying factor and $R_{12}(L)$ or $R_{12}(0)$ and solve for $\langle f \rangle$.

Determining the crosscorrelation coefficient is unfortunately not trivial analytically for most waveform shapes , but it is easily done numerically by computer. The orifice type (rectangular wave) is quite common and the analytical formula for the normalized crosscorrelation coefficient and the RMS value σ are given by

$$R_{12}(L) = \frac{\cos \pi(\tfrac{1}{2} - T/\lambda) - \cos \pi(\tfrac{1}{2} + T/\lambda)}{\sqrt{2}\,\pi\,(T/\lambda - (T/\lambda)^2)^{\frac{1}{2}}}$$

$$\sigma_2 = A\,(T/\lambda - (T/\lambda)^2)^{\frac{1}{2}}.$$

For the sawtooth waveform (), $R_{12}(L)$ and σ_1 are

$$R_{12}(L) = \frac{4\sqrt{6}}{\pi^2} = 0.994$$

$$\sigma_1 = A/\sqrt{12}.$$

No friction factor data are available, but should be nearly that for sine wave roughness. The derivation of these functions is given in Appendix E. Crosscorrelation coefficients for a number of different roughness waveforms are presented in Figures 18 and 19 for projections and in Figure 20 for grooves.

Some waveforms can be imagined where it will be difficult to assign the generalized dimension "T", particularly in rounded forms whose elements have minimum spacing:

It is not now possible to designate such types as projections or grooves, except for the half-round roughness of Nunner.

An example of a waveform for which the correlations do not apply is the ramp wave:

(a) 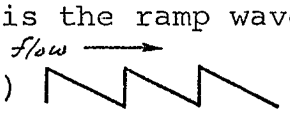

(b) 

In either form, the crosscorrelation coefficient $R_{12}(L)$ is identically zero. No usable friction factor data are available for fully roughened pipes, but it has been shown that form (a) produces a higher friction factor than form (b).

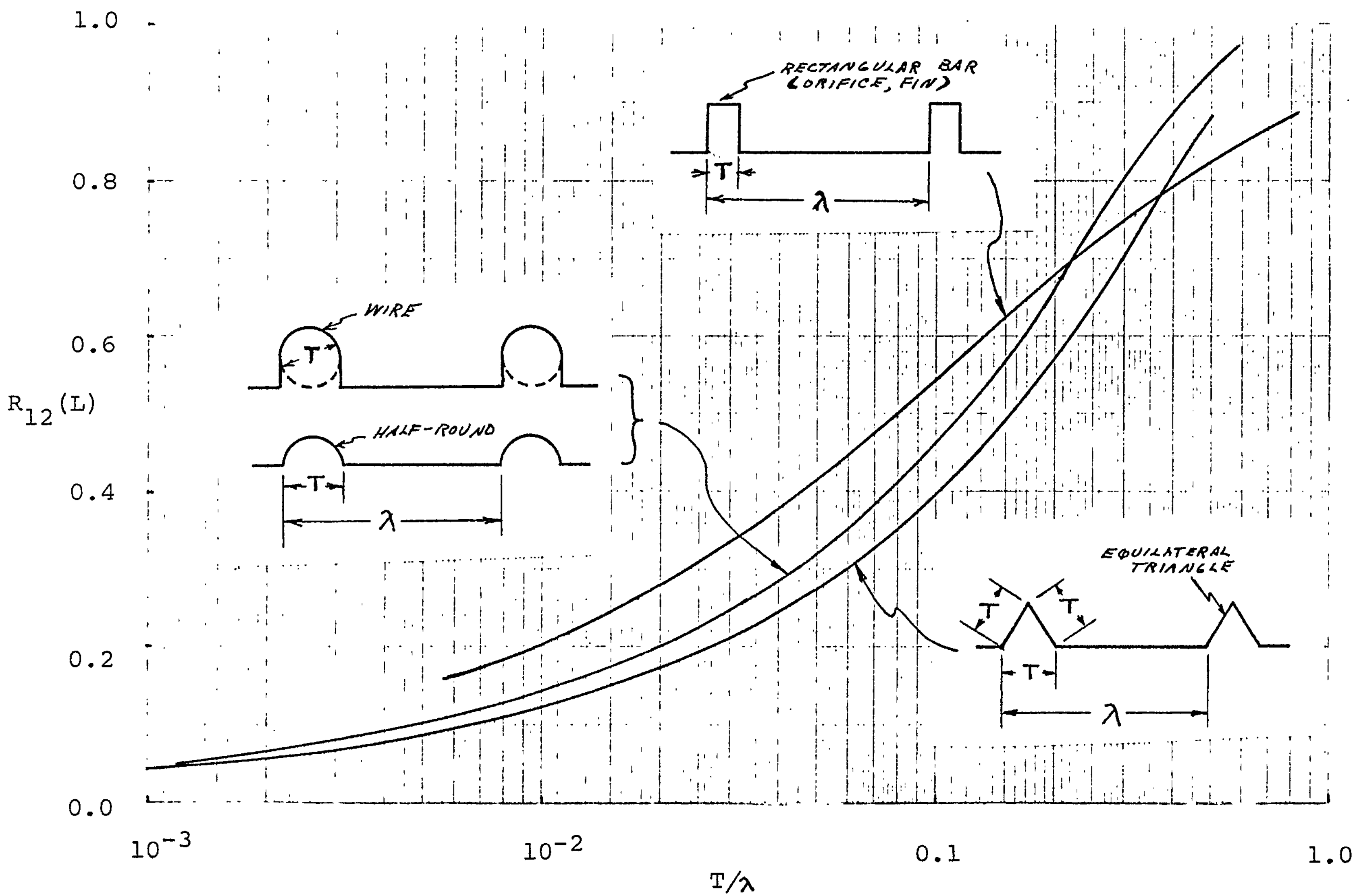

FIGURE 18. CROSSCORRELATION COEFFICIENT FUNCTIONS FOR VARIOUS PROJECTION ROUGHNESS WAVEFORMS

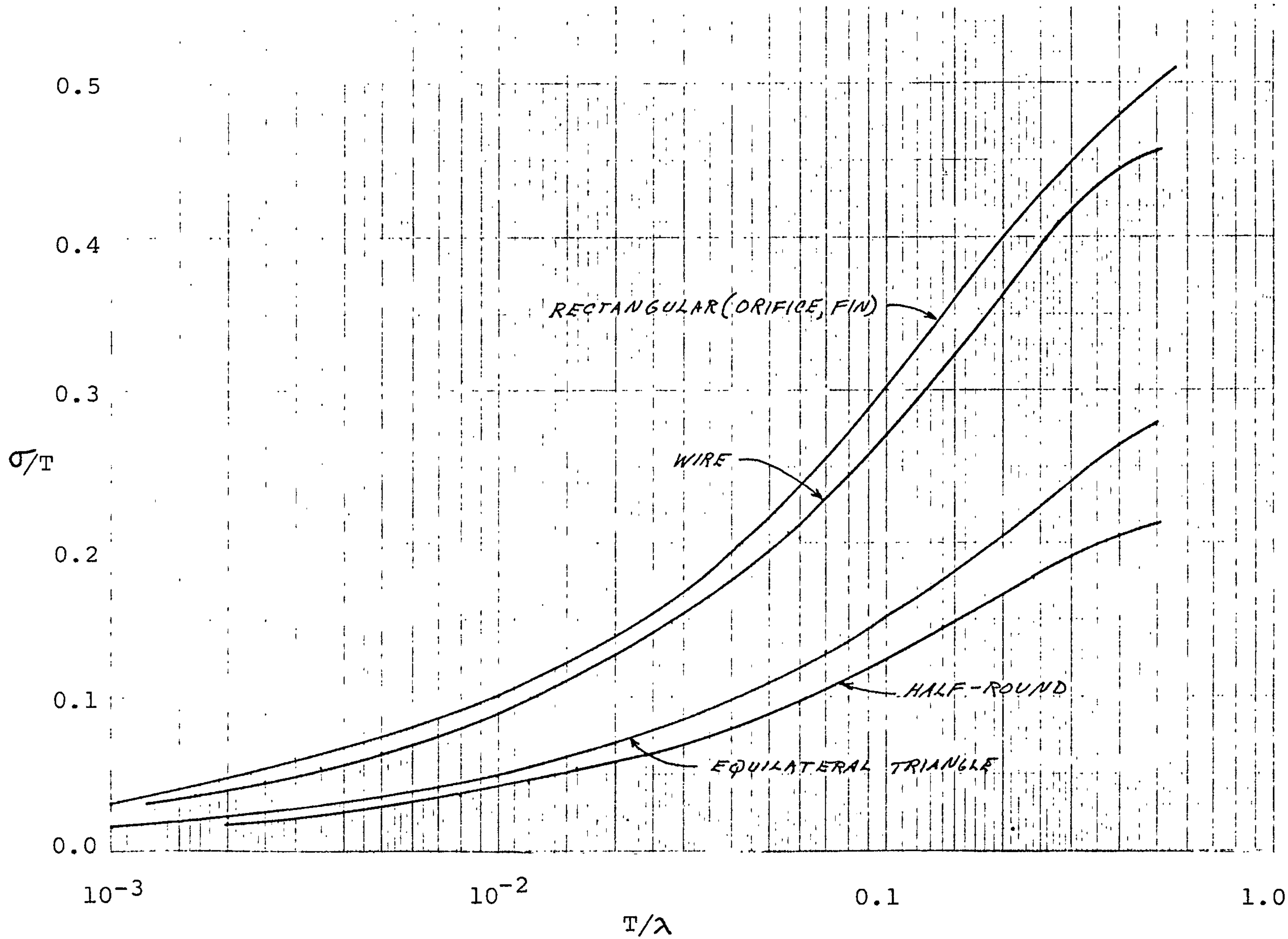

FIGURE 19. ROOT MEAN SQUARE AMPLITUDES FOR VARIOUS PROJECTION ROUGHNESS WAVEFORMS

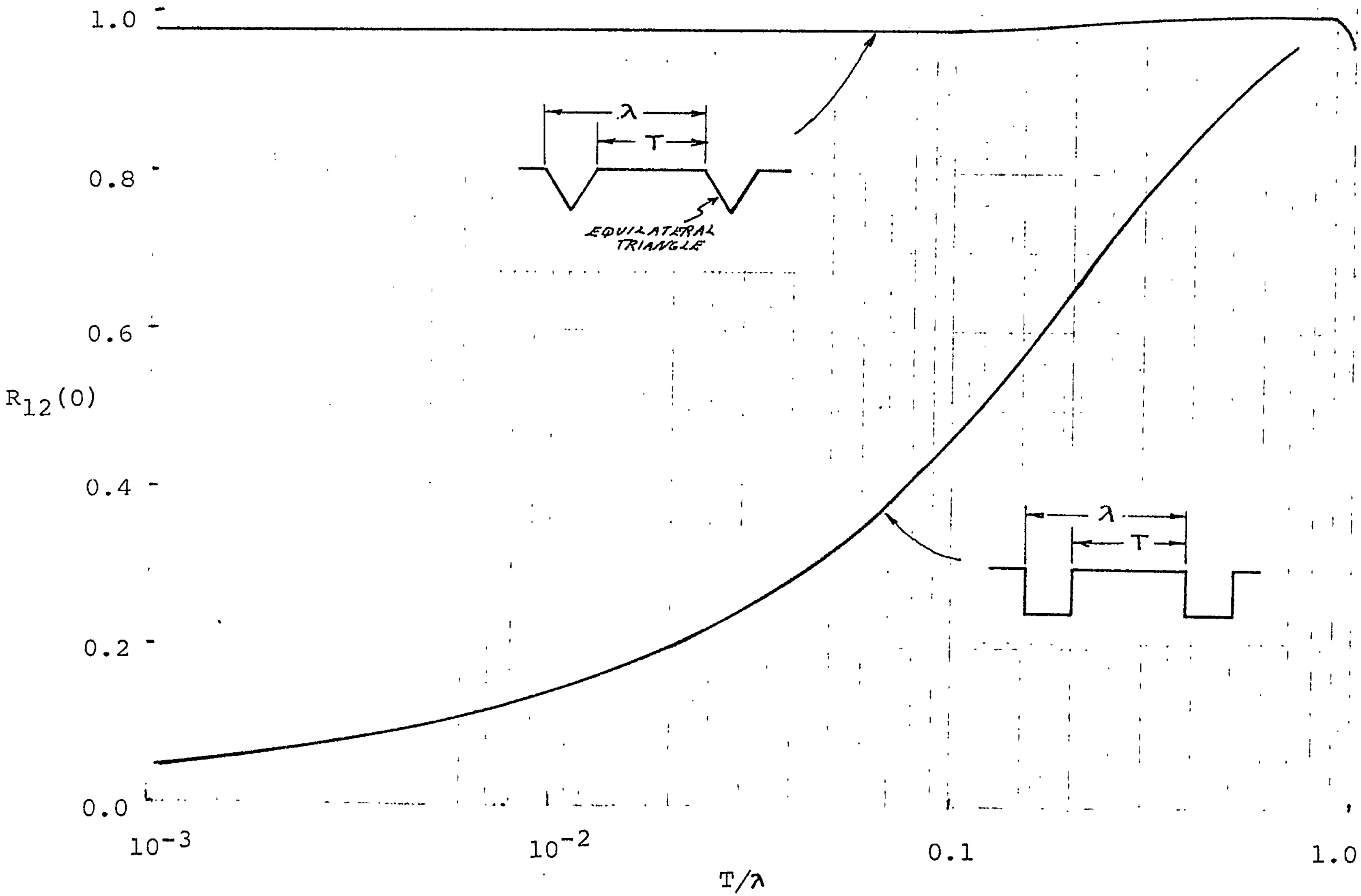

FIGURE 20. CROSSCORRELATION COEFFICIENT FUNCTIONS FOR VARIOUS GROOVE ROUGHNESS WAVEFORMS

Closure

The net interpretation is that the distinct regions of the correlation graphs delineate the parametric space for geometries which are conducive to the existence of a particular flow process in the roughness cavity. This space is quantified in the parameters $\lambda^2/\sigma D_o$ and P^2/TD_o. Numerical criteria have been given so that these processes can be predicted for a given geometry of roughness.

The implication of the various regions is that they represent the transition of one flow process to another with progression of the base variables $\lambda^2/\sigma D_o$ and P^2/TD_o. These transitions certainly must occur and it would therefore be of interest to investigate these points experimentally.

CHAPTER V

CONCLUSIONS AND RECOMMENDATIONS

From the results of this work, it is possible to draw a number of conclusions.

1. Techniques of communications analysis have been shown to be applicable in treating fluid processes which can be related on the basis of averaged properties of the system geometries.

2. It is possible to correlate friction factor data for flow in pipes fully roughened by two-dimensional periodic roughness strictly on the basis of geometry. Friction factors can thus be predicted for a given roughness flow system.

3. It has been shown that such a correlation delineates certain regions within the parametric space which correspond to distinct flow patterns within the roughness cavities so that not only the friction factor but also the flow regime at the wall may be predicted given only the shape of the roughness and the size of the roughness system.

4. Two-dimensional periodic pipe roughness is divided into two main groups according to the wall flow processes they cause to occur: projection type, where the bulk flow interacts with the wall, and groove type, where the flow processes at the wall are contained in the roughness cavities. These distinctions merge into one process for widely-spaced roughness elements.

5. A uniform basis has been established for comparing friction factor data for any such shape of two-dimensional periodic pipe roughness.

6. The minimum diameter D_o is the proper diameter to use for a flow dimension.

7. A linear combination of dimensionless parameters is

necessary to use as a modifying factor to adjust the friction factor on the basis of roughness size.

8. The correlations are valid over the Reynolds number range of about 5×10^3 to 5×10^5 although this spread varies with roughness type. The range is greater for sharp-edged forms, as they seem to be more insensitive to Reynolds number effects than rounded forms.

It is recommended that studies be made of flow over geometries conforming to the intersections of the regions occurring in the correlation graphs. These points may possess desirable flow effects as they are thought to represent geometries where there is the greatest interaction between flow at the wall and flow in the bulk region; hence they could be the most useful for augmentation of heat or mass transfer. As a very wide range of roughness sizes has been investigated, more attention can now be paid to shape effects.

The technique developed here should be applicable to the correlation of friction effects for roughened annular flow and boundary layer flow. These applications are respectively important in nuclear reactors and in wind flow over rough terrain. The latter case could involve a metropolitan area as a roughness in the prediction of pollutant dispersal. The development here has been restricted to two-dimensional processes, but could be extended with little more difficulty to three dimensions.

BIBLIOGRAPHY

1. Augmentation of Convective Heat and Mass Transfer, Winter Annual Meeting of ASME, New York, N. Y., ed. A. E. Bergles, R. L. Webb, Dec. 2, 1970.

2. Benjamin, T. B., J. Fl. Mech. 6, 161(1959).

3. Betterman, D., Int. J. Heat Mass Transfer 9, 153-164(1966).

4. Burck, E., Waerme-u. Stoeff. 2, 87-98(1069).

5. Burck, E., Augmentation of Convective Heat and Mass Transfer, Winter Annual Meeting of ASME, New York, N. Y., ed. A. E. Bergles, R. L. Webb, p. 27(Dec. 2, 1970).

6. Chamberlain, A. R., and N. Bilonok, J. Hyd. Div. Proc ASCE HY3, 86, 67(1960).

7. Chorin, A. J., Mathematics of Computation 22, 745(1969).

8. Clauser, F. H., Advances in Applied Mechanics Vol. IV, Academic Press, New York, 1-51(1956).

9. Davis, R. E., J. Fl. Mech. 42, part 4, 721-731(1970).

10. Dipprey, D. F., and R. H. Sabersky, Int. J. Heat Mass Transfer 6, 329-353(1963).

11. Draper, N. and Smith, H., Applied Regression Analysis, Wiley, New York (1967).

12. Dvorak, F. A., AIAA Journal 7, No. 9, 1752(Sept. 1969).

13. Gibson, A. H., The Philosophical Magazine 50, 199(1925).

14. Gill, W. N. and M. Sher, AIChE Journal 7, (1961).

15. Hama, F. R., Soc. Naval Arch. and Marine Engineering Trans. 62, 333(1954).

16. Heat Transfer 1970, Fourth International Heat Transfer Conference, Paris-Versailles, Vol. II, Forced Convection, Sessions FC1-FC5, 1970.

17. Hinze, J. O., J. W. van Breugel and H. Leijdens, "The Turbulent Boundary Layer along a Saw-tooth Shaped Wall."

18. Kapitsa, P. L., J. Exper. and Theor. Phys. 18, 19(1948).

19. Kellerhals, R., J. Hyd. Div. Proc. ASCE HY1, 89, 201-202 (Jan. 1963).

20. Knudsen, J. G. and Katz, D. L., Chem. Eng. Prog. 46, 490 (1950).

21. Koch, R., VDI Forsch. B, 24, 469(1958).

22. Kolar, V., Int. J. Heat Mass Transfer 8, 639-653(1965).

23. Konobeev, V. I. and N. M. Zhavoronkov, Int. Chem. Eng. 2, No. 3, 431(July 1962).

24. Lamb, H., Hydrodynamics, 6th ed., Cambridge Univ. Press, (1932).

25. Lee, Y. W., Statistical Theory of Communication, Wiley, New York, (1967).

26. Liu, C. K., S. J. Kline, and J. P. Johnston, An Experimental Study of Turbulent Boundary Layers on Rough Walls, Thermosciences Div., Dept. Mech. Eng., Stanford Univ. Report MD-15 (July 1966).

27. Lock, R. C., Proc. Camb. Phil. Soc. 50, 105(1954).

28. May, J. C., Jr., Laws of Turbulent Flow in Rough Pipes, Ph. D. Dissertation, Virginia Polytechnic Inst., Hyd. Eng., (1967).

29. Miles, J. W., J. Fl. Mech. 3, 185(1957).

30. Möbius, H., Phys. Zeit. 41, 202-225(1940).

31. Moody, L. F., Trans. ASME 66, 671(1944).

32. Morris, H. M., Jr., Trans. ASCE 120, 373-410(1955).

33. Motzfeld, H., Z. Angew. Math. Mech. 17, 193(1937).

34. Norman, J. M., H. G. Bossy, Hydraulic Flow Resistance Factors for Corrugated Metal Conduits, U. S. Department of Transportation, Federal Highway Administration, Research and Devel. Report TD 2.2:H99 (Sept. 1970).

35. Nunner, W., VDI Forsch. 455 B 22, 5-39(1956).

36. Perry, A. E. and P. N. Joubert, J. Fl. Mech. 17, 193(1963).

37. Perry, A. E., W. H. Schofield and P. N. Joubert, J. Fl. Mech. 37, part 2, 383(1969).

38. Robertson, J. M., T. H. Burkhart and J. D. Martin, Univ. of Illinois, Urbana, Dept. of Theor. and Appl. Mech. Report T&A. M. No. 279, (May 1965).

39. Roshko, A., NACA TN 3488 (1955).

40. Rotta, J., Ing. Arch., Vol. 18, 277(1950).

41. Sacks, G. M., Proc. ASCE 84, HY3, Paper 1664 (1958).

42. Sams, E. W., NACA RM E52D17 (June 27, 1952).

43. Savage, D. W. and J. E. Myers, AIChE J. 9, No. 5, 695(Sept. 1963).

44. Schlicting, H., Ing. Arch. Vol. 7, No. 1, 1-34(1936).

45. Schlicting, H., Boundary-layer Theory, McGraw-Hill, 6th ed., New York (1968).

46. Sheriff, N. and P. Gumley, Int. J. Heat Mass Transfer 9, 1297-1320(1966).

47. Skoglund, V., J. Aero. Sci. 4, 28(Nov. 1936).

48. Smith, T. N. and R. W. F. Tait, Chem. Eng. Sci. 21, 63-65(1966).

49. Stanton, T., D. Marshall, and R. Houghton, Proc. Roy. Soc. of London A, No. 137, 283(1937).

50. Stevenson, M., Univ. of Maryland, College Park, Md. Technical Note BN-181, (Dec. 1959).

51. Straub, L. and H. M. Morris, Univ. of Minnesota, St. Anthony Falls Hyd. Lab. Tech. Paper No. 3, Series B (July 1950).

52. Streeter, V. L., Proc. ASCE 61, 163-186(1935).

53. Streeter, V. L. and H. Chu, Armour Research Foundation Report Project No. 4918 (Aug. 1949).

54. Sutherland, W. A., Int. J. Heat Mass Transfer 10, 1589-1599(1967).

55. Thring, M. W. and A. Atherton, Trans. Inst. Chem. Eng. 38, No. 5, 235-242(1960).

56. Tripp, W., J. Aero. Sci. 4, 10(Nov. 1936).

57. Verma, S. B. and J. E. Cermak, Technical Report, Fluid Dynamics and Diffusion Laboratory, College of Engineering, Colorado State Univ., Fort Collins, Report No. CER70-71SBV-JEC59 (May 1971).

58. Webster, M. J. and L. R. Metcalf, J. Hyd. Div. Proc. ASCE 85, HY9, Proc. Paper 2148, 35-67(Sept. 1959).

59. Williams, F. and Watts, J., Teat Transfer 1970, Fourth International Heat Transfer Conference, Paris-Versailles 1970, Vol. 2, Session 5, Paper FC5.5 (1970).

60. Worley, F. L., Jr., A Study of Roughness Effects in Turbulent Flow" Ph. D. thesis, Univ. of Houston, Dept. of Chem. Eng.(1965).

61. Wuest, W., Z. Angew. Math. Mech. 29, 239(1949).

62. Yost, A. M., M. S. Thesis, Univ. of Houston, Dept. of Chem. Eng. (1969).

63. Webb, R. L., E. R. G. Eckert, and R. J. Goldstein, Int. J. Heat Mass Transfer 14, 601-617(1971).

64. Nikuradse, J., VDI Forsch. 361 (1933). English translation NACA TM-1292(1965).

SUPPLEMENTARY BIBLIOGRAPHY

Harris, M. J. and J. T. Wilson, J. Brit. Nuclear Energy Conf. 6, 330-336(Oct. 1961).

Kapitsa, P. L., Collected Papers of P. L. Kapitsa, Vol. 2, 1938-1964, Pergamon Press, New York, D. ter Haar, ed. 1965.

Moore, W. L., Proc ASCE J. Hyd. Div. 85, HY3, 25(March 1959).

Robertson, J. M., Proc. 5th Midwest. Conf. oon Fl. Mech., Univ. of Mich. (site) 67-84(April 1957).

Sams, E. W., Reactor Heat Transfer Conf. of 1956, United States Atomic Energy Comm TID-7529 (part1), Book 2, 390(Nov. 1957).

Sheng-tien Hsu and J. F. Kennedy, "Turbulent Flow in Wavy Pipes", J. Fl. Mech. 47, part 3, 481-502(1971).

APPENDIX A

EXPERIMENTAL EQUIPMENT AND RESULTS

FIGURE 21. FLOW CHANNEL

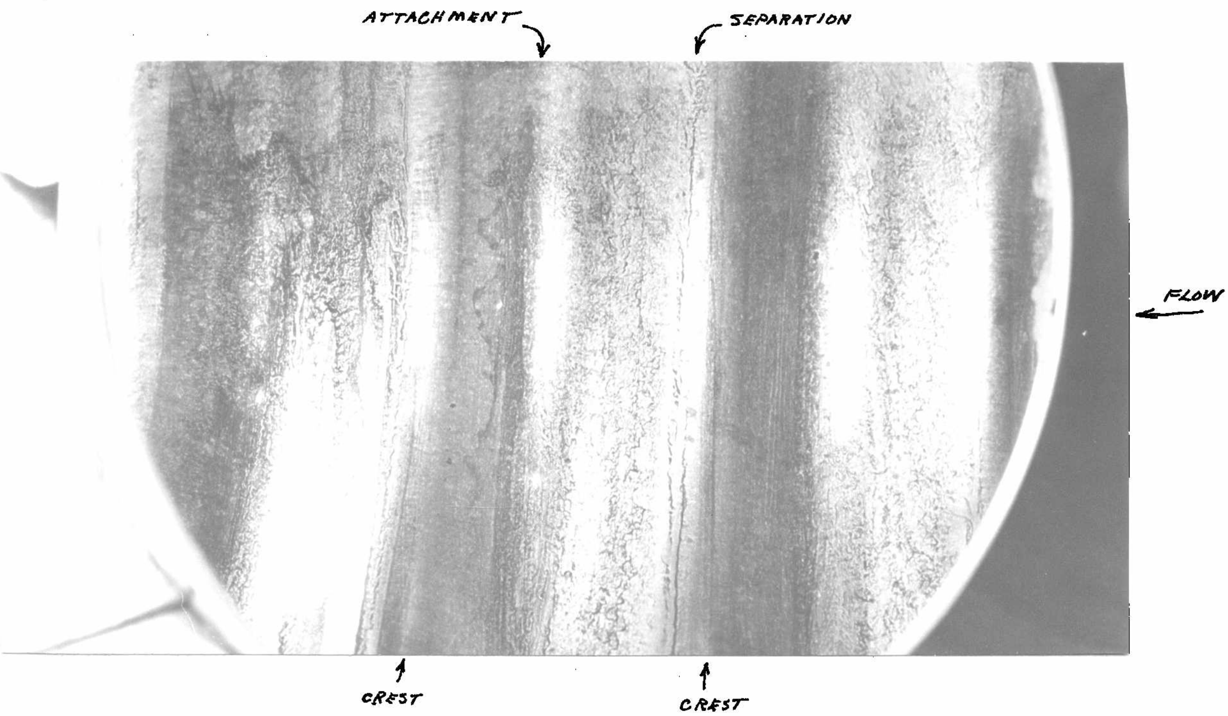

FIGURE 22. CARBON BLACK PATTERN OF VISUALIZATION EXPERIMENT FOR $60{,}000 < N_{Re} < 270{,}000$

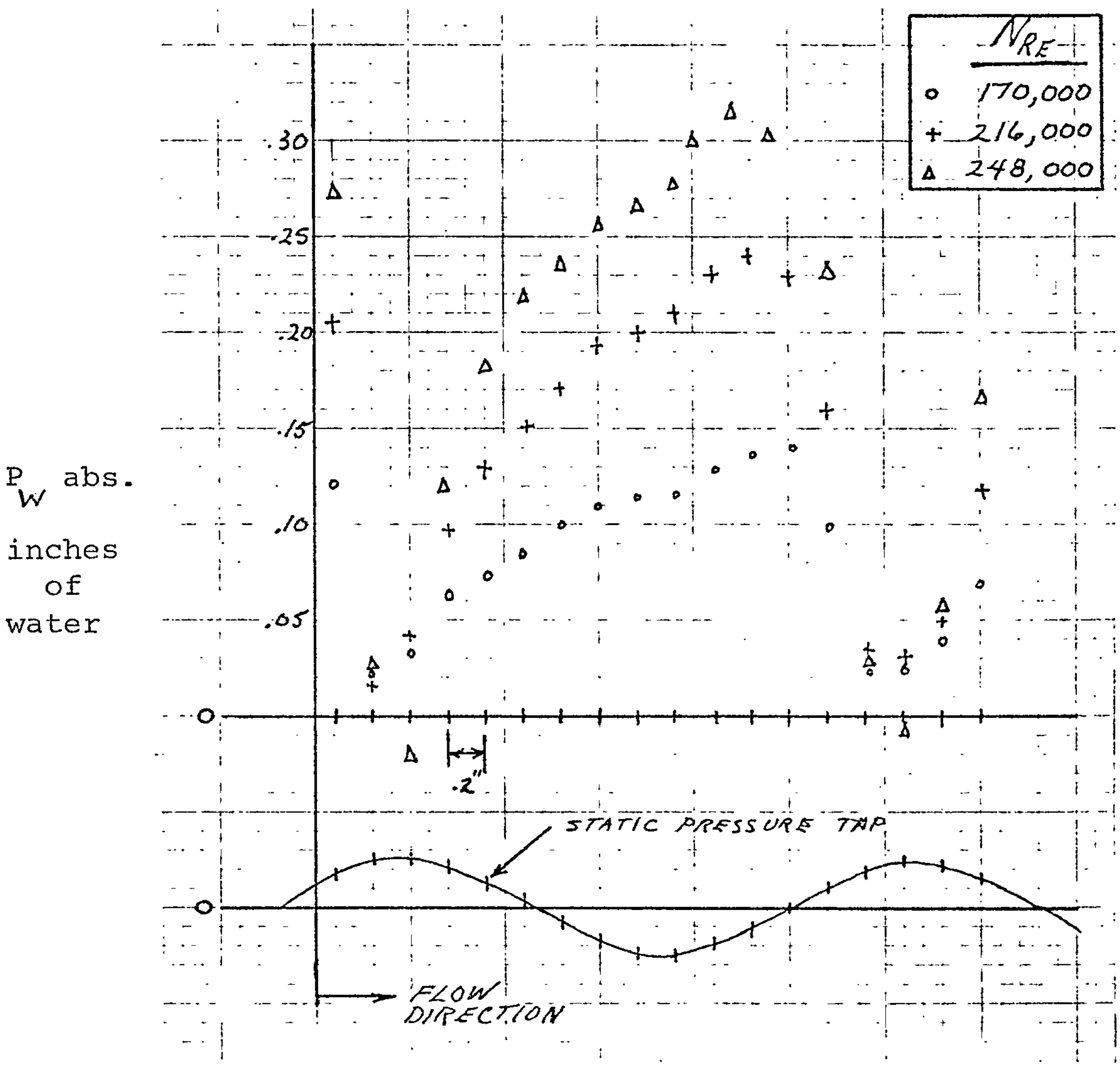

FIGURE 23. WALL STATIC PRESSURE DISTRIBUTION FOR 9" DIAMETER CORRUGATED PIPE

APPENDIX B

LISTING OF DATA USED IN THE CORRELATION OF PROJECTION ROUGHNESS

Dictionary of computer listing of data:

A	amplitude
DO	D_o
F	f, $\langle f \rangle$
FM	$f/(A/\lambda + \sqrt{A\lambda}/D_o + \lambda/D_o)$
LAMBDA	λ
N	identifying number of roughness system, usually corresponding to the author's original notation
NR	Reynolds number code: 14 = $1.\mathrm{x}10^4$, 275 = $2.7\ \mathrm{x}10^5$, etc.
Q	volumetric flow rate
R	$\lambda^2/\sigma D_o$
R12	$R_{12}(L)$
SIGMA	σ
T	length of roughness element

Dimensions of the lengths A, D_o, λ, T, and σ are given in inches, except for those of Konobeev and Zhavoronkov, Nunner, Koch, and Möbius, which are given in millimeters.

[illegible] SINE WAVE — 52

N	NR	DO	A	LAMBDA	T	R12	SIGMA	F	FM	FM*R12	R
1	14	15.790	0.4100	2.0000	0.0	1.000	0.1449	0.0557	0.1696	0.170E 00	0.175E 01
2	14	16.160	0.2400	2.0000	0.0	1.000	0.0849	0.0539	0.1880	0.188E 00	0.292E 01
3	14	15.080	0.7200	4.0000	0.0	1.000	0.2545	0.0911	0.1633	0.163E 00	0.417E 01
4	14	15.400	0.6000	4.0000	0.0	1.000	0.2121	0.0745	0.1538	0.154E 00	0.490E 01
5	14	15.900	0.3000	4.0000	0.0	1.000	0.1060	0.0442	0.1244	0.124E 00	0.949E 01
6	14	15.250	0.6500	8.0000	0.0	1.000	0.2298	[illegible]	0.1132	0.113E 00	0.183E 02
7	14	15.560	0.4400	8.0000	0.0	1.000	0.1555	[illegible]	0.0693	0.693E-01	0.264E 02
8	14	16.020	0.2900	8.0000	0.0	1.000	0.0990	0.0441	0.0701	0.701E-01	0.404E 02
9	14	15.080	0.7200	12.0000	0.0	1.000	0.2545	0.0713	0.0678	0.678E-01	0.375E 02
10	14	15.930	0.2700	12.0000	0.0	1.000	0.0954	0.0358	0.0414	0.414E-01	0.947E 02
12	14	16.230	0.1700	1.0000	0.0	1.000	0.0601	0.0456	0.1773	0.177E 00	0.103E 01
13	14	41.600	4.5000	24.0000	0.0	1.000	1.5907	0.1374	0.1357	0.136E 00	0.870E 01
14	14	10.680	0.4200	4.0000	0.0	1.000	0.1485	0.0925	0.1372	0.137E 00	0.101E 02
15	14	10.950	0.2500	4.0000	0.0	1.000	0.0884	0.0715	0.1377	0.138E 00	0.165E 02
16	14	10.750	0.3500	8.0000	0.0	1.000	0.1237	0.0511	0.0542	0.542E-01	0.481E 02
17	14	10.900	0.2000	8.0000	0.0	1.000	0.0707	0.0411	0.0470	0.470E-01	0.830E 02
18	14	42.450	3.7500	12.0000	0.0	1.000	1.3256	0.1179	0.1565	0.157E 00	0.256E 01
19	14	46.000	2.0000	5.0000	0.0	1.000	0.7070	0.0800	0.1400	0.140E 00	0.769E 00
20	14	48.200	0.8000	5.0000	0.0	1.000	0.2828	0.0534	0.1755	0.175E 00	0.183E 01
21	14	48.000	1.0000	3.0000	0.0	1.000	0.3535	0.0550	0.1274	0.127E 00	0.530E 00
22	14	48.300	0.7000	3.0000	0.0	1.000	0.2474	0.0434	0.1487	0.149E 00	0.753E 00
23	14	49.250	0.7500	2.0000	0.0	1.000	0.2651	0.0523	0.1194	0.119E 00	0.313E 00
24	14	48.600	0.4000	2.0000	0.0	1.000	0.1414	0.0365	0.1405	0.141E 00	0.562E 00
25	14	33.400	3.4000	25.0000	0.0	1.000	1.2726	0.1748	0.1528	0.153E 00	0.147E 02
26	14	18.300	2.0000	15.0000	0.0	1.000	0.7070	0.1563	0.1283	0.128E 00	0.169E 02
27	14	18.340	2.2500	25.7000	0.0	1.000	0.7954	0.0785	0.0412	0.412E-01	0.453E 02
1	15	15.790	0.4100	2.0000	0.0	1.000	0.1449	0.0557	0.1696	0.170E 00	0.175E 01
2	15	16.160	0.2400	2.0000	0.0	1.000	0.0848	0.0539	0.1880	0.188E 00	0.292E 01
3	15	15.080	0.7200	4.0000	0.0	1.000	0.2545	0.0911	0.1633	0.163E 00	0.417E 01
4	15	15.400	0.6000	4.0000	0.0	1.000	0.2121	0.0743	0.1457	0.146E 00	0.490E 01
5	15	15.900	0.3000	4.0000	0.0	1.000	0.1060	0.0432	0.1244	0.124E 00	0.949E 01
6	15	15.250	0.6500	8.0000	0.0	1.000	0.2298	0.0529	0.0698	0.698E-01	0.183E 02
7	15	15.560	0.4400	8.0000	0.0	1.000	0.1555	0.0339	0.0492	0.492E-01	0.264E 02
8	15	16.020	0.2900	8.0000	0.0	1.000	0.0990	0.0234	0.0330	0.330E-01	0.404E 02
9	15	15.080	0.7200	12.0000	0.0	1.000	0.2545	0.0343	0.0332	0.332E-01	0.375E 02
10	15	15.930	0.2700	12.0000	0.0	1.000	0.0954	0.0221	0.0248	0.248E-01	0.947E 02
12	15	16.230	0.1700	1.0000	0.0	1.000	0.0601	0.0455	0.1773	0.177E 00	0.103E 01
13	15	41.600	4.5000	24.0000	0.0	1.000	1.5907	0.1276	0.1357	0.136E 00	0.870E 01
14	15	10.690	0.4200	4.0000	0.0	1.000	0.1485	0.0627	0.1043	0.104E 00	0.101E 02
15	15	10.950	0.2500	4.0000	0.0	1.000	0.0884	0.0447	0.0860	0.860E-01	0.165E 02
16	15	10.750	0.3500	8.0000	0.0	1.000	0.1237	0.0273	0.0289	0.289E-01	0.481E 02
17	15	10.900	0.2000	8.0000	0.0	1.000	0.0707	0.0201	0.0230	0.230E-01	0.830E 02
18	15	42.450	3.7500	12.0000	0.0	1.000	1.3256	0.1179	0.1565	0.157E 00	0.256E 01
19	15	46.000	2.0000	5.0000	0.0	1.000	0.7070	0.0766	0.1330	0.133E 00	0.764E 00
20	15	48.200	0.8000	5.0000	0.0	1.000	0.2828	0.0525	0.1720	0.172E 00	0.183E 01
21	15	48.000	1.0000	3.0000	0.0	1.000	0.3535	0.0550	0.1274	0.127E 00	0.530E 00
22	15	48.300	0.7000	3.0000	0.0	1.000	0.2474	0.0454	0.1487	0.149E 00	0.753E 00
23	15	49.250	0.7500	2.0000	0.0	1.000	0.2651	0.0528	0.1194	0.119E 00	0.313E 00
24	15	48.600	0.4000	2.0000	0.0	1.000	0.1414	0.0365	0.1405	0.141E 00	0.562E 00
25	15	33.400	3.4000	25.0000	0.0	1.000	1.2726	0.1079	0.0917	0.917E-01	0.147E 02
26	15	18.500	2.0000	15.0000	0.0	1.000	0.7070	[illegible]	0.0740	0.740E-01	0.169E 02
27	15	18.340	2.2500	25.7000	0.0	1.000	0.7954	0.0415	0.0216	0.216E-01	0.453E 02

GADDIS SINE WAVE — 1

N	NR	DO	A	LAMBDA	T	R12	SIGMA	F	FM	FM*R12	R
1	15	8.500	0.5000	2.6700	0.0	1.000	0.1767	0.0344	0.1356	0.136E 00	0.475E 01

STREETER SINE WAVE — 3

N	NR	DO	A	LAMBDA	T	R12	SIGMA	F	FM	FM*R12	R
4	15	50.800	0.3350	1.1750	0.0	1.000	0.1574	0.0271	0.0576	0.576E-01	0.223E 00
6	15	50.800	0.4070	2.2100	0.0	1.000	0.1439	0.0350	0.1421	0.142E 00	0.668E 00
7	15	50.200	0.5600	2.2110	0.0	1.000	[illegible]	0.0592	0.1575	0.157E 00	[illegible]

MORRIS SINE WAVE — 2

N	NR	DO	A	LAMBDA	T	R12	SIGMA	F	FM	FM*R12	R
1	15	17.000	0.5000	2.6700	0.0	1.000	0.1767	0.0612	0.1444	0.144E 00	0.237E 01
2	15	23.000	0.5000	2.6700	0.0	1.000	0.1767	0.0545	0.1541	0.154E 00	0.175E 01

GIBSON SINE WAVE — 1

N	NR	DO	A	LAMBDA	T	R12	SIGMA	F	FM	FM*R12	R
1	15	1.900	0.1000	0.4000	0.0	1.000	0.0353	0.1160	0.1989	0.199E 00	0.251E 01

NORMAN AND BOSSY-SINE WAVE CORRUGATED PIPE,D/D**2.5=2 — 10

N	NR	DO	A	LAMBDA	T	R12	SIGMA	F	FM	FM*R12	R
1		24.000	0.5000	2.6700	0.0	1.000	0.1767	0.0930	0.2683	0.268E 00	0.168E 01
2		36.000	0.5000	2.6700	0.0	1.000	0.1767	0.0760	0.2559	0.259E 00	0.112E 01
3		48.000	0.5000	2.6700	0.0	1.000	0.1767	0.0690	0.2547	0.255E 00	0.840E 00
4		60.000	0.5000	2.6700	0.0	1.000	0.1767	0.0610	0.2430	0.243E 00	0.672E 00
5		72.000	0.5000	2.6700	0.0	1.000	0.1767	0.0570	0.2371	0.237E 00	0.560E 00
6		36.000	1.0000	6.0000	0.0	1.000	0.3535	0.1050	0.2616	0.262E 00	0.233E 01
7		48.000	1.0000	6.0000	0.0	1.000	0.3535	0.0930	0.2714	0.271E 00	0.212E 01
8		60.000	1.0000	6.0000	0.0	1.000	0.3535	0.0830	0.2699	0.270E 00	0.170E 01
9		72.000	1.0000	6.0000	0.0	1.000	0.3535	0.0770	0.2711	0.271E 00	0.141E 01
10		84.000	1.0000	6.0000	0.0	1.000	0.3535	0.0720	0.2694	0.269E 00	0.121E 01

NORMAN AND BOSSY-SINE WAVE CORRUGATED PIPE,D/D**2.5=4 — 21

N	NR	DO	A	LAMBDA	T	R12	SIGMA	F	FM	FM*R12	R
1		24.000	0.5000	2.6700	0.0	1.000	0.1767	0.0900	0.2596	0.260E 00	0.168E 01
2		36.000	0.5000	2.6700	0.0	1.000	0.1767	0.0730	0.2487	0.249E 00	0.112E 01
3		48.000	0.5000	2.6700	0.0	1.000	0.1767	0.0640	0.2397	0.240E 00	0.840E 00
4		60.000	0.5000	2.6700	0.0	1.000	0.1767	0.0580	0.2311	0.231E 00	0.672E 00
5		72.000	0.5000	2.6700	0.0	1.000	0.1767	0.0530	0.2205	0.220E 00	0.560E 00
6		36.000	1.0000	6.0000	0.0	1.000	0.3535	0.1010	0.2516	0.252E 00	0.243E 01
7		48.000	1.0000	6.0000	0.0	1.000	0.3535	0.0895	0.2612	0.261E 00	0.212E 01
8		60.000	1.0000	6.0000	0.0	1.000	0.3535	0.0800	0.2602	0.260E 00	0.170E 01
9		72.000	1.0000	6.0000	0.0	1.000	0.3535	0.0725	0.2563	0.256E 00	0.141E 01
10		84.000	1.0000	6.0000	0.0	1.000	0.3535	0.0680	0.2544	0.254E 00	0.121E 01
11		72.000	2.0000	6.0000	0.0	1.000	0.7070	0.1020	0.2195	0.219E 00	0.707E 00
12		96.000	2.0000	6.0000	0.0	1.000	0.7070	[illegible]	[illegible]	0.204E 00	0.530E 00
13		120.000	2.0000	6.0000	0.0	1.000	0.7070	0.0790	0.1917	0.192E 00	0.424E 00
14		[illegible]	2.0000	6.0000	0.0	1.000	0.7070	[illegible]	0.1673	0.167E 00	0.265E 00
15		244.000	2.0000	6.0000	0.0	1.000	0.7070	0.0520	0.1559	0.156E 00	[illegible]
16		36.000	1.0000	3.0000	0.0	1.000	0.3535	0.1000	0.2152	0.215E 00	0.707E 00
17		72.000	1.0000	3.0000	0.0	1.000	0.3535	0.0730	[illegible]	0.133E 00	0.354E 00
18		[illegible]	1.0000	3.0000	0.0	1.000	0.3535	0.0510	0.1617	0.162E 00	0.236E 00
19		[illegible]	2.0000	[illegible]	0.0	1.000	[illegible]	[illegible]	[illegible]	[illegible]	[illegible]
20		[illegible]	2.5000	[illegible]	0.0	1.000	0.8837	[illegible]	0.2281	0.228E 00	[illegible]
21		[illegible]	2.5000	9.0000	0.0	1.000	[illegible]	[illegible]	0.2114	0.211E 00	[illegible]

SINE WAVE ROUGHNESS

STEVENSON WIRE ROUGHNESS 5

N	NR	DO	A	LAMBDA	T	R12	SIGMA	F	FM	FM*R12	R
1	15	7.430	0.0420	12.0000	0.0420	0.083	0.0022	0.0210	0.0123	0.102E-02	0.669E 04
2	15	7.430	0.0420	6.0000	0.0420	0.118	0.0031	0.0256	0.0290	0.342E-02	0.154E 04
3	15	7.430	0.0420	3.0000	0.0420	0.169	0.0044	0.0355	0.0765	0.130E-01	0.273E 03
4	15	7.430	0.0420	1.5000	0.0420	0.240	0.0062	0.0435	0.1650	0.395E-01	0.485E 02
5	15	7.430	0.0420	0.7500	0.0230	0.341	0.0087	0.0560	0.3097	0.106E 00	0.872E 01

SACKS WIRE ROUGHNESS 15

N	NR	DO	A	LAMBDA	T	R12	SIGMA	F	FM	FM*R12	R
1	414	2.000	0.0100	1.0000	0.0100	0.141	0.0039	0.0266	0.0479	0.673E-02	0.558E 03
2	414	2.000	0.0100	2.0000	0.0100	0.099	0.0026	0.0256	0.0235	0.237E-02	0.315E 04
3	414	2.000	0.0100	4.0000	0.0100	0.070	0.0024	0.0244	0.0116	0.816E-03	0.179E 05
4	414	2.000	0.0100	6.0000	0.0100	0.057	0.0004	0.0230	0.0074	0.422E-03	0.487E 05
5	414	2.000	0.0100	8.0000	0.0100	0.050	0.0003	0.0226	0.0053	0.264E-03	0.101E 06
1	15	2.000	0.0100	1.0000	0.0100	0.141	0.0019	0.0260	0.0464	0.653E-02	0.558E 03
2	15	2.000	0.0100	2.0000	0.0100	0.099	0.0036	0.0222	0.0206	0.205E-02	0.315E 04
3	15	2.000	0.0100	4.0000	0.0100	0.070	0.0004	0.0200	0.0095	0.669E-03	0.179E 05
4	15	2.000	0.0100	6.0000	0.0100	0.057	0.0004	0.0194	0.0062	0.356E-03	0.489E 05
5	15	2.000	0.0100	8.0000	0.0100	0.050	0.0003	0.0198	0.0045	0.226E-03	0.101E 06
1	215	2.000	0.0100	1.0000	0.0100	0.141	0.0009	0.0250	0.0446	0.628E-02	0.558E 03
2	215	2.000	0.0100	2.0000	0.0100	0.099	0.0004	0.0208	0.0193	0.192E-02	0.315E 04
3	215	2.000	0.0100	4.0000	0.0100	0.070	0.0004	0.0192	0.0087	0.609E-03	0.179E 05
4	215	2.000	0.0100	6.0000	0.0100	0.057	0.0004	0.0174	0.0056	0.319E-03	0.489E 05
5	215	2.000	0.0100	8.0000	0.0100	0.050	0.0003	0.0168	0.0041	0.202E-03	0.101E 06

NUNNER HALF-ROUND 10

N	NR	DO	A	LAMBDA	T	R12	SIGMA	F	FM	FM*R12	R
2	14	46.000	2.0000	150.0000	2.0000	0.217	0.2569	0.0385	0.0099	0.216E-02	0.217E 04
3	14	46.000	2.0000	40.0000	2.0000	0.446	0.4929	0.0959	0.0779	0.349E-01	0.707E 02
4	14	42.000	4.0000	80.0000	4.0000	0.446	0.9540	0.1030	0.0433	0.193E-01	0.155E 03
5	14	42.000	4.0000	40.0000	4.0000	0.641	1.3180	0.1270	0.0939	0.602E-01	0.289E 02
6	14	42.000	4.0000	20.0000	4.0000	0.844	1.6400	0.1345	0.1513	0.134E 00	0.581E 01
2	714	46.000	2.0000	150.0000	2.0000	0.217	0.2560	0.0320	0.0082	0.179E-02	0.217E 04
3	714	46.000	2.0000	40.0000	2.0000	0.445	0.4920	0.0825	0.0741	0.330E-01	0.707E 02
4	714	42.000	4.0000	80.0000	4.0000	0.446	0.9540	0.1040	0.0437	0.195E-01	0.155E 03
5	714	42.000	4.0000	40.0000	4.0000	0.641	1.3180	0.1475	0.1090	0.699E-01	0.289E 02
6	714	42.000	4.0000	20.0000	4.0000	0.894	1.6400	0.1450	0.1631	0.144E 00	0.581E 01

NUNNER ORIFICE 2

N	NR	DO	A	LAMBDA	T	R12	SIGMA	F	FM	FM*R12	R
1	14	46.000	2.0000	40.0000	2.5000	0.376	0.4941	0.1065	0.0956	0.360E-01	0.719E 02
1	714	46.000	2.0000	40.0000	2.5000	0.363	0.4541	0.1130	0.1014	0.368E-01	0.718E 02

SAMS SQUARE THREAD---PROJECTION TYPE 1

N=	NR	DO	A	LAMBDA	T	R12	SIGMA	F	FM	FM*R12	R
1	15	0.500	0.0065	0.0094	0.0047	0.900	0.0032	0.0504	0.0694	0.625E-01	0.544E-01

STREETER AND CHU--- SQUARE THREAD:ORIFICE TYPE 2

N	NR	DO	A	LAMBDA	T	R12	SIGMA	F	FM	FM*R12	R
4(III)	15	4.547	0.0510	0.2210	0.0550	0.734	0.0221	0.0677	0.2236	0.164E 00	0.487E 00
5(III)	15	4.547	0.0510	0.4430	0.0550	0.519	0.0165	0.0953	0.3880	0.201E 00	0.257E 01

KOCH ORIFICE ROUGHNESS NRE=100000 7

N	NR	DO	A	LAMBDA	T	R12	SIGMA	F	FM	FM*R12	R
6	14	40.000	5.0000	40.0000	1.0000	0.204	0.7070	0.2621	0.1526	0.311E-01	0.849E 02
7	14	40.000	5.0000	325.0000	1.0000	0.079	0.2759	0.0734	0.0082	0.647E-03	0.954E 04
8	14	40.000	5.0000	980.0000	1.0000	0.045	0.1595	0.0225	0.0011	0.497E-04	0.150E 06
10	14	30.000	10.0000	95.0000	1.0000	0.144	1.0050	0.3898	0.0881	0.127E-01	0.319E 03
11	14	30.000	10.0000	327.0000	1.0000	0.078	0.5522	0.1477	0.0115	0.902E-03	0.645E 04
12	14	30.000	10.0000	990.0000	1.0000	0.045	0.3193	0.0467	0.0013	0.585E-04	0.100E 06
13	14	25.000	12.5000	325.0000	1.0000	0.079	0.6923	0.1156	0.0074	0.583E-03	0.616E 04

MOBIUS ORIFICE ROUGHNESS 12

N	NR	DO	A	LAMBDA	T	R12	SIGMA	F	FM	FM*R12	R
1	15	4.499	0.2500	2.5000	0.2500	0.464	0.0750	0.1597	0.1921	0.891E-01	0.135E 02
2	15	4.497	0.2500	4.7500	0.2500	0.332	0.0558	0.1271	0.0911	0.302E-01	0.899E 02
3	15	4.494	0.2500	9.2500	0.2500	0.235	0.0435	0.0839	0.0346	0.814E-02	0.470E 03
4	15	4.594	0.1429	4.7500	0.2500	0.332	0.0332	0.0597	0.0422	0.140E-01	0.148E 03
5	15	3.900	0.5491	4.7500	0.2500	0.332	0.1226	0.2913	0.1609	0.534E-01	0.472E 02
6	15	4.853	0.0742	4.7500	0.2500	0.332	0.0156	0.0295	0.0264	0.879E-02	0.281E 03
7	15	4.273	0.3475	10.2500	0.3500	0.265	0.0631	0.1123	0.0391	0.104E-01	0.389E 03
8	15	4.674	0.1499	2.9500	0.1500	0.332	0.0335	0.0951	0.1186	0.394E-01	0.519E 02
9	15	4.810	0.0727	1.4250	0.0750	0.332	0.0152	0.0655	0.1582	0.525E-01	0.260E 02
10	15	4.935	0.0982	1.9000	0.1000	0.332	0.0219	0.0914	0.1745	0.579E-01	0.334E 02
11	15	9.360	0.4995	5.0000	0.5000	0.464	0.1495	0.2020	0.2517	0.117E 00	0.179E 02
12	15	8.020	0.4985	9.5000	0.5000	0.332	0.1113	0.1172	0.0861	0.286E-01	0.909E 02

MAY--ORIFICE TYPE 17

N	NR	DO	A	LAMBDA	T	R12	SIGMA	F	FM	FM*R12	R
15	15	2.755	0.2379	2.4390	0.4890	0.656	0.0743	0.1500	0.1252	0.821E-01	0.238E 02
17	15	3.196	0.2613	2.2500	0.2500	0.470	0.0521	0.2030	0.1517	0.424E-01	0.193E 02
16	15	3.196	0.2613	4.2500	0.2500	0.342	0.0612	0.1730	0.0988	0.347E-01	0.922E 02
19	15	3.196	0.2603	8.2500	0.2500	0.250	0.0445	0.1200	0.0391	0.975E-02	0.477E 03
20	15	3.196	0.2603	16.2500	0.2500	0.177	0.0320	0.0700	0.0122	0.215E-02	0.258E 04
21	15	3.196	0.2603	32.2500	0.2500	0.125	0.0229	0.0390	0.0035	0.443E-03	0.143E 05
22	15	2.755	0.4976	4.4890	0.4890	0.425	0.1550	0.2600	0.1139	0.552E-01	0.472E 02
23	15	2.755	0.4977	8.4890	0.4890	0.349	0.1160	0.2200	0.0565	0.197E-01	0.226E 03
24	15	2.755	0.4976	16.4900	0.4890	0.247	0.0844	0.1400	0.0198	0.490E-02	0.117E 04
25	15	2.755	0.4976	32.4890	0.4890	0.175	0.0606	0.0730	0.0055	0.962E-03	0.632E 04
26	15	2.755	0.4976	64.4890	0.4890	0.124	0.0432	0.0370	0.0015	0.180E-03	0.350E 05
27	15	2.248	0.7696	6.7550	0.7550	0.491	0.2397	0.2950	0.0679	0.334E-01	0.647E 02
28	15	2.248	0.7696	12.7550	0.7550	0.353	0.1795	0.2000	0.0281	0.991E-02	0.403E 03
29	15	2.248	0.7696	24.7550	0.7550	0.259	0.1309	0.1230	0.0092	0.232E-02	0.206E 04
30	15	1.751	1.0030	9.0200	1.0200	0.494	0.3176	0.2230	0.0315	0.156E-01	0.146E 03
31	15	1.751	1.0030	17.0200	1.0200	0.358	0.2351	0.1400	0.0114	0.409E-02	0.695E 03
32	15	1.751	1.0030	33.0200	1.0200	0.262	0.1735	0.0760	0.0034	0.864E-03	0.359E 04

SAVAGE--FIN ROUGHNESS , PROJECTION TYPE 6

N	NR	DO	A	LAMBDA	T	R12	SIGMA	F	FM	FM*R12	R
6	15	4.065	1.0000	[illegible]	0.0980	0.117	[illegible]	0.3255	0.0781	0.912E-02	0.507E 03
5	15	4.065	[illegible]	[illegible]	[illegible]	0.149	0.1047	0.344	0.1251	0.187E-01	0.151E 03
19	15	5.565	0.2500	[illegible]	[illegible]	[illegible]	[illegible]	0.114	[illegible]	0.113E 00	0.472E [illegible]
20	15	5.565	0.2500	[illegible]	0.0880	0.434	0.0700	0.151	[illegible]	0.127E 00	0.254E 01
21	15	5.565	0.2500	[illegible]	[illegible]	[illegible]	0.317	0.177	[illegible]	0.551E-01	0.140E 02
22	15	5.565	0.2500	[illegible]	[illegible]	0.246	[illegible]	[illegible]	[illegible]	0.530E-01	0.253E 02

PROJECTION ROUGHNESS

APPENDIX C

LISTING OF DATA USED IN THE CORRELATION OF GROOVE ROUGHNESS

Dictionary of computer listing of data:

A	amplitude
DO	D_o
F	f, $\langle f \rangle$
FM	$f \cdot (P/S + \sqrt{AP}/D_o + \sqrt{P/D_o})$
LAMBDA	λ
N	identifying number of roughenss system, usually corresponding to the author's original notation
NR	Reynolds number code: 14 = $1.\times10^4$, 275 = 2.7×10^5, etc.
R	P^2/TD_o
R12	$R_{12}(0)$
SIGMA	σ
T	length of roughness element

Dimensions of the lengths A, D_o, λ, T, and σ are given in inches, except for those of Kolar and Koch, which are given in millimeters.

MAY RECTANGULAR GROOVE 32

N	NR	DU	A	LAMBDA	T	R12	SIGMA	F	FM	FM/R12	P
1	15	3.196	0.2593	0.5000	0.2500	0.825	0.0156	0.0340	0.0230	0.278E-01	0.792E-01
2	15	2.755	0.5023	0.9890	0.4890	0.824	0.0125	0.0430	0.0369	0.448E-01	0.186E 00
3	15	2.248	0.7595	1.5050	0.7550	0.826	[illegible]	[illegible]	0.0557	0.675E-01	0.331E 00
4	15	1.751	1.0040	2.0200	1.0200	0.827	0.2500	0.0540	0.0851	0.103E 00	0.560E 00
5	15	3.196	0.2350	0.7500	0.2500	0.766	0.0139	0.0620	0.0558	0.726E-01	0.313E 00
6	15	2.755	0.2373	0.9890	0.4890	0.924	0.0156	0.0530	0.0473	0.574E-01	0.186E 00
7	15	2.755	0.4965	1.2390	0.4890	0.792	0.0507	0.0700	0.0755	0.953E-01	0.418E 00
8	15	2.755	0.4992	1.4890	0.4890	0.764	0.0551	0.0760	0.0958	0.125E 00	0.742E 00
9	15	2.248	0.7620	2.2550	0.7550	0.747	0.1253	0.1350	0.1774	0.231E 00	0.133E 01
10	15	1.751	1.0041	3.0200	1.0200	0.759	0.2236	0.1300	0.2959	0.385E 00	0.224E 01
11	15	3.196	0.2521	1.2500	0.2500	0.679	0.0100	0.1370	0.1668	0.246E 00	0.125E 01
12	15	2.755	0.2373	1.4890	0.4890	0.764	0.0138	0.1050	0.1353	0.177E 00	0.742E 00
13	15	2.248	0.7511	3.7550	0.7550	0.680	[illegible]	0.1790	0.4073	0.599E 00	0.530E 01
14	15	1.751	1.0031	5.0200	1.0200	0.637	0.1618	0.1720	0.5482	0.804E 00	0.896E 01
16	15	2.755	0.4986	2.4890	0.4890	0.676	0.0499	0.1720	0.3640	0.450E 00	0.297E 01
15	15	2.755	0.2373	2.4890	0.4890	0.676	0.0335	0.1600	0.2543	0.421E 00	0.297E 01
17	15	3.196	0.2613	2.2500	0.2500	0.567	0.0052	0.2300	0.3477	0.613E 00	0.501E 01
18	15	3.196	0.2603	4.2500	0.2500	0.449	0.0035	0.1700	0.3670	0.863E 00	0.200E 02
19	15	3.196	0.2603	8.2500	0.2500	0.338	0.0018	0.1200	0.3535	0.105E 01	0.601E 02
20	15	3.196	0.2603	16.2500	0.2500	0.247	0.0009	0.0730	0.2691	0.109E 01	0.320E 03
21	15	3.196	0.2603	32.2500	0.2500	0.177	0.0005	0.0390	0.1967	0.111E 01	0.128E 04
22	15	2.755	0.4976	4.4890	0.4890	0.563	0.0242	0.2600	0.6361	0.113E 01	0.119E 02
23	15	2.755	0.4977	8.4890	0.4890	0.445	0.0136	0.2200	0.7196	0.162E 01	0.475E 02
24	15	2.755	0.4976	16.4900	0.4890	0.335	0.0072	0.1450	0.6089	0.182E 01	0.190E 03
25	15	2.755	0.4976	32.4890	0.4890	0.246	0.0037	0.0730	0.4243	0.173E 01	0.760E 03
26	15	2.755	0.4976	64.4890	0.4890	0.175	0.0018	0.0370	0.2903	0.166E 01	0.304E 04
27	15	2.248	0.7506	6.7550	0.7550	0.568	0.0558	0.2830	0.9265	0.163E 01	0.212E 02
28	15	2.248	0.7506	12.7550	0.7550	0.449	0.0312	0.2000	0.8990	0.200E 01	0.848E 02
29	15	2.248	0.7506	24.7550	0.7550	0.339	0.0165	0.1200	0.7298	0.215E 01	0.339E 03
30	15	1.751	1.0030	9.0200	1.0200	0.571	0.1002	0.2200	0.9858	0.173E 01	0.358E 02
31	15	1.751	1.0030	17.0200	1.0200	0.451	0.0542	0.1400	0.8612	0.191E 01	0.143E 03
32	15	1.751	1.0030	33.0200	1.0200	0.341	0.0299	0.0750	0.6402	0.188E 01	0.573E 03

SAMS SQUARE THREAD 2

N	NR	DU	A	LAMBDA	T	R12	SIGMA	F	FM	FM/R12	R
2	15	0.500	0.0095	0.0195	0.0085	0.806	0.0000	0.0432	0.0196	0.244E-01	0.285E-01
3	15	0.500	0.0042	0.0094	0.0047	0.827	0.0000	0.0240	0.0089	0.107E-01	0.940E-02

STREETER AND CHU----SQUARE THREAD ,GROOVE-LIKE 3

N	NR	DO	A	LAMBDA	T	R12	SIGMA	F	FM	FM/R12	R
1(I_r)	15	4.547	0.0255	0.0555	0.0273	0.823	0.0002	0.0260	0.0093	0.119E-01	0.641E-02
2(I_m)	15	4.547	0.0510	0.1110	0.0550	0.824	0.0007	0.0290	0.0112	0.136E-01	0.125E-01
3(I_L)	15	4.538	0.0920	0.2090	0.0990	0.824	0.0021	0.0290	0.0126	0.153E-01	0.227E-01

TRIPP SQUARE GROOVE 2

N	NR	DO	A	LAMBDA	T	R12	SIGMA	F	FM	FM/R12	P
108	15	2.060	0.1250	0.6250	0.5000	0.880	0.0025	0.0270	0.0121	0.138E-01	0.152E-01
205	15	3.800	0.1250	0.6250	0.5000	0.880	0.0025	0.0224	0.0081	0.926E-02	0.822E-02

KOLAR V-GROOVE ROUGHNESS 3

N	NR	DU	A	LAMBDA	T	R12	SIGMA	F	FM	FM/R12	R
1	15	26.000	0.5000	0.8000	0.2000	0.979	0.0287	0.0390	0.0197	0.202E-01	0.692E-01
2	15	26.000	1.0000	1.6000	0.4000	0.981	0.1150	0.0515	0.0304	0.310E-01	0.138E 00
3	15	26.000	1.5000	2.4000	0.6000	0.932	0.2580	0.0608	0.0401	0.408E-01	0.206E 00

SKOGLUND V-GROOVE 2

N	NR	DO	A	LAMBDA	T	R12	SIGMA	F	FM	FM/R12	R
1	15	0.479	0.0125	0.0650	0.0475	0.922	0.0000	0.0430	0.0144	0.147E-01	0.688E-02
2	15	0.920	0.0125	0.0600	0.0475	0.962	0.0000	0.0350	0.0097	0.998E-02	0.358E-02

KOCH--GROOVE TYPE 2

N	NR	DU	A	LAMBDA	T	R12	SIGMA	F	FM	FM/R12	R
5	14	40.000	5.0000	19.6000	1.0000	0.423	1.2100	0.2294	0.3559	0.841E 00	0.865E 01
9	14	30.000	16.0000	39.2000	1.0000	0.313	2.4755	0.2333	0.5657	0.181E 01	0.486E 02

SAVAGE--FIN ROUGHNESS , GROOVE TYPE 15

N	NR	DU	A	LAMBDA	T	R12	SIGMA	F	FM	FM/R12	P
1	15	4.065	1.0000	1.0000	0.0580	0.522	0.0291	0.1440	0.1458	0.279E 00	0.233E 01
2	15	4.065	1.0000	2.0000	0.0880	0.397	0.0419	0.1830	0.2743	0.716E 00	0.102E 02
3	15	4.065	1.0000	3.0000	0.0880	[illegible]	0.0283	0.2510	0.4440	0.139E 01	0.237E 02
4	15	4.065	1.0000	5.0000	0.0880	0.273	0.0171	0.3210	0.7531	0.286E 01	0.574E 02
5	15	4.065	1.0000	[illegible]	0.0880	0.210	[illegible]	0.3490	1.0045	0.478E 01	0.175E 03
6	15	4.065	1.0000	13.0000	0.0880	0.166	0.0065	[illegible]	[illegible]	0.426E 01	0.466E 03
8	15	4.565	0.7500	[illegible]	0.0880	0.655	[illegible]	0.1120	0.0741	0.113E 00	0.423E 00
10	15	4.565	0.7500	[illegible]	0.0880	0.333	0.0159	0.2560	0.4570	0.136E 01	0.211E 02
11	15	4.565	0.7500	[illegible]	0.0880	0.273	[illegible]	[illegible]	[illegible]	0.248E 01	0.601E 02
12	15	4.565	0.7500	[illegible]	0.0880	0.210	[illegible]	0.2720	0.7296	0.347E 01	0.156E 03
14	15	5.065	[illegible]	[illegible]	0.0880	0.655	0.0362	[illegible]	[illegible]	0.123E 00	0.341E 00
15	15	5.065	[illegible]	[illegible]	0.0880	0.522	[illegible]	0.1440	0.1460	0.279E 00	0.187E 01
16	15	5.065	[illegible]	[illegible]	[illegible]	0.333	[illegible]	[illegible]	0.4346	0.130E 01	0.130E 02
17	15	5.065	[illegible]	[illegible]	[illegible]	0.210	[illegible]	[illegible]	0.5114	0.243E 01	0.140E 03
19	15	5.565	[illegible]	[illegible]	0.0880	0.655	[illegible]	[illegible]	[illegible]	0.135E 00	0.347E 00
20	15	5.565	[illegible]	[illegible]	[illegible]	0.522	[illegible]	[illegible]	[illegible]	0.325E 00	0.170E 01
21	15	5.565	[illegible]	[illegible]	[illegible]	0.397	[illegible]	[illegible]	0.2437	0.634E 00	0.746E 01
22	15	5.565	[illegible]	[illegible]	[illegible]	[illegible]	[illegible]	[illegible]	0.2871	0.862E 00	0.173E 02

GROOVE ROUGHNESS

APPENDIX D

STATISTICAL ANALYSIS OF REGIONS OF FRICTION FACTOR CORRELATIONS

Dictionary of computer listings:

BO	β_0 --intercept in straight line least squares fit
B1	β_1 -- slope in straight line least squares fit
F	F-statistic calculated by MSR/MSSR
FS	F-statistic from χ^2 distribution
MSR	mean square due to regression = $\sum(Y_i-\bar{Y})^2$
MSSR	mean square about regression = $\sum(Y_i-YHAT_i)^2/(NP-2)$
NP	number of data points
REG	region
SUMSQ	sum of squares about regression = $\sum(Y_i-YHAT_i)^2$
TV	"Student t" statistic
Y	value of ordinate, from data
YHAT	value of ordinate, from least squares estimate
$\bar{Y}$	mean value of Y = $\sum Y_i/NP$
95% Y+	upper 95% confidence value of the mean
95% Y-	lower 95% confidence value of the mean
X	value of abscissa

LOG X	Y	YHAT	Y-YHAT	95% Y+	95% Y-
-1.2646	0.0625	0.0629	-0.0004	0.0631	0.0627
-0.6517	0.0976	0.1178	-0.0202	0.1175	0.0981
-0.5047	0.1174	0.1146	0.0028	0.1160	0.1132
-0.5141	0.1174	0.1165	0.0008	0.1170	0.1152
-0.3262	0.1131	0.1317	-0.0187	0.1404	0.1231
-0.3137	0.1575	0.1327	0.0248	0.1442	0.1211
-0.3124	0.1641	0.1327	0.0313	0.1473	0.1182
-0.2754	0.1274	0.1355	-0.0081	0.1392	0.1317
-0.2754	0.1274	0.1355	-0.0081	0.1392	0.1317
-0.2351	0.1405	0.1384	0.0021	0.1394	0.1374
-0.2351	0.1405	0.1384	0.0021	0.1394	0.1374
-0.1751	0.1421	0.1425	-0.0007	0.1432	0.1425
-0.1232	0.1487	0.1466	0.0021	0.1476	0.1457
-0.1232	0.1487	0.1466	0.0021	0.1476	0.1457
-0.1142	0.1400	0.1473	-0.0073	0.1507	0.1439
-0.1142	0.1330	0.1473	-0.0143	0.1539	0.1406
0.0100	0.1773	0.1564	0.0208	0.1662	0.1467
0.0100	0.1773	0.1564	0.0208	0.1662	0.1467
0.2425	0.1696	0.1734	-0.0038	0.1753	0.1716
0.2425	0.1696	0.1734	-0.0038	0.1753	0.1716
0.2437	0.1541	0.1735	-0.0194	0.1828	0.1643
0.2634	0.1720	0.1750	-0.0030	0.1764	0.1735
0.2634	0.1750	0.1750	0.0000	0.1750	0.1750

REG= 1 B0=0.15565 B1=0.07334 NP= 23 SUMSQ=0.0097
MSR= 0.146E-01 MSSR=.00000 TV=2.06 F= 0.156E 09 FS=4.33

REGION 1

LOG X	Y	YHAT	Y-YHAT	95% Y+	95% Y-
0.3752	0.1484	0.1805	-0.0321	0.1900	0.1711
0.4005	0.1939	0.1730	0.0209	0.1841	0.1718
0.4044	0.1269	0.1776	-0.0507	0.1925	0.1626
0.4081	0.1565	0.1772	-0.0207	0.1833	0.1711
0.4081	0.1565	0.1772	-0.0207	0.1833	0.1711
0.4093	0.2014	0.1771	0.0244	0.1842	0.1699
0.4659	0.1880	0.1714	0.0166	0.1762	0.1665
0.4659	0.1880	0.1714	0.0166	0.1762	0.1665
0.5201	0.1631	0.1555	0.0077	0.1578	0.1533
0.5201	0.1631	0.1555	0.0077	0.1578	0.1533
0.6762	0.1356	0.1498	-0.0142	0.1539	0.1457
0.6901	0.1538	0.1484	0.0054	0.1499	0.1468
0.6901	0.1457	0.1484	-0.0027	0.1492	0.1476
0.7640	0.1441	0.1409	0.0033	0.1418	0.1399
0.7640	0.1337	0.1409	-0.0072	0.1429	0.1388
0.9397	0.1357	0.1229	0.0128	0.1266	0.1192
0.9397	0.1357	0.1229	0.0128	0.1266	0.1192
0.9466	0.1056	0.1223	-0.0172	0.1278	0.1179
0.9772	0.1244	0.1191	0.0053	0.1206	0.1176
0.9772	0.1244	0.1191	0.0053	0.1206	0.1176
1.0031	0.1372	0.1164	0.0209	0.1224	0.1104
1.0031	0.1043	0.1164	-0.0121	0.1198	0.1129
1.1467	0.0851	0.1018	-0.0167	0.1066	0.0970
1.1674	0.1529	0.0997	0.0532	0.1149	0.0844
1.1674	0.0917	0.0997	-0.0080	0.1020	0.0974
1.2144	0.1377	0.0945	0.0432	0.1069	0.0821
1.2184	0.0859	0.0945	-0.0084	0.0969	0.0920
1.2284	0.1283	0.0934	0.0347	0.1034	0.0834
1.2286	0.0760	0.0934	-0.0174	0.0990	0.0878
1.2517	0.1167	0.0910	0.0257	0.0984	0.0837
1.2614	0.1182	0.0901	0.0281	0.0981	0.0820
1.2616	0.0638	0.0901	-0.0262	0.0959	0.0842
1.2677	0.0891	0.0894	-0.0004	0.0895	0.0893
1.2853	0.0924	0.0876	0.0048	0.0890	0.0863
1.3775	0.0821	0.0782	0.0039	0.0793	0.0771
1.4151	0.0525	0.0744	-0.0217	0.0807	0.0681
1.4223	0.0883	0.0736	0.0146	0.0779	0.0694
1.4223	0.0492	0.0736	-0.0245	0.0807	0.0666
1.4610	0.0602	0.0697	-0.0095	0.0725	0.0670
1.4610	0.0699	0.0697	0.0002	0.0698	0.0697
1.5232	0.0579	0.0634	-0.0055	0.0649	0.0618
1.5742	0.0332	0.0581	-0.0250	0.0654	0.0509
1.5742	0.0678	0.0581	0.0097	0.0610	0.0553
1.5836	0.0530	0.0572	-0.0042	0.0584	0.0560
1.6060	0.0380	0.0549	-0.0167	0.0598	0.0500
1.6060	0.0701	0.0549	0.0152	0.0593	0.0505
1.6559	0.0216	0.0498	-0.0280	0.0580	0.0416
1.6557	0.0412	0.0498	-0.0086	0.0523	0.0473
1.6738	0.0552	0.0483	0.0073	0.0501	[illegible]
1.6738	0.0534	0.0480	0.0054	0.0496	0.0464
1.6823	0.0289	0.0471	-0.0182	0.0524	0.0418
1.6823	0.0542	0.0471	0.0071	0.0492	0.0450

REG= 2 B0=0.21883 B1=-.10263 NP= 52 SUMSQ=0.2095
MSR= 0.963E-01 MSSR=.00300 TV=2.01 F= 0.964E 05 FS=4.04

REGION 2

LOG X	LOG Y	LOG YHAT	LOG Y-YHAT	LOG 95% Y+	LOG 95% Y-
1.6869	-1.4031	-1.3636	-0.0395	-1.3277	-1.3995
1.7151	-1.4050	-1.3657	-0.0393	-1.3354	-1.3763
1.8476	-1.4500	-1.4678	0.0006	-1.4654	-1.4701
1.8494	-1.4810	-1.4679	-0.0132	-1.4642	-1.4713
1.8564	-1.4341	-1.4731	0.0390	-1.4577	-1.4885
1.8564	-1.4438	-1.4731	0.0293	-1.4653	-1.4809
1.9193	-1.6390	-1.5209	-0.1181	-1.4894	-1.5524
1.9193	-1.3283	-1.5209	0.1926	-1.4696	-1.5722
1.9279	-1.4769	-1.5274	0.0505	-1.5139	-1.5409
1.9289	-1.5069	-1.5282	0.0213	-1.5225	-1.5339
1.9537	-1.5194	-1.5470	0.0276	-1.5396	-1.5543
1.9585	-1.5441	-1.5507	0.0066	-1.5489	-1.5524
1.9651	-1.4591	-1.5557	0.0966	-1.5300	-1.5814
1.9764	-1.3832	-1.5643	0.1811	-1.5161	-1.6125
1.9764	-1.6050	-1.5643	-0.0407	-1.5534	-1.5751
2.1652	-1.8073	-1.7077	-0.0996	-1.6813	-1.7342
2.1703	-1.8541	-1.7116	-0.1424	-1.6738	-1.7494
2.1788	-1.7290	-1.7181	-0.0109	-1.7152	-1.7210
2.1899	-1.7144	-1.7265	0.0121	-1.7233	-1.7297
2.1899	-1.7102	-1.7265	0.0163	-1.7222	-1.7309
2.3933	-1.7058	-1.8507	0.1449	-1.8123	-1.8890
2.4359	-1.8873	-1.9134	0.0261	-1.9065	-1.9203
2.4481	-2.0567	-1.9227	-0.1340	-1.8872	-1.9581
2.5032	-1.8978	-1.9645	0.0667	-1.9469	-1.9822
2.5904	-1.9841	-2.0308	0.0467	-2.0185	-2.0432
2.6055	-2.0040	-2.0423	0.0384	-2.0322	-2.0525
2.6718	-2.0894	-2.0927	0.0032	-2.0918	-2.0935
2.6788	-2.0108	-2.0980	0.0871	-2.0750	-2.1210
2.7050	-2.0402	-2.1179	0.0778	-2.0974	-2.1385
2.7467	-2.1718	-2.1496	-0.0222	-2.1437	-2.1554
2.7467	-2.1849	-2.1496	-0.0354	-2.1402	-2.1589
2.7467	-2.2020	-2.1496	-0.0524	-2.1357	-2.1634
2.8419	-2.3878	-2.2220	-0.1659	-2.1782	-2.2657
3.0679	-2.3099	-2.3737	0.0638	-2.3716	-2.4158
3.1870	-2.4754	-2.4842	0.0088	-2.4792	-2.4891
3.3190	-2.6351	-2.5844	-0.0507	-2.5711	-2.5978
3.3372	-2.7466	-2.5983	-0.1482	-2.5592	-2.6375
3.3372	-2.6651	-2.5983	-0.0668	-2.5807	-2.6160
3.4114	-2.6668	-2.6547	-0.0121	-2.6515	-2.6579
3.4993	-2.6875	-2.7207	0.0332	-2.7119	-2.7294
3.4983	-2.6256	-2.7207	0.0950	-2.6956	-2.7458
3.4983	-2.7158	-2.7207	0.0049	-2.7194	-2.7220
3.5549	-3.0634	-2.7637	-0.2997	-2.6845	-2.8429
3.7855	-3.2345	-2.9390	-0.2955	-2.8607	-3.0172
3.8010	-3.0170	-2.9507	-0.0663	-2.9332	-2.9683
3.8099	-3.0450	-2.9575	-0.0875	-2.9343	-2.9807
3.9391	-2.9917	-3.0556	0.0639	-3.0387	-3.0726
3.9793	-3.1889	-3.0862	-0.1026	-3.0590	-3.1135
4.1540	-3.3536	-3.2189	-0.1347	-3.1831	-3.2548
4.2518	-3.0884	-3.2933	0.2049	-3.2387	-3.3479
4.2518	-3.1748	-3.2933	0.1185	-3.2617	-3.3249
4.2518	-3.2157	-3.2933	0.0776	-3.2726	-3.3140
4.5437	-3.7458	-3.5151	-0.2307	-3.4533	-3.5769
4.6894	-3.3748	-3.6258	0.2510	-3.5583	-3.6933
4.6894	-3.4960	-3.6258	0.1298	-3.5909	-3.6607
4.6894	-3.4488	-3.6258	0.1770	-3.5782	-3.6734
5.0012	-4.2319	-3.8627	-0.3692	-3.7626	-3.9628
5.0041	-3.6956	-3.8649	0.1693	-3.8190	-3.9108
5.0041	-3.5785	-3.8649	0.2864	-3.7873	-3.9425
5.0041	-3.6468	-3.8649	0.2182	-3.8058	-3.9240
5.1773	-4.3041	-3.9965	-0.3076	-3.9127	-4.0803

REG= 3 B0=-.60247 B1=-.75987 NP= 61 SUMSQ=0.0491
MSR= 0.387E 02 MSSR=.00160 TV=2.01 F= 0.241E 05 FS=4.04

REGION 3

LOG X	LOG Y	LOG YHAT	LOG Y-YHAT	LOG 95% Y+	LOG 95% Y-
-2.4467	-2.0053	-2.0884	0.0831	-2.0400	-2.1368
-2.1934	-1.9250	-1.9795	0.0545	-1.9486	-2.0103
-2.1623	-1.8337	-1.9661	0.1324	-1.8913	-2.0409
-2.0849	-2.0336	-1.9328	-0.1008	-1.8763	-1.9894
-2.0269	-1.9691	-1.9078	-0.0612	-1.8737	-1.9420
-1.9017	-1.8674	-1.8540	-0.0134	-1.8466	-1.8614
-1.8190	-1.8599	-1.8185	-0.0414	-1.7956	-1.8413
-1.6439	-1.8165	-1.7431	-0.0734	-1.7030	-1.7833
-1.5456	-1.6135	-1.7009	0.0874	-1.6532	-1.7485
-1.1597	-1.6953	-1.5349	-0.1604	-1.4471	-1.6228
-1.1067	-1.5555	-1.5121	-0.0434	-1.4883	-1.5359
-0.8587	-1.5086	-1.4054	-0.1031	-1.3481	-1.4628
-0.7315	-1.2409	-1.3507	0.1098	-1.2891	-1.4124
-0.7315	-1.3486	-1.3507	0.0021	-1.3495	-1.3519
-0.6826	-1.3891	-1.3297	-0.0594	-1.2962	-1.3632
-0.5046	-1.1378	-1.2532	0.1153	-1.1869	-1.3194
-0.4796	-1.1707	-1.2424	0.0717	-1.2011	-1.2837

REG= 4 B0= -1.036 B1=0.43007 NP= 17 SUMSQ=0.0008
MSR= 0.131E 01 MSSR=.00034 TV=2.05 F= 0.386E 04 FS=4.21

REGION 4

LOG X	LOG Y	LOG YHAT	LOG Y-YHAT	LOG 95% Y+	LOG 95% Y-
-0.4602	-0.8704	-0.9845	0.1141	-0.9376	-1.0314
-0.4193	-0.9085	-0.9591	0.0509	-0.9385	-0.9802
-0.3793	-1.0207	-0.9348	-0.0860	-0.8996	-0.9699
-0.3741	-0.9463	-0.9316	-0.0147	-0.9256	-0.9376
-0.2519	-0.9872	-0.8564	-0.1309	-0.8033	-0.9094
-0.1294	-0.7520	-0.7810	0.0290	-0.7693	-0.7927
-0.1294	-0.9018	-0.7810	-0.1208	-0.7325	-0.8296
0.0975	-0.6097	-0.6414	0.0317	-0.6288	-0.6540
0.1224	-0.6361	-0.6260	-0.0101	-0.6221	-0.6300
0.2300	-0.4953	-0.5598	0.0646	-0.5343	-0.5854
0.2709	-0.5537	-0.5347	-0.0190	-0.5272	-0.5422
0.3502	-0.4146	-0.4859	0.0713	-0.4577	-0.5141
0.3664	-0.5542	-0.4759	-0.0783	-0.4450	-0.5068
0.4726	-0.3469	-0.4106	0.0637	-0.3855	-0.4357
0.4726	-0.3759	-0.4106	0.0346	-0.3969	-0.4243
0.6995	-0.2126	-0.2710	0.0584	-0.2479	-0.2940
0.7245	-0.2225	-0.2556	0.0331	-0.2426	-0.2687
0.8730	-0.1945	-0.1642	-0.0303	-0.1522	-0.1762
0.9370	-0.0753	-0.1247	0.0494	-0.1052	-0.1446
0.9522	-0.0946	-0.1155	0.0207	-0.1072	-0.1238
1.0094	-0.1452	-0.0803	-0.0649	-0.0545	-0.1061
1.0747	0.0526	-0.0402	0.0928	-0.0031	-0.0772
1.2354	-0.0647	0.0606	-0.1253	0.1110	0.0102
1.2791	0.1154	0.0857	0.0297	0.0977	0.0738
1.3016	-0.0639	0.0996	-0.1633	0.1654	0.0339
1.3245	0.1334	0.1135	0.0199	0.1216	0.1054
1.3266	0.2123	0.1148	0.0975	0.1542	0.0754
1.3748	0.1439	0.1445	-0.0006	0.1448	0.1442
1.5543	0.2373	0.2549	-0.0176	0.2622	0.2477

REG= 5 B0=-.70138 B1=0.61526 NP= 27 SUMSQ=0.0078
MSR= 0.428E 01 MSSR=.00001 TV=2.01 F= 0.372E 06 FS=4.06

REGION 5

TABULATED DATA OF STATISTICAL ANALYSIS OF
REGRESSIONS OF REGIONS OF CORRELATION PLOTS

APPENDIX D

DERIVATION OF CROSSCORRELATION COEFFICIENTS

DERIVATION OF $R_{12}(L)$ FOR RECTANGULAR BAR (ORIFICE)

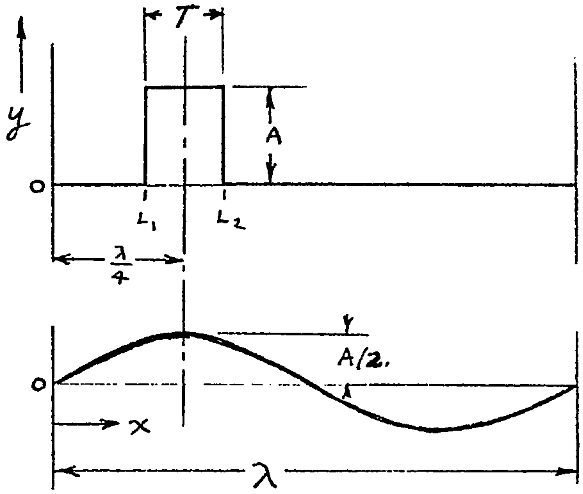

$$F_2(x) = \begin{cases} A & \frac{\lambda}{4}-\frac{T}{2} < x < \frac{\lambda}{4}+\frac{T}{2} \\ 0 & \text{elsewhere} \end{cases}$$

$$\eta_2 = \frac{AT}{\lambda}$$

$$F_1(x) = \frac{A}{2} \sin \frac{2\pi x}{\lambda}$$

$$\eta_1 = 0.$$

$$r_{12}(L) = \frac{1}{\lambda} \int_0^{\lambda} (F_1(x+L) - \eta_1)(F_2(x) - \eta_2)\, dx$$

$$r_{12}(L) = \frac{1}{\lambda}\left\{ \int_0^{\left(\frac{\lambda}{4}-\frac{T}{2}\right)=L_1} (0-\eta_2)\frac{A}{2}\sin\frac{2\pi x}{\lambda}\,dx + \int_{L_1}^{L_2=\frac{\lambda}{4}+\frac{T}{2}} (A-\eta_2)\frac{A}{2}\sin\frac{2\pi x}{\lambda}\,dx + \int_{L_2}^{\lambda}(0-\eta_2)\frac{A}{2}\sin\frac{2\pi x}{\lambda}\,dx \right\}$$

$$= \frac{1}{\lambda}\left\{ \left[-\frac{\eta_2 A}{2}\left(\frac{\lambda}{2\pi}\right)\left(-\cos\frac{2\pi x}{\lambda}\right)\right]_0^{L_1} + \left[\frac{(A-\eta_2)A\lambda}{4\pi}\left(-\cos\frac{2\pi x}{\lambda}\right)\right]_{L_1}^{L_2} + \left[\frac{-\eta_2 A\lambda}{4\pi}\left(-\cos\frac{2\pi x}{\lambda}\right)\right]_{L_2}^{\lambda} \right\}$$

$$= \frac{1}{\lambda}\left\{ \frac{\eta_2 A\lambda}{4\pi}\left(\cancel{\cos L_1\left(\frac{2\pi}{\lambda}\right)} - \cancel{1}\right) + \frac{A^2\lambda}{4\pi}\left(-\cos\frac{2\pi}{\lambda}L_2 + \cos\frac{2\pi}{\lambda}L_1\right) + \frac{\eta_2 A\lambda}{4\pi}\left(\cancel{\cos\frac{2\pi L_2}{\lambda}} - \cancel{\cos\frac{2\pi}{\lambda}L_1}\right) + \frac{\eta_2 A\lambda}{4\pi}\left(\cancel{1} - \cancel{\cos\frac{2\pi}{\lambda}L_2}\right)\right\}$$

$$r_{12}(L) = \frac{A^2}{4\pi}\left[\cos\frac{2\pi}{\lambda}\left(\frac{\lambda}{4}-\frac{T}{2}\right) - \cos\frac{2\pi}{\lambda}\left(\frac{\lambda}{4}+\frac{T}{2}\right)\right]$$

$$r_{12}(L) = \frac{A^2}{4\pi}\left[\cos\pi\left(\frac{1}{2}-\frac{T}{\lambda}\right) - \cos\pi\left(\frac{1}{2}+\frac{T}{\lambda}\right)\right]$$

normalize by σ_1 and σ_2:

$$\sigma^2 = \frac{1}{\lambda}\int_0^{\lambda} (F(x)-\eta)^2 dx$$

$$\therefore \qquad \sigma_1 = .707\,\frac{A}{2}$$

$$\sigma_2^2 = \frac{1}{\lambda}\left[\int_0^{\lambda-T} (0-\eta_2)^2 dx + \int_0^{T} (A-\eta_2)^2 dx\right]$$

$$= \frac{1}{\lambda}\left[\eta_2^2(\lambda-T) + (A-\eta_2^2)T\right]$$

$$= \frac{1}{\lambda}\left[\eta_2^2\lambda - \cancel{\eta_2^2 T} + A^2T - 2A\eta_2 T + \cancel{\eta_2^2 T}\right]$$

$$= \eta_2^2 + \frac{A^2T}{\lambda} - \frac{2A\eta_2 T}{\lambda}$$

but $\eta_2 = \frac{AT}{\lambda}$;

$$\sigma_2^2 = \frac{A^2T^2}{\lambda^2} + \frac{A^2T}{\lambda} - \frac{2A^2T^2}{\lambda^2}$$

$$= A^2\left(\frac{T}{\lambda} - \frac{T^2}{\lambda^2}\right)$$

$$\therefore \quad \boxed{\sigma_2 = A\left(\frac{T}{\lambda} - \frac{T^2}{\lambda^2}\right)^{1/2}}$$

hence, to normalize

$$R_{12}(L) = \frac{r_{12}(L)}{\sigma_1\sigma_2} = \frac{\frac{A^2}{4\pi}\left[\cos\pi\left(\frac{1}{2}-\frac{T}{\lambda}\right) - \cos\pi\left(\frac{1}{2}+\frac{T}{\lambda}\right)\right]}{.707\,\frac{A}{2}\left(A\left(\frac{T}{\lambda}-\frac{T^2}{\lambda^2}\right)^{1/2}\right)}$$

$$\boxed{R_{12}(L) = \frac{\cos\pi\left(\frac{1}{2}-\frac{T}{\lambda}\right) - \cos\pi\left(\frac{1}{2}+\frac{T}{\lambda}\right)}{.707\,(2\pi)\left(T/\lambda - T^2/\lambda^2\right)^{1/2}}}$$

DERIVATION OF $R_{12}(L)$ FOR SAWTOOTH WAVEFORM

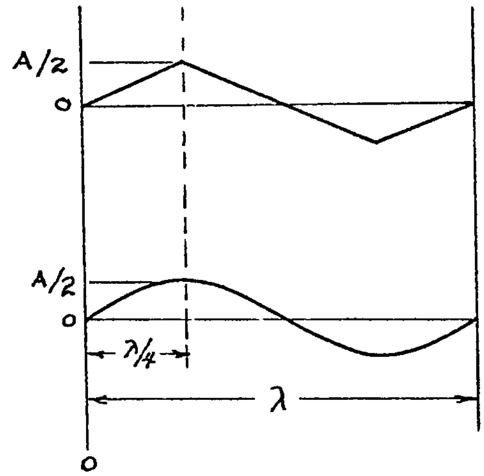

$$F_2(x) = \frac{2Ax}{\lambda} \quad \left\{ 0 < x \le \lambda/4 \right.$$

$$\eta_2 = 0.$$

$$F_1(x) = \frac{A}{2} \sin\left(\frac{2\pi x}{\lambda}\right)$$

$$\eta_1 = 0.$$

BECAUSE OF SYMMETRY, WE NEED ONLY INTEGRATE FROM $0 \to \lambda/4$ AND MULTIPLY BY 4:

$$r_{12}(L) = 4 \cdot \frac{1}{\lambda} \int_0^{\lambda/4} F_1(x) F_2(x)\, dx$$

$$= 4 \cdot \frac{1}{\lambda} \int_0^{\lambda/4} \frac{A}{2} \sin\left(\frac{2\pi x}{\lambda}\right) \frac{2Ax}{\lambda}\, dx$$

$$= \frac{4A^2}{\lambda^2} \left[\left(\frac{\lambda}{2\pi}\right)^2 \sin \frac{2\pi x}{\lambda} - \frac{x\lambda}{2\pi} \cos \frac{2\pi x}{\lambda} \right]_0^{\lambda/4}$$

$$= \frac{4A^2}{\lambda^2} \left[\left(\frac{\lambda}{2\pi}\right)^2 (1 - 0) - \frac{\lambda}{2\pi}\left[0 - 0 \right] \right]$$

$$r_{12}(L) = \frac{A^2}{\pi^2}$$

$$\sigma_2^2 = 4 \cdot \frac{1}{\lambda} \int_0^{\lambda/4} \left(\frac{2Ax}{\lambda}\right)^2 dx$$

$$= \frac{4}{\lambda} \left(\frac{2A}{\lambda}\right)^2 \frac{x^3}{3} \Big|_0^{\lambda/4}$$

$$= \frac{A^2}{12}$$

$$\boxed{\sigma_2 = \frac{A}{\sqrt{12}}}$$

$$\boxed{R_{12}(L) = \frac{r_{12}(L)}{\sigma_1 \sigma_2} = \frac{A^2/\pi^2}{\left(.707\frac{A}{2}\right)\left(\frac{A}{\sqrt{12}}\right)} = \underline{\underline{0.994}}}$$

APPENDIX E

NOMENCLATURE

A	waveform amplitude, peak-to-peak
c	wave velocity
D	nominal diameter
D_o	minimum diameter of rough pipe
d	volumetric average diameter
e	sand-grain roughness height
$\mathcal{E}$	eddy viscosity
$\mathcal{E}'$	roughness eddy viscosity
f, $\langle f \rangle$	Darcy friction factor = $8\,\tau_w/\rho\,\bar{U}^2$ averaged over a wave-length of roughness
F_i	function of the waveform i
F	F statistic
k	constant
k	wave number
L	phase difference length of two waveforms
m	constant power in power-law velocity distribution
n	wave number
n_p	number of data points
N_{Re}	Reynolds number
p_o	wall pressure
P	length of cavity of groove roughness

P_o	wall pressure amplitude
p_w	wall static pressure
Q	volumetric flow rate
$\mathbb{R}e$	roughness Reynolds number
R	$= \lambda^2/\sigma D_o$ for projection roughness and P^2/TD_o for groove roughness
$R_{12}(L)$	crosscorrelation coefficient for projection roughness
$R_{12}(0)$	crosscorrelation coefficient for groove roughness
S	wetted perimeter of a roughness element over a wavelength
T	length of crest of a roughness element
U	point velocity, time averaged
$\bar{U}$	space- averaged velocity
U_o	centerline (maximum) velocity
U_*	shear velocity $= \sqrt{\tau_w/\rho}$
ΔU	$U_o - U$
x	longitudinal direction of flow in a pipe
X	abscissa in least-squares regression
y	direction normal to flow(radial direction in round pipes)
Y	ordinate in least-squares regression

Greek symbols

$\beta 1$	slope in linear least-squares equation
$\beta 0$	intercept in linear least-squares equation
Δ	amplitude

ϵ	equivalent sand-grain roughness height
η	wavelength-averaged mean
λ	wavelength
μ	dynamic viscosity
ν	kinematic viscosity
ν_e	modified kinematic viscosity for rough surfaces
π	3.14159
ρ	density
σ	root mean square of amplitude
Σ	a summation
τ_o	smooth wall shear stress
τ_w	total rough wall shear stress
ϕ	functional dependency